

AD-A133666



DIRECT SHEAR FAILURE IN REINFORCED CONCRETE BEAMS UNDER IMPULSIVE LOADING

Dr Timothy J. Ross

September 1983

Final Report

Approved for public release; distribution unlimited.

DTIC FILE COPY

DTIC
 ELECTE
 OCT 18 1983
 A

AIR FORCE WEAPONS LABORATORY
 Air Force Systems Command
 Kirtland Air Force Base, NM 87117

This final report was prepared by the Air Force Weapons Laboratory, Kirtland Air Force Base, New Mexico, under Job Order 88091343. Dr Timothy J. Ross (NTESA) was the Laboratory Project Officer-in-Charge.

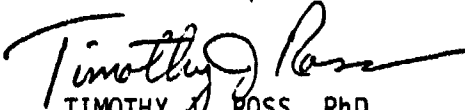
When Government drawings, specifications, or other data are used for any purpose other than in connection with a definitely Government-related procurement, the United States Government incurs no responsibility or any obligation whatsoever. The fact that the Government may have formulated or in any way supplied the said drawings, specifications, or other data is not to be regarded by implication, or otherwise in any manner construed, as licensing the holder, or any other person or corporation; or as conveying any rights or permission to manufacture, use, or sell any patented invention than may in any way be related thereto.

This report has been authored by an employee of the United States Government. Accordingly, the United States Government retains a nonexclusive, royalty-free license to publish or reproduce the material contained herein, or allow others to do so, for the United States Government purposes.

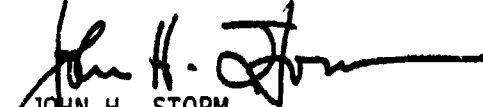
This report has been reviewed by the Public Affairs Office and is releasable to the National Technical Information Services (NTIS). At NTIS, it will be available to the general public, including foreign nations.

If your address has changed, if you wish to be removed from our mailing list, or if your organization no longer employs the addressee, please notify AFWL/NTESA, Kirtland AFB, NM 87117 to help us maintain a current mailing list.

This report has been reviewed and is approved for publication.


TIMOTHY J. ROSS, PhD
Project Officer


PAUL E. MINTO
Captain, USAF
Chief, Applications Branch

FOR THE COMMANDER

JOHN H. STORM
Colonel, USAF
Chief, Civil Engrg Research Division

DO NOT RETURN COPIES OF THIS REPORT UNLESS CONTRACTUAL OBLIGATIONS OR NOTICE ON A SPECIFIC DOCUMENT REQUIRES THAT IT BE RETURNED.

UNCLASSIFIED

SECURITY CLASSIFICATION OF THIS PAGE (When Data Entered)

REPORT DOCUMENTATION PAGE		READ INSTRUCTIONS BEFORE COMPLETING FORM
1. REPORT NUMBER AFWL-TR-83-84	2. GOVT ACCESSION NO. AD-A133666	3. RECIPIENT'S CATALOG NUMBER
4. TITLE (and Subtitle) DIRECT SHEAR FAILURE IN REINFORCED CONCRETE BEAMS UNDER IMPULSIVE LOADING		5. TYPE OF REPORT & PERIOD COVERED Final Report
		6. PERFORMING ORG. REPORT NUMBER
7. AUTHOR(s) Dr. Timothy J/ Ross		8. CONTRACT OR GRANT NUMBER(s)
9. PERFORMING ORGANIZATION NAME AND ADDRESS Air Force Weapons Laboratory (NTESA) Kirtland Air Force Base, NM 87117		10. PROGRAM ELEMENT, PROJECT, TASK: AREA & WORK UNIT NUMBERS 62601F/88091343
11. CONTROLLING OFFICE NAME AND ADDRESS Air Force Weapons Laboratory (NTESA) Kirtland Air Force Base, NM 87117		12. REPORT DATE September 1983
		13. NUMBER OF PAGES 226
14. MONITORING AGENCY NAME & ADDRESS (if different from Controlling Office)		15. SECURITY CLASS. (of this report) Unclassified
		15a. DECLASSIFICATION/DOWNGRADING SCHEDULE
16. DISTRIBUTION STATEMENT (of this Report) Approved for public release; distribution unlimited.		
17. DISTRIBUTION STATEMENT (of the abstract entered in Block 20, if different from Report)		
18. SUPPLEMENTARY NOTES Copyrighted by Timothy Jack Ross for his dissertation for his Degree of Doctor of Philosophy at Stanford University.		
19. KEY WORDS (Continue on reverse side if necessary and identify by block number)		
Reinforced Concrete	Structural Damage	Viscoelastic
Impulsive Loads	Stochastic Processes	Laplace Transform
Direct Shear	Beams	Normal Mode
Failure Curves	One-way Slabs	
Elastic Failure	Timoshenko Theory	
20. ABSTRACT (Continue on reverse side if necessary and identify by block number)		
<p>Direct shear failures in reinforced concrete elements have been believed to occur only along existing slip planes such as construction joints or crack surfaces, or in short members such as corbels where the shear span is very small. These failures typically have been classified in terms of static forces and mechanisms. Recent dynamic tests have shown the possible existence of direct shear failure phenomena in reinforced concrete slabs which do not have small shear spans and which are subjected to impulsive loading distributed along the</p> <p style="text-align: right;">see → (over)</p>		

20. ABSTRACT (Continued).

slap span. A technique is needed to examine these failures.

An analytic procedure is developed, using the classical elastic Timoshenko beam theory, to define conditions under which reinforced concrete beams and one-way slabs can fail in a direct shear mode when subjected to distributed impulsive loading. The procedure is based on the assumption that incipient failure occurs in direct shear when the beam support shear exceeds a strength threshold before the support bending moment attains its ultimate capacity. The Timoshenko theory is extended to include rotational beam-end restraint and to account for visco-elastic material response to assess qualitatively the influence of rate effects on shear and bending moment.

Dynamic failure in direct shear is presumed to behave in accordance with currently accepted static shear transfer mechanisms. Dynamic failure criteria are extrapolated from static criteria with the use of an enhancement factor based on increased material strengths due to load rate. Failure curves, defining peak pressure versus rise time domains where direct shear failure is possible, are compared to experimental evidence for specific beam geometries and load rates. Post failure deterministic and stochastic models are introduced as candidates for analysis beyond incipient shear failure.

It is concluded that direct shear failures can be predicted for certain combinations of load parameters. Rate effects enhance shear forces more than bending moments during transient response. Strength enhancement due to load rate reduces the domain of load parameters over which a direct shear failure can take place, whereas a relaxation of beam-end restraint increases this domain considerably.

Accession No. _____

Classification _____

By _____

Distribution/Availability Codes

Dist	Avail and/or Special
A	

NSA
COPY INSPECTED

Acknowledgements

Research is a very insidious and capricious process; involving as it does a subtle interplay between fact and preconception, while at the same time creating feelings of despair one day and euphoric optimism the next. And because research primarily is inclined to be a solitary experience, a need develops on the part of the researcher to associate and interact with individuals who are sympathetic with his plight. The thinking, study, and research represented by this dissertation could not have been accomplished by the author without the helpful efforts and thoughtful consideration of these individuals. Therefore, it is a pleasure to preface this dissertation by acknowledging those special individuals who favorably influenced the author during the course of his graduate studies and doctoral research. Many people contributed to the development of this work in both a technical and emotional sense, but the author is especially grateful:

To my advisor Professor Helmut Krawinkler, whose guidance and suggestions on the research, whose knowledge of reinforced concrete failures, and whose meticulous attention to detail on the presentation of issues and concepts within the dissertation have made this investigation worthwhile and worthy of publication;

To Professor Haresh Shah for his participation on my reading committee and whose enthusiasm in probability and statistics initiated my interests in this field;

To Professor William Weaver, Jr. for his participation on my reading committee, his helpful comments on the normal mode method, and his being an excellent example in personal organization;

To my good friend and colleague, Dr. Felix Wong, whose many discussions and suggestions and whose extensive knowledge of analytic procedures provided me with ideas necessary to attack my research problems;

To Professor Ted Zsutty for his participation at my dissertation defense and for his humorous and enlightening remarks on the vagaries of analyzing reinforced concrete;

To Professor Michael Taksar for his review of Chapter 6 and his lively discussions on stochastic modeling;

To Professor Walter Austin, Rice University, for his teaching me not to take any research subject too seriously;

To my many colleagues at the Blume Center for their friendship, and to my office partners Vahid Sotoudeh and Auguste Boissonnade, whose knowledge of mathematics and critiques of my defense presentation were helpful;

To my parents for their love and understanding throughout my rather sporadic and extended graduate experience;

To my dear children, Bradley and Amethyst, whose smiles and innocence helped me keep this research in perspective, and whose love for their Daddy gave me every reason to be optimistic;

And especially to my beloved wife Carol for her professional preparation of the manuscript, for her patience and understanding of my erratic and often unexplained behavior, for her confidence in me, and mostly for the love and encouragement she gave me when I needed it most.

The experimental data used in this dissertation was provided by the Defense Nuclear Agency and the U.S. Army Corps of Engineers. This research was supported by the U.S. Department of the Air Force and is gratefully acknowledged.

This dissertation is dedicated to the memory of my dear friend Captain Steven Aksomitas, USAF.

Table of Contents

	<u>Page</u>
Acknowledgements	i
Table of Contents	iii
List of Tables	vi
List of Figures	vii
List of Symbols	xi
Chapter 1. Introduction	1
1.1 Problem Statement	1
1.2 Background	2
1.3 Major Assumptions	3
1.4 Objectives and Scope	5
1.5 Summary	7
Chapter 2. Direct Shear Failure Mechanisms	9
2.1 Introduction	9
2.2 Behavior Under Static Loads	10
2.2.1 Initially Cracked Concrete	10
2.2.2 Initially Uncracked Concrete	12
2.3 Behavior Under Dynamic Loads	15
2.3.1 Response Definition	15
2.3.2 Shear Key Tests	15
2.3.3 Pushoff Element Tests	17
2.4 Summary	18
Chapter 3. Failure Criteria	20
3.1 Introduction	20
3.2 Rate Effects on Material Properties	22
3.2.1 Strength Properties	25
3.2.2 Elastic Properties	25
3.3 Flexural Failure Criteria	26
3.4 Direct Shear Failure Criteria	27
3.5 Summary	32

Table of Contents (continued)

	<u>Page</u>
Chapter 4. Experimental Data Base	34
4.1 Introduction	34
4.2 Test Description	34
4.2.1 Configuration	35
4.2.2 Instrumentation	35
4.3 Data Analysis	36
4.3.1 Interface Pressure	37
4.3.2 Active Steel Strain	40
4.3.3 Post Failure Measurements	42
4.4 Summary	43
Chapter 5. Elastic Beam Theory	44
5.1 Introduction	44
5.2 Timoshenko Beam	46
5.2.1 Normal Mode Method	47
5.2.1.1 Flexure-Shear Mode	53
5.2.1.2 Thickness-Shear Mode	58
5.2.1.3 Convergence	61
5.2.1.4 Shear and Moment Analysis	62
5.2.2 Rate Effects on Response	65
5.2.2.1 Strain Rate	66
5.2.2.1.1 Laplace Transform Solution	69
5.2.2.1.2 Elastic and Strength Effects	78
5.2.2.2 Load Rate	81
5.2.3 Failure Curves	83
5.3 Shear Beam	85
5.3.1 Normal Mode Method	86
5.3.2 Strain Rate Effects	89
5.4 Comparisons to Data	91
5.5 Summary	93

Table of Contents (continued)

	<u>Page</u>
Chapter 6. Post Failure Models	95
6.1 Introduction	95
6.2 Simplified Deterministic Models	96
6.3 Stochastic Models	99
6.3.1 Shear Slip Model: Wiener Process	103
6.3.1.1 Moments	103
6.3.1.2 First Passage Probability	106
6.3.2 Shear Slip Rate Model: Ornstein-Uhlenbeck Process	107
6.3.2.1 Moments	107
6.3.2.2 First Passage Probability	110
6.4 Summary	110
 Chapter 7. Summary and Conclusions	 112
7.1 Summary	112
7.2 Conclusions	113
7.3 Recommendations for Future Work	115
 References	 119
Tables	124
Figures	130
Appendix A - Interface Pressure Loading	180
Appendix B - Concrete Fracturing	194
Appendix C - Shear Transfer in Reinforced Concrete	198

List of Tables

<u>Table</u>	<u>Title</u>	<u>Page</u>
4.1	Test Groups and Test Designation	124
4.2	Physical Parameters for Each Test Group	125
4.3	Summary of Test Results	126
5.1	Example of Reinforced Concrete Beam Properties	127
5.2	Test Group Beam Parameters	128
5.3	Comparison of Analysis Prediction and Experimental Data	129

List of Figures

<u>Figure</u>	<u>Title</u>	<u>Page</u>
1.1	Classification of Direct Shear Failures into Three Regimes	130
2.1	Initially Cracked and Initially Uncracked Concrete Beams	131
2.2	Force Transfer Mechanisms in Direct Shear for an Initially Cracked Concrete Section	132
2.3	Dowel Reinforcement Patterns Across a Crack Plane	133
2.4	Effect of Concrete Strength on Shear Transfer Strength of Initially Cracked Specimens	133
2.5	Shear Transfer Strength vs. Reinforcement Parameter $\rho_s f_y$ for Specimens With and Without an Initial Crack Along the Shear Plane	134
2.6	Shear Transfer in Initially Uncracked Concrete	134
2.7	Typical Shear Failure for a Corbel	135
3.1	Effect of Strain Rate on Strength of Concrete, Steel and Aluminum	136
3.2	Strength Enhancement and Modulus Enhancement Factors for Concrete Versus Strain Rate	137
3.3	Strength Enhancement and Modulus Enhancement Factors for Concrete Versus Load Rate (Stress Rate)	138
3.4	Shear Friction Plus Cohesion Approach	139
3.5	Relationship of Principal Stresses ($\sigma_3 > \sigma_1$) for Mohr-Coulomb Criterion	139
4.1	Test Configuration for the WES Tests	140
4.2	Test Element Construction Details, Test Group I	141
4.3	Test Element Construction Details, Test Groups II and III	142
4.4	Example Test Instrumentation Layout, Test Groups II and III	143

List of Figures (continued)

<u>Figure</u>	<u>Title</u>	<u>Page</u>
4.5	Post Test View of Test Element DS1-1	144
4.6	Post Test View of Test Element DS1-2	144
4.7	Post Test View of Test Element DS1-4	145
4.8	Post Test View of Test Element DS1-5	145
4.9	Post Test View of Test Element DS2-1	146
4.10	Post Test View of Test Element DS2-2	146
4.11	Post Test View of Test Element DS2-4	147
4.12	Post Test View of Test Element DS1-3	147
4.13	Post Test View of Test Element DS2-3	148
4.14	Post Test View of Test Element DS2-5	148
4.15	Post Test View of Test Element DS2-6	149
4.16	Post Test Schematic of Test Element FH1	149
4.17	Failure Mode Determination Using Interface Pressure Measurements	150
4.18	Active Measurements for FH1: Flexural Failure	151
4.19	Active Measurements for DS1-1: Direct Shear Failure	152
4.20	Active Measurements for DS1-3: Direct Shear Failure	153
4.21	Post Failure Measurements for DS2-1: Direct Shear Failure	154
4.22	Post Failure Measurements for DS2-5: Direct Shear Failure	155
5.1	Timoshenko Beam Model and Idealized Interface Pressure Loading ..	156
5.2	Elastic Wave Velocity Curves for a Solid Circular Cylinder of Radius a	157
5.3	Timoshenko Beam Wave Configurations	158
5.4	Dispersion Relations for a Timoshenko Beam	158
5.5	Timoshenko Beam Element	159
5.6	Fourier Amplitude Spectrum for Idealized Interface Pressure Pulse 0.6 msec Duration	160
5.7	Fourier Amplitude Spectrum for Idealized Interface Pressure Pulse 2 msec Duration	160

List of Figures (continued)

<u>Figure</u>	<u>Title</u>	<u>Page</u>
5.8	Normalized Support Shear and Moment vs. Time for Example Beam: Fixed-Ends, $P_0 = 5000$ psi	161
5.9	Normalized Support Shear and Moment vs. Time for Example Beam: Fixed-Ends, $P_0 = 2000$ psi	161
5.10	Direct Shear Failure Time t' , vs. Peak Pressure for Example Beam	162
5.11	Flexure Failure Time, t'' , vs. Peak Pressure for Example Beam	162
5.12	Normalized Support Shear and Moment vs. Time for Example Beam: $R = 4EI/L$, $P_0 = 5000$ psi	163
5.13	Linear Viscoelastic Model	164
5.14	Rate Effect Ratio (RER) vs. Time for Example Beam	165
5.15	Strain Rate Effects on Shear Failure Time, t' , for Example Beam ($\Omega = 1$)	166
5.16	Strain Rate Effects on Shear Failure Time, t' , for Example Beam ($\Omega = 1.5$)	166
5.17	Strength Enhancement Effects on Normalized Support Shear of Example Beam	167
5.18	Modulus Enhancement Effects on Normalized Support Shear of Example Beam	167
5.19	Direct Shear Failure Time Parameters	168
5.20	Construction of Failure Curves	169
5.21	Failure Curve for Example Beam; Fixed-Ends, No Strength Enhancement	169
5.22	Influence of Beam-End Restraint on Failure Curve of Example Beam	170
5.23	Influence of Strength Enhancement Factor on Failure Curve of Example Beam; Fixed-Ends	170

List of Figures (continued)

<u>Figures</u>	<u>Title</u>	<u>Page</u>
5.24	Influence of Reinforcement Ratio on Failure Curve of Example Beam; Fixed-Ends	171
5.25	Influence of L/d Ratio on Failure Curve of Example Beam; Fixed-Ends	171
5.26	Comparison of Support Shear Forces for a Timoshenko Beam and a Shear Beam; Fixed-Ends	172
5.27	Domain of Equivalence for Support Shear Forces	172
5.28	Comparison of Failure Curve and Test Data: Group I Beams	173
5.29	Comparison of Failure Curve and Test Data: Group II Beams	174
5.30	Comparison of Failure Curve and Test Data: Group III Beams	175
6.1	Post Failure Model: Rigid-Body Slab Motion	176
6.2	Shear Stiffness vs Shear Displacement for a Precracked Shear Plane	177
6.3	Stochastic Processes: Wiener and Ornstein Uhlenbeck	178
6.4	Test Roof Slab Velocity	179

List of Symbols

A	= beam cross-sectional area
A_s	= area of total longitudinal steel
A_s'	= area of tension steel
$A(\omega), B(\omega)$	= components of Fourier amplitude
A_i, B_i	= functions in Laplace variable s , $i = 0,3,4$
A_n, B_n	= constants
a	= first passage barrier
a_i, b_i	= constants $i = 0,1,2$
b	= beam width (unity)
C	= concrete cohesive strength
C_i, C_i'	= constants $i = 1,2,3,4$
c	= elastic wave speed
c_0	= elastic longitudinal wave speed
c'	= shear viscosity function
DIF	= dynamic increase factor
$D(p)$	= characteristic equation in Laplace variable p
d	= beam effective depth
E	= beam modulus of elasticity
$E\{\cdot\}$	= expected value
f_c	= concrete compressive strength
f_y	= steel yield strength
f_x	= probability density function
f_t	= concrete tensile strength
G	= beam elastic shear modulus
$G_n(t)$	= variable function of time
$G_n(x,s)$	= n^{th} derivative function in Laplace variable s
$H(u)$	= unit step function
$h(u)$	= impulse response function
h	= thickness of beam
I	= beam moment of inertia
i	= indice number
j	= complex number
K_1, K_1', K_2	= constants for a given mode

List of Symbols (continued)

k'	= shear deformation coefficient
k	= shear stiffness function
L	= beam length
L_p^{-1}	= inversion operator for Laplace variable p
M	= beam bending moment
M_u	= ultimate bending moment capacity
M_{ur}	= ultimate bending moment with rate effects
\overline{M}_s	= applied concentrated moment
\overline{M}	= Laplace function of bending moment
m	= beam mass
$m_x(t)$	= mean function
n	= mode number
P_0	= peak interface pressure
$Pr\{ \cdot \}$	= probability function
p	= Laplace variable for space
P_1, P_2	= roots of Laplace characteristic equation
q	= applied transverse distributed load on beam
$\overline{q}, \overline{\overline{q}}$	= Laplace functions of distributed load q
R	= rotational beam-end restraint
r	= beam radius of gyration
s	= Laplace variable for time
T_a	= first passage time
$T_n(t)$	= variable function of time
t	= time
t_i	= time variables $i = 0, 1, 2, \dots$
$U(t)$	= Ornstein-Uhlenbeck process
u	= dummy variable
V	= shear force
V_d	= dowel force
V_e	= total shear resistance along crack planes
V_u	= ultimate shear capacity
V_{ur}	= ultimate shear capacity with rate effects
\overline{V}	= Laplace function of the shear force
$Var\{ \cdot \}$	= variance function

List of Symbols (continued)

v_{max}	= maximum shear stress
v_u	= ultimate shear stress
v_o	= initial transverse velocity
$W(t)$	= Wiener process
$\dot{W}(t)$	= White noise error term
w	= reinforcement index
w_o	= initial crack width
$X(t)$	= transverse displacement stochastic process
$X(\omega)$	= Fourier amplitude
x	= distance along the beam axis
x_o	= initial transverse displacement
Y_n	= beam n^{th} normal mode due to deflection
y	= beam transverse deflection
$\overline{y}, \overline{\overline{y}}$	= Laplace functions on y
z	= subscript to denote rate effects
α	= damping factor
α'	= viscous parameter for compression
β	= elastic constant
$\Gamma(u)$	= standardized normal distribution function
γ	= constant for a given mode
γ_{xy}	= shear angle
δ, δ'	= constants for a given mode
δ_o	= initial shear slip
ϵ	= constant
ζ	= constant in Laplace analysis
η	= viscous parameter for shear
θ	= constant
θ'	= initial crack inclination angle
λ	= wavelength
μ, μ'	= constants for a given mode
ν	= Poissons ratio
ξ, ξ'	= constants for a given mode

List of Symbols (Continued)

π	= constant 3.14159
π_i	= constants for a given mode $i = 1, 2, 3, 4$
ρ	= beam density
ρ_s	= steel reinforcement ratio
$\dot{\sigma}$	= load rate
$\sigma_x(t)$	= standard deviation function
σ^2	= variance
τ	= dummy variable
τ_s	= shear stress
Φ_n	= beam n^{th} normal mode due to bending rotation
ϕ	= beam angle of rotation due to bending
$\bar{\phi}, \underline{\phi}$	= Laplace functions of ϕ
ϕ	= concrete internal angle of friction
ϕ_1, ϕ_2	= differentiable functions of time
Ψ	= elastic modulus enhancement function
ψ, ψ'	= constants for a given mode
ω	= frequency
ω'	= first thickness-shear frequency
ω_n	= beam n^{th} natural frequency
Ω	= strength enhancement factor

Chapter 1

Introduction

1.1 Problem Statement

Reinforced concrete beams and one-way slabs can fail in a variety of mechanisms. They can fail in a flexural mode where plastic hinges form at locations where the ultimate bending capacity is attained. They can fail in a combined flexure-shear mode which is characterized by the formation of inclined tension cracks and flexural cracks within the shear span of the elements. They can fail in a shear-compression mode where diagonal tension cracking reduces the element to a tied-arch mechanism and the load is transferred to the supports in direct compression in a truss-like action. And last, these elements can fail in a direct shear mode. As defined here, failure connotes the condition at which a structural element can not sustain any further increase in external load without excessive and irreversible deformations.

Direct shear failures in reinforced concrete structures generally occur at locations near supports or joints of the elements which comprise the structure. Most of what is known about direct shear failures in concrete results from static testing. These tests suggest that direct shear failures can arise under two general situations. First, failure can occur near a support where shear forces are high and where a pre-existing crack surface has formed through the thickness of the member. Second, direct shear failure can occur near a joint or support where the shear-span (defined as the ratio of moment to shear force under a concentrated load condition) is less than about one-half the effective depth of the member, such as would exist for a short corbel.

Recent dynamic tests on shallow-buried reinforced concrete box structures subjected to impulsive pressures, however, have shown that direct shear failures in the roof slab of these structures can occur in situations where there are no existing crack planes through the thickness of the roof slab and where the loading is distributed along the span of the member and not concentrated near a support.

At present there is no analytic method to assess and explore these recent dynamic direct shear failures. This absence of a method for assessing the relevant issues associated with dynamic direct shear failures provides the genesis for the development of the elastic model described herein.

1.2 Background

To understand the problem of a slab failing in direct shear from a distributed dynamic pressure, a brief discussion is provided of the mechanics of the roof of a shallow buried box loaded by ground shock wave. This shock wave is induced from a surface blast wave and, as it impinges on the roof, the impedance (density times dilatational wave speed) mismatch between the soil cover and the concrete roof results in the wave being partially reflected and transmitted in accordance with classical wave propagation theory. The transmitted wave becomes the actual interface pressure which provides the loading to the roof-slab causing subsequent motion. This interface pressure and subsequent structural interaction are discussed in more detail in Appendix A.

An assessment of the shearing action in a reinforced concrete slab under impulsive loading (which is manifested in the form of interface pressures) must consider several issues associated with both the dynamics of response and the mechanical

behavior of the material. The response of the member will include very early time wave propagation phenomena and later, transient vibrational characteristics. The material behavior of reinforced concrete will be influenced by rate effects on the elastic and strength properties in shear.

In the particular case of reinforced concrete beams or slabs subjected to impulsive loads, wave propagation through the thickness of the member is associated with times much smaller than the times corresponding to propagation along its length. However, shear failures can occur at times soon after a wave has traversed the thickness of the beam (see Appendix A for a plausible failure scenario). Inasmuch as beam models do not account for wave phenomena associated with beam thickness, it is important to keep in mind that early time shear failures may very well involve the mechanics of both wave action and beam action. In a more exact three dimensional sense, shearing action is initiated very early when waves diffract at the intersection of a beam and supporting wall, often called a reentrant corner. A flexure phenomenon in the three-dimensional sense is not initiated until much later when the beam attains some momentum of its own. This occurs after waves have transversed the beam thickness many times. On the other hand, beam action, although neglecting wave action through the thickness, provides for an immediate comparison between the magnitudes of shearing forces and bending moments.

1.3 Major Assumptions

The difference in response action and time of response described in Section 1.2 leads to the first important assumption made in this work. Since the major effort here is to compare shear and moment at the support, beam action will be assumed to give a sufficiently accurate picture of direct shear in the presence of a moment

influence. In this sense it will be possible to determine whether a direct shear failure mechanism will occur prior to a bending failure mechanism, but questions regarding the actual time to shear failure would be answered more appropriately with a detailed three-dimensional analysis which includes wave action.

The second assumption involves the modeling of a one-way roof slab as a beam of unit width. This is a common procedure so long as the properties along the long dimension of the slab are relatively homogeneous. However, this assumption does contain a minor error in terms of the slab stiffness which should be pointed out here. A one-way slab under loading normal to its plane is in a state of plane strain, whereas a beam under the same loading condition is in a state of plane stress because there are no tractions on its lateral surfaces. This difference arises from the Poisson effect and results in the beam model underestimating the elastic slab stiffness. This effect is small and is given by the expression $(1 + \nu)(1 - 2\nu)/(1 - \nu)$, which is the ratio of beam stiffness to slab stiffness and where ν is Poissons ratio.

The third assumption involves the presumption that an elastic theory can adequately describe the attainment of maximum capacity which has been defined as the failure level. The use of elastic models in describing response up to failure is believed to be adequate because of the existence of small strains, the very short times involved, and the brittle nature of shear failures in concrete, all of which have been seen in recent dynamic tests.

Perhaps one of the biggest voids to fill is in the identification of a failure criterion for direct shear under dynamic loading. This area is lacking in adequate dynamic test data and thus cannot be addressed sufficiently in this study. To accomplish

the task of this research, the fourth assumption is that dynamic direct shear failure modes can be described in terms of the static failure mechanisms previously dealt with at length in the literature. Unlike static loads, under which fractures are initiated and propagated according to the stress and strain field existing throughout the concrete member, impulsive loads create transient islands of high stresses and strain whose location may change before an initiated crack has time to propagate. Under static loads the weakest elements in the concrete mass will control locations and levels of cracking whereas under impulsive loads the weakest link in the concrete mass may not have time to crack because of local transient conditions. A qualitative discussion of this process is provided in Appendix B.

Fifth, it is assumed that the failure criteria in direct shear is not a function of the bending moment and that the failure criteria in flexure is not a function of the shear force. Static test data on normally reinforced concrete beams with adequate shear reinforcement have shown that the presence of a shear force has little influence on flexure failure levels and that the presence of a moment has little influence on direct shear failure levels.

1.4 Objectives and Scope

This study will investigate the nature of direct shear failures in reinforced concrete beams under the action of uniformly distributed impulsive loading. In pursuing this investigation the first objective is to develop an elastic model which describes support shear forces during the period over which a direct shear failure is considered more likely than a flexural failure. The second objective is to define the conditions under which a direct shear failure can be realized. These conditions will be specified in terms of beam geometry, material properties, and loading

parameters. The third objective is to determine the influence of rate effects on both shearing forces and the conditions required to realize a direct shear failure. The fourth objective is to introduce simple models which can describe beam behavior after an incipient direct shear failure has occurred. These simple post failure models should be useful for an assessment of the uncertainties inherent in the actual failure process.

The scope of this research effort can be summarized by referring to Figure 1.1. This figure shows that the direct shear failure process can be classified into three distinct regimes, all of which receive various degrees of attention in this dissertation. The first regime, involving the characterization of a direct shear failure level using an elastic approach, embodies the bulk of the work conducted for this dissertation. The second regime involves the actual concrete fracturing and shearing process under impulsive load conditions. Very little is known about this process and so it is assumed that the dynamic failure mechanism in direct shear is similar to the static failure mechanism about which there is considerable information. Naturally, this second regime currently involves many uncertainties. The third regime is associated with the post failure condition of the slab or beam after the strength level has been reached and increased external load produces a situation involving large deformations and inelastic material response in both the reinforcing steel and the concrete. The third regime, involving post failure conditions, is treated in an introductory fashion in this dissertation by attempting to account for some of the uncertainties inherent in the initial conditions posed by the second regime.

The direct shear failure mechanisms developed from static testing and limited dynamic element tests are summarized in Chapter 2. Failure criteria developed from static testing in both flexural and direct shear modes are provided in Chapter 3 along with simple empirical adjustments to these static criteria to account for strength increases under the influence of loading rate. Recent dynamic tests which have shown direct shear failures in roof slabs are described in Chapter 4.

Chapter 5 describes the development of elastic beam models which are defined by linear partial differential equations. The analytic results are compared to data gathered on one-way slabs loaded with impulsive blast pressures. Rate effects on initial elastic properties, strength properties, and the time domain over which shear dominates bending moments are also studied in Chapter 5. Another issue investigated in Chapter 5 is the effect of support restraint on the shear phenomenon and the relative importance of shear force versus bending moment.

Linear models describing post-failure response are defined in Chapter 6 by ordinary differential equations based on the presumption of a well defined failure plane. These models are formulated for both deterministic and stochastic situations in an effort to account for uncertainties in the failure process. Finally, conclusions and recommendations are made in Chapter 7 regarding the applications of the models developed herein and the focus of future work in this area.

1.5 Summary

Direct shear failure in reinforced concrete under impulsive loads is relatively undocumented because of the paucity of data showing failure characteristics. The

combined effects of beam action and wave action are likely to be important in developing models to understand the dynamic direct shear phenomenon. This research makes an initial attempt to understand this phenomenon by considering elastic beam action to describe incipient shear failure conditions.

The major assumptions made in this endeavor are: 1) Wave propagation through the beam thickness is neglected in favor of a simpler one dimensional beam model which assesses both bending moment and shear; 2) one-way slab response under plane strain conditions can be adequately treated by a beam model; 3) elastic behavior is presumed to adequately describe response to incipient failure in direct shear; 4) direct shear failure in the dynamic case is assumed to behave in accordance with shear transfer mechanisms used to describe static situations; and 5) failure is simply described by either shear or moment reaching its respective strength capacity first in the beam response history.

The effects of load rate and beam-end restraint are investigated. Failure curves developed from elastic beam models are compared with experimental data on one-way slabs which failed in direct shear. Simple models to describe post failure behavior are introduced. Recommendations are made regarding future research into dynamic direct shear failures.

Chapter 2

Direct Shear Failure Mechanisms

2.1 Introduction

The American Concrete Institute code (ACI '77) indicates that, under static loads, direct shear failures can arise under conditions near a support where shear forces are high. The existence of a crack plane through the thickness of a beam can be important to the behavior of a beam in direct shear. For this case, called initially cracked concrete, shear failure occurs along the crack plane. The ACI refers to this direct shear behavior as shear-friction. In shear-friction, shear transfer is accomplished along the crack plane by a frictional resistance to sliding between the faces of the crack.

Although not explicitly acknowledged by ACI, direct shear can also occur in some situations in uncracked or monolithic concrete. For initially uncracked concrete, shear transfer is accomplished through the combined actions of shear and compression in small "concrete struts" which are formed by a series of small diagonal cracks which form along a shear plane after load is applied to the beam. For the initially uncracked case "slip" is characterized by the rotation and compression of these small struts.

Although the basic behavior of these two cases is different, both are referred to in the static sense as direct shear failures. Figure 2.1 displays the two cases of initially cracked and uncracked concrete beams and their appearance after the imposition of a shearing force across the shear plane. A summary of experimental

studies on shear transfer mechanisms in general, of which direct shear failure is a subset, is presented in Appendix C.

Information on behavioral mechanisms in direct shear under impulsive conditions is not available. The only available data on dynamic direct shear failures is provided in two past experimental studies, where dynamic load levels causing direct shear failure are compared to associated static load levels.

2.2 Behavior Under Static Loads

2.2.1 Initially Cracked Concrete

For direct shear along an initially cracked beam section where the crack inclination is almost vertical, the force transfer mechanisms are described by the model in Figure 2.2, which shows a small section along the beam axis containing the crack. The surfaces of cracks in concrete are usually rough. The cracks follow a generally irregular path, which is further disturbed as the cracks pass around the coarse aggregate inclusions in the concrete, as shown in Figure 2.2a. Application of a static shear force V , as shown in the model of Figure 2.2b, causes shear displacement or slipping and also causes the cracked surfaces to separate slightly. This separation induces tension in the reinforcement crossing the shear plane. This induced tension force in the reinforcement is balanced by an equal compression force in the concrete and acts normal to the crack plane as shown in Figures 2.2a and 2.2b. The normal compressive force produces a frictional resistance to sliding between the faces of the crack plane which serves to resist an applied shear force acting along this plane. The relative movement of the concrete crack faces causes a shear action to develop in the longitudinal reinforcing bars which cross the crack

plane. The resistance of the bars to the shearing action shown as dowel forces in Figure 2.2c, also serves to resist the applied shear force.

For normally reinforced (i.e., underreinforced) concrete beams, the separation of the crack faces along the shear plane eventually creates tensile strains sufficient to cause yielding in the longitudinal reinforcing steel or compressive strains sufficient to create crushing of the concrete. At ultimate strength the yield force in the steel is equal to the compressive force normal to the crack plane and the frictional resistance along the crack is proportional to this normal force.

As mentioned there is also a shear resistance along a defined crack plane due to the dowel action of reinforcement crossing the crack plane. Mattock and Hawkins '72 point out that after extensive slip along the crack plane the dowel reinforcement can actually kink at the crack plane, as shown in Figure 2.3, and provide extra resistance due to a component of the reinforcement force in the direction of slippage.

In the ACI adopted shear-friction theory, frictional resistance provided along a crack is a function only of the maximum normal force across the crack, which in turn is determined by the yield strength in the steel. Mattock and Hawkins '72 state that this observation is consistent with the shear-friction concepts since the coefficient of friction is also independent of concrete strength.

However, concrete strength can be an important parameter when combined with certain magnitudes of the reinforcement index, $\rho_s f_y$. For example, for low strength concrete actual crushing of the concrete will occur for small values of

$\rho_s f_y$, and for high strength concrete crushing will occur for large values of $\rho_s f_y$. This change in behavior caused by crushing of concrete can be seen in Figure 2.4 for a 2500 psi (pounds-per-square inch) concrete. For high values of induced compressive stress across the crack plane, which corresponds to high values of the parameter $\rho_s f_y$, the ultimate shear strength of initially cracked and initially uncracked specimens are the same, as seen in Figure 2.5. Mattock and Hawkins '72 explain this by stating: "In a heavily reinforced shear plane, or one subject to a substantial externally applied normal compressive stress, it is possible for the theoretical shear resistance due to friction and dowel effects to become greater than the shear which would cause failure in an initially uncracked specimen having the same physical characteristics. In such a case, the crack in the shear plane "locks up" and the behavior and ultimate strength then become the same as for an initially uncracked specimen."

2.2.2 Initially Uncracked Concrete

For initially uncracked concrete specimens which eventually fail in direct shear, short diagonal tension cracks develop along the shear plane (see Figure 2.6) and a truss-like mechanism develops. The ultimate shear strength is then developed as the inclined "miniature" concrete struts fail under a combination of compression and shear. Tests on corbels by Kriz and Raths '65 revealed that direct shear failures in reinforced concrete under static loads are realized in specimens for which the ratio of shear span to effective depth (M/Vd) is less than 0.2. In some of the reported tests shear failures occurred at higher M/Vd ratios but these were generally more likely when high percentages of reinforcement were used. The shear failures described by Kriz and Raths '65 were characterized by the development of a series of short inclined cracks along the plane of the interface

between the column and the corbel, as shown in Figure 2.7. A direct shear failure then occurred by an overall shearing along the plane weakened by these inclined cracks.

Mattock and Hawkins '72 have proposed hypotheses for the behavior of initially uncracked reinforced concrete specimens based on a statically indeterminate truss analogy. As load is applied initially the concrete is uncracked and the dowel steel is unstressed. A direct shear stress will occur along the shear plane in the concrete and eventually as the external shear force is increased, short inclined diagonal tension cracks will form along the length of the shear plane. The short cracks develop when the principal tensile stress in the concrete becomes equal to the tensile strength of the concrete.

As the shear load is increased, short parallel diagonal struts develop between the inclined cracks as shown in Figure 2.6. Since these struts are continuous with the concrete on either side of the shear plane, both a compression and transverse shear force will exist in each strut and the external shear will be resisted by the components of these forces which are in the direction of the shear plane. Furthermore, as these struts tend to compress and rotate, the consequent displacements normal and parallel to the shear plane will stress the transverse dowel steel until it eventually reaches its yield strength. This of course is based on the presumption that the concrete does not fail first in compression. A direct shear failure will finally occur when the small struts fail under their combined stress state as the dowel steel attains its yield strength.

Under a condition where no external load acts normal to the shear plane, the failure plane in initially uncracked reinforced concrete specimens can shift slightly from the shear plane to a plane parallel to the shear plane, as shown in Figure 2.6. This occurs when the ends of the small inclined cracks propagate in a direction parallel to the shear plane as the small struts rotate slightly. When these parallel cracks start to coalesce the shear stress in the struts increases locally based on a reduced shear plane area and failure occurs when the locally higher shear stresses reach a critical value.

For initially uncracked concrete, Mattock '74 found that no slip or separation occurred along the shear plane until the small diagonal cracks formed along the shear plane at shear stresses of 400 to 700 psi. Mattock '74 also found that at failure some of the small diagonal cracks coalesce to form major cracks parallel to the shear plane and the small inclined concrete struts spalled in compression. In this case no slip, in the true sense of the word, occurred. Rather, relative motion parallel and normal to the shear plane occurred as a result of the rotation and compression of the small inclined concrete struts as the reinforcement across the shear plane stretched in tension. Furthermore, the shear resistance after ultimate decreased more rapidly than in initially uncracked concrete as the "slip" increased. The curve shown in Figure 2.5 for uncracked concrete can be modeled quite well using the statically indeterminate truss analogy developed by Mattock and Hawkins '72.

2.3 Behavior Under Dynamic Loads

2.3.1 Response Definition

Only two studies on direct shear resistance of reinforced concrete specimens subjected to impulsive loads could be found. These studies were primarily concerned with general failure levels. In these studies the most cited parameter was the dynamic increase factor (DIF). This is the ratio between the load at which shear failure occurs due to a dynamically applied load divided by the statically applied load to failure. The major contrast between these two dynamic studies and the static studies described in Section 2.2 is that the latter were extensive and they illuminated the parameters of interest in the identification of shear transfer mechanisms. In the limited dynamic studies these detailed investigations were lacking and results focused mainly on the change in the DIF as a function of the change in loading conditions and the strength of the concrete and steel used in the reinforced concrete elements.

2.3.2 Shear Key Tests

Perhaps the first known controlled experiments on concrete elements subjected to dynamic shear were conducted by Hansen et al.'61. In these experiments a series of comparable static and dynamic tests on three types of concrete shear keys was completed. The objective of these tests was to determine the magnitude of ultimate shear strength of the concrete shear keys under dynamic conditions. Three types of keys were considered: type 1: Plain concrete, type 2: Plain concrete under directly imposed compressive stress normal to the shear plane, and type 3: Concrete reinforced by diagonally embedded dowels. For each of the three types two specimens were tested statically and four specimens were tested dynamically.

For dynamic loadings, rise time to peak load was 25 to 40 milliseconds and for the static loads the rise time was on the order of 10 to 15 minutes total load duration. The load in the case of the static test was continually increased in steps up to failure while in dynamic tests it was applied in several triangular pulses of constant duration but increasing in magnitude until a pulse corresponding to failure was reached. As the dynamic failure was always sudden, a few small magnitude load pulses were first applied before causing failure to obtain information about the stress strain characteristics and general behavior of the keys.

For these tests, the dynamic strength was greater than the static strength especially for type 2 and type 3 specimens. But the crack patterns and brittleness of failure appeared to be similar between static and dynamic cases. Type 2 specimens showed a striking increase in strength due to the existence of compression across the shear plane. Also, for type 2 specimens the tendency to direct shear type failures was more pronounced than in either the type 1 or type 3 categories. Specimens of type 3 also showed an increase in strength over those of type 1.

In studying the behavior of each specimen and comparing and grouping the results recorded, Hansen '61 saw an important feature common to all three types: a high strength of concrete in pure shear, particularly under dynamic loading. The DIF for the three specimen types averaged 1.15 for type 1, approximately 1.6 for type 2, and about 1.3 for type 3. It was also observed that the tendency for a diagonal tension failure, as opposed to direct shear type failure, was greatly reduced when compression across the shear plane was present. In fact, the presence of this compression was directly correlated with the enhancement of shear strength in a

direct shear sense. Compression across the shear plane on these key elements and doweling appeared to be very helpful in increasing the shear resistance as well as making failure less brittle.

It was observed that the quality and strength of the coarse aggregates rather than the compressive strength of the concrete governed the strength of keys in dynamic shear. Bond failure of the cementing gel (indicating stronger gravel) gave a higher strength than when shearing took place on weak gravel. The deflections of the brittle shear failures both in static and dynamic tests were comparatively small in magnitude, ranging from .003 to .018 inches.

2.3.3 Pushoff Element Tests

A second study conducted under dynamic loads was done by Chung '78. This experimental work investigated the shear resistance of concrete joints to dynamic, static, and cyclic loadings. The test specimens were concrete pushoff elements. There were 48 specimens, equally divided into two series. In series A the shear plane was not reinforced while in series B two 5 millimeter diameter mild steel stirrups were placed across the shear plane equivalent to 0.43 percent of the area of the shear plane. Secondary reinforcement was provided in each specimen to strengthen it against any unexpected bending.

Each of the series of specimens was divided into four groups for testing purposes. Specimens of the first group were tested under static loads and served as control specimens. Specimens of the second group were subjected to impact loading. Specimens in the third and fourth groups were first subjected to cyclic loading of low magnitude and then were tested to failure by impact loads. For the impact

loadings the rise time was on the order of 0.8 milliseconds (msec). Test results show that series B specimens could absorb some 40% more impulse than series A specimens. The difference was due to the provision of shear reinforcement in the former. The steel reinforcement provided a clamping force across the shear plane, and sustained the load for a longer period before failure, as was seen from the force-time curves. The results showed that the DIF for series A specimens averaged 1.8 while the average DIF for series B specimens was 1.9. These DIF figures show the strong enhancement in shear strength afforded by high load rates.

2.4 Summary

Under static loads direct shear failure in initially cracked reinforced concrete is characterized by slippage along the crack plane. Shear resistance is provided by a combination of friction on the crack faces and dowel action of the transverse reinforcing steel. This mechanism of shear resistance depends on the reinforcement ratio and the dowel steel strength, but shows little sensitivity to concrete strength for lightly reinforced elements. In direct shear failure in initially uncracked concrete under static loads, short inclined cracks form along the shear plane to produce a series of small diagonal struts. Subsequent slip and separation along the shear plane is caused by compression and rotation of these struts. Concrete strength is an important parameter in the behavior of initially uncracked concrete. The ultimate shear resistances of cracked and uncracked concrete are comparable under high normal stresses across the shear plane.

The dynamic tests have led to the following two conclusions. First, the dynamic shear strength of the shear plane is greater than the static shear strength. The dynamic strength increase may amount to 90% of the static shear strength at a

rate of stressing around 1750 ksi/sec (Kips-per-square inch/second). Second, a small amount of reinforcement across the shear plane is essential for improving the ductility of the specimen and for increasing its impulse capacity.

Chapter 3

Failure Criteria

3.1 Introduction

The determination of how and when a reinforced concrete element is predicted to fail under a given set of loading and support conditions is dependent on the failure criteria. In formulating failure criteria for concrete under the state of stress which exists in a beam, it is necessary to properly define the term failure. Concepts such as material yielding, initiation of cracking, load carrying capacity, and the extent of deformation have been used in the past to define failure. In this dissertation failure will be defined to occur when a concrete element reaches its ultimate load carrying capacity. Whether this capacity is reached in terms of a shearing mechanism or a flexure mechanism is dependent on the state of stress in the beam and which of the mechanisms is realized first in the beam response history.

Chen '82 indicates that concrete failures can be classified as being either tensile or compressive. With respect to the definition of failure given in the previous paragraph, tensile failure is defined by the formation of major cracks and the loss of tensile strength normal to the crack faces and compressive failure is described by the development of many small cracks and the loss of strength. However, most concrete elements rarely undergo a uniaxial state of stress even though the most commonly used strength parameters are based on uniaxial test properties.

Chen '82 summarizes several state-of-the-art failure models for concrete under a general stress state, but the most common and perhaps simplest failure model used

is the Mohr-Coulomb criterion combined with a tension cut off value. This criterion is very similar to the shear friction concepts described earlier in that they both are functions of the internal angle of friction of concrete, they both are dependent on the normal force across a potential crack plane and they both base failure on an ultimate shear capacity along a crack plane. Except for the provision of concrete cohesion (inherent shear stress under a zero normal stress condition) in the Mohr-Coulomb criteria the two are equivalent.

An important question in this dissertation, as outlined in Chapter 1, is whether a flexure failure or a direct shear failure occurs first in a beam under rapid load conditions. Obviously both flexural and shear stresses exist in the beam and in a rigorous failure criterion their interaction would be accounted for. However, Park and Paulay '75 have indicated that experiments with normally reinforced concrete beams with adequate shear reinforcement show that the shear force has no recognizable influence on the development of flexural capacity. But a close relationship does exist among flexure, shear, bond, and anchorage in the shear span of a beam. For example, when large shear forces are transmitted at a section at the ultimate moment capacity, the distribution of the flexural strains in the concrete and steel are affected. In this case the capacity of the flexural compression zone is reduced because the shear force can only be carried in this zone after widening of cracks in the tension zone. Looking at the converse situation, where moments are present at sections under ultimate shear, Mattock '74 has found that the action of a moment less than the flexural ultimate strength of a cracked section does not reduce the shear which can be transferred across the crack plane.

Experiments on beams have shown that: 1) shear forces do not influence the development of flexural capacity and 2) flexure forces do not influence the shear capacity. Because of this it should be possible to formulate separate failure criteria for flexure and for shear.

3.2 Rate Effects on Material Properties

It is well known that rate effects increase the strength and initial stiffness of construction materials. For example, Figure 3.1 (from Davies '81) shows a comparison of the ratio of dynamic strength to static strength versus strain rate for three common materials — concrete, steel, and aluminum. These curves are, of course, valid only for a particular grade of steel or aluminum or a particular 28 day strength for concrete. The respective curves for the three materials vary according to the initial strength. In general, the higher the initial strength the lower is the strength enhancement for a given strain rate (see Crum '59 and Cowell '65 for reinforcing steel strength enhancement). Even for a given initial strength, the data shows a random scatter of dynamic strengths for a given load rate.

The available data on rate effects on steel and concrete (see bibliographies in Bresler '74 and Bazant & Byung '82) indicates that the increase in yield strength of high-grade steel and the increase in compressive strength of concrete are comparable in the range of strain rates between 0.1/sec and 10/sec.

Figure 3.1 shows that the increase in dynamic steel strength can be higher than that for concrete strength for some strain rates. However, the "steel curve" in Figure 3.1 is for mild steel and the corresponding curve for a high-grade steel is lower and is actually comparable to the "concrete curve" in Figure 3.1 for strain

rates in the range of 0.1/sec to 10/sec. For this reason it is assumed in this dissertation that rate influences are the same on the strength properties of both concrete and steel.

Data such as that presented by Watstein and Boresi '52 and shown in Figures 3.2 and 3.3 can be used to develop empirical relationships between strength and strain rate for concrete specimens. However, Bazant and Byung '82 have done this for an extensive data base containing information from many past studies. The empirical formulas for strain rate effects on elastic and strength properties have severe limitations. The data presented by Watstein and Boresi '52 is for an "average" strain rate for each test. Since the response of an elastic element to a time-varying load produces a strain-rate which varies with time, the data can only be used in the expected value, or mean, sense. The empirical relationships developed by Bazant and Byung '82, also derived from constant strain-rate test results, are inapplicable when the order of magnitude of strain rate greatly differs from time-step to time-step in a dynamic analysis. This latter problem is usually of little consequence when the structure is constantly in motion. Furthermore, Bazant's procedure is only used to determine strain rate effect on the initial tangent modulus rather than the incremental change in modulus through the loading history.

The rate effect problem can be simplified considerably by allowing elastic and strength properties to be functions of the "average" strain rate or average stress rate (or load rate) for a particular dynamics problem. This is justified further by the fact that the large majority of strain rate test results are gathered from constant or average rate tests.

If strain rate effects on elastic properties are modeled, the governing equations of motion become nonlinear. This is because in the constitutive model there will be a product between the dependent variables. That is, there will be a function of strain rate times a differential operator on strain. Solutions of equations of this type are solved numerically and certain numerical errors and instabilities can arise as mentioned by Bazant and Byung '82. Furthermore, the numerical solution procedures are implicit and require updated elastic coefficients at each time-step which violates the original intent of developing a simple model. Despite these problems, solutions can be obtained but there is an easier procedure with the use of stress rate.

Stress rate effects on uniaxial concrete elastic and strength properties are also available from tests conducted by Watstein and Borezi '52. But stress rate also involves nonlinear equations since it is proportional to strain rate. This difficulty can be overcome by assuming that load rate is an approximation to stress rate. It is important to keep in mind that load rate is not the same as the stress rate of the material. The former is associated only with the external rate of increase of loading whereas the latter involves the internal rate of response. The rate of response is the phenomenon affecting the material but little data exists on this rate. Therefore, the load rate is taken here as an approximation of the true response rate of the material.

Use of load rate is inherently more tractable since the change in elastic coefficients in the equation of motion is explicit, i.e., it depends on the characteristics of the external load and not internal response. Obviously, in the real world material changes result from internal rates of straining, but from a

mathematical point of view load rate effects are available from tests and are much more convenient to work with since the equations of motion still remain linear.

3.2.1 Strength Properties

Under the assumption that load rate and stress rate are equivalent (generally load rate is only an upper bound to stress rate for impulsive loading) it is possible to determine the enhancement in strength properties as a function of load rate. The lower portion of Figure 3.3 shows normalized concrete strength as a function of stress rate. Letting the load rate be the same as stress rate, the enhancement of concrete strength, denoted as Ω , due to load rate effects can be found from the lower portion of Figure 3.3.

A correlation between average load rate and average strain rate can be found by comparing the data shown in Figures 3.2 and 3.3. The strength enhancement factor, Ω , can be used to estimate the increase in capacity of a beam under dynamic conditions.

It is interesting to compare the strength enhancement factors shown in Figures 3.2 and 3.3 to the dynamic increase factors (DIF) for concrete strength in a shearing mode given in Section 2.3. This comparison reveals the possibility that concrete strength enhancement might be higher in a direct shear mode than in a uniaxial compressive mode.

3.2.2 Elastic Properties

Again under the assumption that load rate is equivalent to stress rate, the enhancement of the concrete elastic modulus can be determined from test data.

The upper portion of Figure 3.3 shows normalized concrete elastic modulus as a function of the stress rate (hereafter referred to as load rate). The concrete elastic modulus enhancement factor, denoted as Ψ , is the ordinate of the plot shown in the upper portion of Figure 3.3.

A correlation between average strain rate and average load rate for the elastic modulus enhancement factor also can be determined by comparing the curves in the upper portions of Figures 3.2 and 3.3. The elastic modulus enhancement factor, Ψ , can be used to approximate initial elastic properties of a beam experiencing dynamic response.

3.3 Flexure Failure Criteria

Failure in a flexural mode is defined here when a beam reaches its ultimate moment capacity. Generally for fixed beams this capacity will occur at a support. The most common expression for ultimate moment capacity, without a capacity reduction factor, for a singly reinforced beam is given as

$$M_u = f'_c w b d^2(1-0.59w) \quad (3-1)$$

where

f'_c = uniaxial compressive strength of concrete (28-day cylinder strength)

w = reinforcement index = $A'_s f_y / b d f'_c$

b = width of the beam

d = effective depth of the beam

A'_s = area of steel on the tension side

f_y = yield strength of the steel

This equation is valid as long as the steel in the cross-section is less than the steel at a balanced design. For all the beams in this dissertation this condition is never violated. Since the beams in this dissertation are actually doubly reinforced it may be more appropriate to use the ultimate strength formula pertaining to a condition where compression steel is present. In this case, however, the ultimate moment computed using either approach is very nearly the same because the actual percentage reinforcement is much less than the percentage associated with a balanced condition. Physically this means that the centroid of the compression steel is close to the neutral axis of the beam so that the increase in ultimate moment due to the compression steel is small.

Assuming the rate influence on concrete and steel to be the same, Equation (3-1) is augmented by a factor which is dependent on the load rate influence on concrete and steel strength. Equation (3-1) becomes,

$$M_{ur} = \Omega M_u \quad (3-2)$$

where M_{ur} = ultimate moment with rate effects
 Ω = strength enhancement factor

3.4 Direct Shear Failure Criteria

Over the last 15-20 years considerable experimental testing and analysis has been accomplished in the area of direct shear failures under static loads. Most of the test specimens have involved small shear-span to depth ratios (M/Vd) in an attempt to study near-vertical crack planes, or they have been push-off elements in which a shear plane is predefined. Before selecting the direct shear failure criterion to be

used in this dissertation, a review is provided of a few of the past failure criteria in direct shear.

For conditions of very low (M/Vd) ratios (i.e., less than 0.2), Somerville '74 argued that, since the dominant structural action will be direct shear, some merit should be given to a "shear friction plus cohesion" approach. This is a modification of the shear friction theory outlined by Mast '68 and later adopted by the ACI, in which cohesion in concrete is considered and the reinforcement plays a reduced role. In the shear friction theory the reinforcement acts as a tension member rather than as a dowel and the friction angle is independent of concrete strength or stress level. The Somerville approach is shown in Figure 3.4, where C is the apparent cohesive strength of the concrete and $\tan \phi$ is taken to lie in the range 0.75-1.00 to match data for very low and very high percentages of steel. This approach has been considered by the European Committee for Concrete and test data from Hermansen '72 exists to support the theory for low (M/Vd) ratios.

Mattock '74 points out that the "shear friction" hypothesis leads to conservative (low) estimates of shear transfer strength because it neglects effects such as dowel action and the shearing off of asperities on the crack faces. An artificially high coefficient of friction (1.4 for monolithic concrete) is used to compensate for the neglect of these other effects. Mattock '74 further states that the shear friction theory does not adequately reflect the mechanism of shear transfer for initially uncracked concrete, but this difference has been discussed in this dissertation in Chapter 2.

In another study Mattock '74 addressed the influence of moment across the shear plane. He found that the action of a moment less than the flexural ultimate strength of a cracked section does not reduce the shear which can be transferred across the crack. To arrive at this conclusion Mattock compared the measured ultimate shear strength to the calculated shear strength based on two methods of calculation -- shear friction theory for a shear failure and the ultimate moment capacity (divided by the eccentricity of loading) for a flexural failure. Mattock determined that if the calculated strength was the lesser of the two methods, then in all cases the actual strength exceeded the calculated strength. Furthermore, he determined that the ultimate shear strength across a crack in monolithic concrete can occur simultaneously with the ultimate flexural strength.

Hawkins '81 proposed a direct shear resistance function which relates shear resistance to shear-slip along a crack plane whether or not an actual crack exists. In addition to describing shear stiffness and ultimate shear, his resistance function provides an estimate of the shear ductility up to a collapse in shear. The Hawkins criterion in the initial elastic stage of response is based on tests conducted at the University of Washington and the Delft Technical University where specimens were studied for their initial shear stiffness and their ultimate shear capacity.

Inasmuch as the experimental data to be used in this dissertation (outlined in Chapter 4) involves structures which presumably did not have a precracked shear plane, use will be made of the Hawkin's criterion which, because of its origins, is valid for specimens both with and without a precracked shear plane. Mattock '74 actually points out that, for high values of $\rho_s f_y$ (the roof slabs in Chapter 4 have $\rho_s f_y$ values up to 1,500 psi), the difference in ultimate capacity for initially

cracked and initially uncracked specimens is negligible. The Hawkin's criterion can be shown to be very similar to the concept of "shear friction plus cohesion" postulated by Somerville '74.

As shown in Figure 3.5, the envelope of failure produced by a Mohr-Coulomb criterion is a description of shear friction with cohesion, given by the equation

$$v_{\max} = C + \rho_{\frac{2}{3}} f_y \tan \tilde{\phi} \quad (3-3)$$

where v_{\max} = maximum shear stress

C = cohesion

$\tilde{\phi}$ = internal angle of friction

From geometry it can be shown that the cohesion can be given in terms of the concrete uniaxial tensile strength, f'_t , as

$$C = \frac{f'_t}{2} \frac{1 + \sin \tilde{\phi}}{\cos \tilde{\phi}} \quad (3-4)$$

The uniaxial tensile strength of concrete is usually expressed in terms of its uniaxial compressive strength, f'_c , since the latter is used extensively in design and testing. Quite often the split cylinder strength of concrete is used to approximate the tensile strength. Chen '82 estimates this value as

$$f'_t = 7.5 \sqrt{f'_c} \quad (\text{psi}) \quad (3-5)$$

Equation (3-3) then becomes

$$v_{\max} = 3.75 \sqrt{f'_c} \frac{1 + \sin \tilde{\phi}}{\cos \tilde{\phi}} + \rho_s f_y \tan \tilde{\phi} \quad (\text{psi}) \quad (3-6)$$

and $V_u = v_{\max} bh$

where V_u = ultimate shear capacity

ρ_s = total percentage of steel crossing the shear plane = A_s/bh

h = beam thickness (depth)

b = beam width

The Hawkins '81 criterion is developed from tests and is given by

$$V_u = \left\{ 8 \sqrt{f'_c} + 0.8 \rho_s f_y \right\} bh \leq 0.35 f'_c bh \quad (\text{psi}) \quad (3-7)$$

The Hawkins criterion agrees very closely with Equations (3-6). The upper limit on shear stress of the Hawkins criterion ($0.35 f'_c$) is higher than the upper bound for shear friction given by ACI 318-77 ($0.2 f'_c$ or 800 psi) but the lower figure is for design and is conservative and doesn't reflect the actual strengths. In fact the Hawkins limit of $0.35 f'_c$ appears conservative when compared to the upper limit established by the U.S. Air Force AFSC '73. The Air Force limit of $0.51 f'_c$ however, was achieved by applying a compressive stress normal to the crack plane during the slip process.

Again for rapid loadings, and in the absence of data to provide a dynamic failure criterion, Equation (3-7) is adjusted by a function to account for strength enhancement due to load rate effects. For a dynamic direct shear failure criteria, Equation (3-7) becomes

$$V_{ur} = \Omega V_u \quad (3-8)$$

where V_{ur} = ultimate shear with rate effects

Ω = strength enhancement function

3.5 Summary

The failure criteria are an integral element in any study which seeks to determine the resistance levels at which a structural element can no longer sustain increased loading. Failure criteria are dependent on the mechanism of failure and as such, can depend on geometry as well as material strength properties. In the absence of detailed experimental studies on direct shear failures under impulsive loads, the dynamic criteria is taken as the static criteria multiplied by a factor which is greater than or equal to one and which accounts for an increase in resistance due to load rate.

Experimental data on rate effects for both reinforcing steel and concrete show random variation and variation with initial strength properties. Based on the large scatter of data and some central tendencies, the enhancement of both concrete and steel is assumed to be the same for strain rates above 0.1/sec. This assumption is for exploratory purposes and can be refined further in future efforts. The

enhancement in steel is seen to have more effect on the moment criteria than the direct shear criteria under this assumption.

The interaction of shear and moment is complex even under static conditions. Experimental data on reinforced concrete elements shows that ultimate direct shear capacities are not influenced by the presence of moment up to the ultimate flexural capacity of the element. The interaction of shear and moment under impulsive loads is presumed to behave the same as under static conditions.

Comparison of the strength enhancement factor Ω for dynamic uniaxial compressive tests on concrete elements, shown in Figures 3.2 and 3.3, and the DIF for concrete pushoff elements subjected to dynamic shear (described in Section 2.3) shows that the latter is usually higher. This may indicate that concrete is stronger in a shearing mode under dynamic loads than is normally revealed under standard dynamic uniaxial test conditions.

Chapter 4

Experimental Data Base

4.1 Introduction

The data used for comparison purposes in this dissertation comes from a series of eleven tests during the period 1981-1982 and one test in 1979 on reinforced concrete boxes conducted by the U.S. Corps of Engineers, Waterways Experiment Station (WES). Kiger and Slawson '82 and Kiger and Getchell '79 have documented the available data on these tests. These tests comprise a good sample for comparison because they were all fabricated and tested in a similar manner. The eleven tests during the period 1981-1982 were accomplished for the expressed purpose of studying direct shear failures in reinforced concrete elements. The twelfth test is provided here as an illustration of a case where a flexural failure dominated the response. Of interest in these tests was the response of the roof element of the box-like structure near the walls, i.e., at the roof-wall interface.

The twelve tests all had known design physical characteristics and all responded in a different fashion. Some roof elements failed in direct shear and collapsed, some failed in direct shear and did not collapse, and one did not fail in direct shear. Since the only variations in the tests were the load on and the strength of the roof element, it is possible to correlate load conditions with strength characteristics in analyzing the data.

4.2 Test Description

The test specimens are grouped into three categories, defined as Groups I, II, and III in Table 4.1. The test configuration for the tests is shown in Figure 4.1. As

shown in the figure the reinforced concrete elements were covered with a very shallow layer of soil and subjected to a high-intensity blast pressure which was uniform across the span of the test structure.

4.2.1 Test Configuration

Test specimens within each group had the same overall dimensions, fabrication scheme, soil cover, design concrete strength, and design steel strength. The major variations among the groups of tests were the span-to-thickness ratio and the reinforcement ratio. Figures 4.2 and 4.3 show cross-sectional details for the three test groups and Table 4.2 displays the physical parameters for each group.

Each test structure was loaded with a high-explosive induced blast pressure and, although some structures were subjected to the same design loading, the characteristics of the loading varied among the tests. These characteristics include the peak pressure along the span, the rise time to peak and the decay characteristics of the pressure pulse.

4.2.2 Instrumentation

Figure 4.4 shows a typical instrumentation diagram of the WES tests. Active interface pressure gages measure the pressure transferred from the soil layer above the roof to the roof slab itself. This interface pressure phenomenon and resulting interaction are described in Chapter 1 and Appendix A. This interface pressure is the actual loading to which the roof element responds. Once this pressure is specified the effects of the soil layer can be ignored because the interaction between soil and structure has been taken into account.

Active steel strain gages on the longitudinal steel were used in all tests to measure the response of the structure. In addition, in Group II and III tests high-speed photography was used to record the response of the underside of the roof. This photography shows the response of the roof after failure in direct shear, where the roof slab moves away from the supports as a rigid-body. Finally, in Group II and III tests passive scratch gages on the steel reinforcing is available to estimate the maximum strains exhibited in the steel in the roof.

A correlation of the active steel strain data and the interface pressure data reveals the type of failure mode (direct shear, flexure, etc.) and the approximate time of failure. For direct shear, the failure level is defined as the peak pressure along the span which existed prior to the initial "slip" of the roof slab along a shear plane.

4.3 Data Analysis

Figures 4.5 through 4.11 show post-test photographs of those test structures believed to have failed in direct shear at the roof-to-wall interface and seen to have subsequently collapsed. In all these cases the failure plane is vertical or near vertical and the roof is completely severed from the walls. Figures 4.12 through 4.15 show post-test photographs of those structures which did not collapse, but still are believed to have failed in direct shear. The twelfth specimen, designated FH1 and reported by Kiger and Getchell '79, did not fail in direct shear. Figure 4.16 shows a schematic of the post test condition of FH1. The roof slab in this test responded in flexure and did experience some structural damage as shown. These presumptions of failure type are determined from the interface pressure readings which will be described next.

4.3.1 Interface Pressure

Typically the interface pressure measurements are available at three locations along the roof span. Figure 4.4 show these locations. The readings at the location over a wall give an idea of the pressure time distribution over a point that moves very little, i.e., a nearly rigid boundary. This case can be thought of as a limiting condition for a rigid slab (see discussion in Appendix A). Another pressure measurement point is at the centerline of the slab. These readings truly reveal the interaction effect caused by a flexible slab, i.e., the slab centerline initially undergoes the most movement along the slab. Finally, the third reading is on the slab just interior to a supporting wall. This reading is important because it reveals the nature of the response of the slab. If this measurement closely resembles the measurement over a wall it shows that the response is likely to be flexure or flexure-shear. If on the other hand this near-support measurement closely resembles the readings at the slab centerline it is likely that a slip along a crack-plane has occurred near the support. This is because the only way the interface pressure near the support can decay as quickly as the pressure at the centerline decays (which is much faster than the pressure decay over a wall) is for the slab near the support to move away from the overlying soil as quickly as the centerline moves away from the soil. This indicates a "slip" condition (see Section 2.1) and very clearly reveals a direct shear failure.

The schematic in Figure 4.17a shows a condition where a direct shear failure is not indicated. Initially all three pressure readings rise to the same approximate peak value with the same rise time. This is the interface pressure discussed in Chapter 1 and Appendix A. Beyond the peak pressure the three measurements begin to differ. At the span center the pressure begins to drop quickly as the roof

begins to move downward away from the soil. At the measurement over the wall the decay characteristics after peak pressure are much slower than at the center, indicating that the load over the wall stays at a relatively higher level, reflecting the near-rigid condition over the wall. And the readings over the span near the support show a decay after peak pressure that is slower than at the span center, indicating that this point is also undergoing very little movement away from the soil. Then the displacement profile along the span probably looks something like a fixed-ended beam responding in the first flexural mode. A specific example of a flexural response is seen in the interface pressure readings of the FH1 structure, shown in Figure 4.18.

On the other hand, Figure 4.17b shows a condition of a probable direct shear failure with subsequent collapse. Again, all three pressure readings rise to the same approximate peak in about the same length of time. The pressure readings at the span center and over the structure wall are about the same as in the previously discussed case. However, the pressure reading over the span near the support shows a marked difference from the previous case. Here, after peak pressure is attained, the pressure decays very rapidly as does the pressure reading at the span center. This sudden drop in pressure indicates the roof at this location is moving away from the soil much more quickly than the whole structure is moving down as a rigid-body (this rigid-body motion can be correlated to the vertical pressure over the wall). Interface pressure readings for test structure DS1-1, shown in Figure 4.19, reveal an initial direct shear failure.

Evidence of the subsequent collapse of the roof element shown schematically in Figure 4.17b is also provided in the interface pressure readings. After the pressure

has decayed to zero, or near zero, there is a small interval of time in which the load stays at this low level and then the pressure suddenly jumps up slightly. This effect is termed "reloading" and it corresponds to the case where the soil overburden, having been previously separated from the roof span, moves downward until it "catches up" with the roof slab and recontacts or reloads this surface. Because the shear resistance impedes the downward slip, the momentum of the slab is reduced and the velocity of the slab becomes lower than the velocity of the soil and eventual recontact is established. In cases where the slab actually collapsed, there was sufficient impulse in the interface pressure after "reload" not only to overcome the aggregate interlock and dowel action but to break the longitudinal steel in a membrane-type mechanism of the slab.

Figure 4.17c shows a condition where the initial failure was probably in direct shear but there was no subsequent collapse. In this case the pressure readings at all three locations along the roof span are similar to those in the previous case of a catastrophic direct-shear failure (collapse). However, after recontact was established there was apparently insufficient impulse left in the load pulse to overcome the combined mechanisms alluded to in the previous paragraph. This is evidenced by the reload magnitude to remain at a significant level. These features can be seen in the interface pressure measurements of test structure DS1-3, shown in Figure 4.20. For the purposes of this dissertation the two response conditions shown in Figure 4.17b and Figure 4.17c can both be designated as initial or incipient direct shear failures.

Table 4.3 summarizes the average peak interface pressure and approximate rise time experienced in all twelve test specimens. These peak pressures are those

which existed on the roof slab prior to failure in a particular mode. These test results will be used later in Chapter 5 as a comparison to elastic beam analyses.

4.3.2 Active Steel Strain

The interface pressure data outlined above provide an indication of the time to failure and the external load level at failure. The loading data do not reveal, however, the internal state of stress creating the failure mechanism. For a direct-shear failure mechanism it is necessary to determine if shearing stresses dominate over bending stresses in the early time prior to failure. Active strain measurements in the longitudinal steel can provide the necessary information regarding whether a shearing action or flexure action is occurring. Unfortunately, the strain records for very early times associated with a slip phenomenon are subject to high data recording noise and the response in this region is indiscernable. However, strains beyond an initial shear failure do provide information on whether a flexure or a membrane mode of response is indicated.

For a fixed-end beam undergoing downward motion of the first flexural mode, the bending moment at the support will create a stress condition where axial strains near the top fibers of the beam will be in tension and the axial strains near the bottom fibers will be in compression. At the center of the beam (again assuming the beam to be moving downward in the first mode, i.e., the first quarter cycle of response) the stress-strain condition will be reversed. That is, there will be compressive strains near the top of the beam and tensile strains near the bottom.

For a beam responding in a membrane mode, after a direct shear failure creates a shear zone at the support, the axial strains at both the top and bottom fibers in the

beam will be in tension. This arises from the fact that in a membrane mode beam fibers are in simple tension. Figure 4.19 shows active longitudinal steel strain measurements in the roof element of test structure DS1-1. On the strain diagrams positive strain values denote tension and negative values are compression. The strains in Figure 4.19 show predominant tension for both bottom and top steel at the right support beyond 2.5 milliseconds. All the measurements exhibit an oscillatory character, especially at early times (i.e., less than 1 msec), because the higher modes of vibration may have contributed to the response and because of signal noise. This specific test structure failed initially in direct shear and subsequently collapsed.

Figure 4.18 shows active strain measurements for test structure FH1. Here, the strains at the center are primarily compression on the top and tension on the bottom indicating a predominant flexural response. This test structure did not fail in direct shear, but apparently developed flexural hinges.

After a slab fails in direct shear, as discussed earlier, there is a time interval where the load is reduced to near zero. At this stage the slab still has momentum and the steel reinforcing enters a membrane mode where both top and bottom bars are being stretched in tension. This resistance to steel stretching and the frictional resistance provided along the shear zone slows the slab down and allows the soil to "reload" the slab. Now with more load on the slab and a plastic shear hinge formed at the shear zone the steel strains increase at a much faster rate. The steel strains increase until either the impulse on the slab disappears or the reinforcing bars break and the slab collapses. An example of this later-time

(beyond 1 msec) phenomenon, where the slab does not collapse, can be seen in the tension strain readings at the support of test structure DS1-3 in Figure 4.20.

4.3.3 Post Failure Measurements

Measurements of the roof slab response after an initial direct shear failure can be found in permanent steel strains from passive scratch gages and in high-speed photography of the underside of the roof slab. The permanent steel strain data gives an indication of the magnitude of the large inelastic strains reached before collapse and the distribution of these strains along the span. Figures 4.21a and 4.22a show sample data of this type for test specimens DS2-1 and DS2-5, respectively. The high speed photographic data provides an indication of the times associated with very large deformations beyond failure and a visual description of the post failure modes of response. Figures 4.21b and 4.22b show the slab displacement profiles versus time for test specimens DS2-1 and DS2-5, respectively.

Generally, the data shows that after direct shear failure the slab behaves according to a mix of three different response modes. First there is a shear deformation mode at the slab ends which provides for a near-rigid body response over the slab. Second, the slab behaves in a membrane mode in which the steel in the shear zones near the supports is being pulled in tension. And third, the slab behaves in a flexural mode because of residual bending strength, with the response similar to that of a simply supported beam.

All three of these modes occur together to various degrees in the post failure regimes of slab response. The data in Figures 4.21 and 4.22 clearly reveal these different modes and their occurrence in the response history.

4.4 Summary

Data from twelve high explosive pressure tests on reinforced concrete one-way roof slabs are presented. Slab surface loading versus time is provided by interface pressure readings, and slab response is documented by active and passive steel strain measurements and high-speed photography. Indications of early time (less than 1 msec) direct shear failure are provided by interface pressure measurements. Response after incipient shear failure can be seen in strain measurements and high-speed photographic documentation. Test evidence indicates that eleven slabs failed initially in direct shear and one slab failed in flexure.

Chapter 5

Elastic Beam Theory

5.1 Introduction

In this dissertation, the primary objective of the analysis of direct shear failures in beams and one-way slabs under distributed impulsive loads is to determine how the load and resistance parameters influence the failure modes discussed in Chapter 3. Because the experimental data does not discern the very early time relationship between shear and flexure, a model capable of assessing both these actions is needed. In order to make the analysis mathematically tractable an elastic one-dimensional theory is desired. In this study the well known Timoshenko beam is used as the analytic model. The major assumptions involved in the use of this model have been summarized in Section 1.3.

The most important assumption involves the use of an elastic theory to describe beam response prior to failure. Generally, concrete is presumed to be elastic until cracking takes place, after which it is assumed to be beyond the elastic stage. However, this dissertation assumes that elastic beam theory can adequately represent beam behavior to the point of an incipient shear failure. This assumption can be justified by the following reasoning. First, experimental results show direct shear failures tend to be brittle, indicating elastic response prior to extensive cracking. Second, response times to failure are so short (less than 1 msec) that excessive deformations associated with inelastic behavior are never realized. Furthermore, the elastic studies described in this dissertation can be used as a point of departure for future efforts which may study inelastic failure mechanisms.

Two extensions to the current Timoshenko theory are addressed in this study. First, the influence of a variable beam-end rotational stiffness (beam-end restraint) on direct shear failure is investigated. And second, the elastic theory is expanded to include viscoelastic material properties in order to investigate strain rate effects on direct shear failure.

Failure curves showing the effects of load parameters on the direct shear failure domain for specific beam geometries are developed using the elastic Timoshenko theory. These curves identify the range of load parameters within which an incipient direct shear failure is indicated by analysis. The expression "incipient direct shear failure" refers to the maximum support shear force that a beam member can sustain in a direct shear failure mode. The failure curves will show the effects of load rate on the direct shear failure domain.

Load parameters obtained from experiments are compared to analytic results with the use of failure curves developed for the rates of loading seen in the tests. This comparison reveals the adequacy of the elastic beam models and serves to highlight areas requiring further work.

Finally, a simple shear beam is introduced as a substitute for the Timoshenko beam for purposes of predicting shearing forces. The two different theories (shear beam and Timoshenko beam) are compared to determine the special conditions of the loading, beam-end restraints, and strain rates under which they provide comparable support shear forces.

5.2 Timoshenko Beam

The classical one-dimensional Bernoulli-Euler theory for flexural vibrations of elastic beams becomes an inadequate model when higher modes need to be considered. Lamb '17 first recognized that this theory was not suitable for transverse impulsive-type loadings because the propagation velocity of the disturbance approaches infinity as its wave-length approaches zero. Both rotary inertia and shearing deformations become increasingly important in the higher modes. Rayleigh, in 1877, extended the theory to account for the effect of rotary inertia and Timoshenko '21 augmented the equations to include the effect of transverse-shear deformation. (The contributions of rotary inertia and transverse-shear deformations usually attributed to Lord Rayleigh and Stephen Timoshenko, respectively, were originally outlined by M. Breese, 1859.) Both of these corrections depend on the cross-sectional properties of the beam. Timoshenko also showed that a finite propagation velocity along the beam was predicted regardless of the size of the wave length.

In analyzing the conditions when shear exceeds bending moment in a beam model, the analysis to follow on the Timoshenko beam is divided into three major sections. The first section discusses an elastic Timoshenko beam under the action of a rapidly applied triangular load using the normal mode method. Throughout this dissertation the interface pressure versus time profiles are approximated as shown in Figure 5.1. The second section discusses the analysis of a Timoshenko beam, augmented to account for strain rate effects, using Laplace transform techniques. In this case the elastic properties of the beam are augmented by viscoelastic properties in an attempt to model rate effects. The third section develops the

concept of a failure curve which describes the domain of load parameters within which a direct shear failure is indicated by analysis.

5.2.1 Normal Mode Method

Solution of the Timoshenko equations for a variety of loading and initial conditions has been accomplished by several investigators. Colton '73 summarizes many of these solution methods. Analysis of the Timoshenko beam under forced motions was accomplished by Herrmann '55 who developed a general solution for time dependent boundary conditions using the property of orthogonality of the principal (normal) modes of free vibration. Huang '61 also provided the normal modes and natural frequencies of free vibration for six different beam-end conditions. Bleich and Shaw '60 discussed the early stage dominance of shear stresses in a Timoshenko beam excited by an initial velocity distribution. This dissertation extends the analysis of a Timoshenko beam under forced motions for an elastic support boundary condition (Figure 5.1).

The governing equations for the elastic Timoshenko beam are limited in terms of the response details which they can predict. This limitation arises because not all generalized deformations are permitted in the beam theory. These limitations can be highlighted by comparing beam theory to the exact three-dimensional theory of elasticity. This comparison can then be used as a guide in interpreting results based on the approximate beam theory.

In the exact three-dimensional elastic theory displacements at all points through the beam thickness and all along the beam length are considered. This results in an infinite number of wave propagation modes and an infinite number of

deformational and stress states. In contrast to this is the approximation made in beam theory where the displacement distribution through the thickness is assumed constant and only a finite number of wave types are predicted. For example, the Bernoulli-Euler theory predicts one wave type, that being flexural waves. The Timoshenko theory predicts two wave types — a flexure-shear type and a thickness-shear type. For each given type of wave an infinite number of modes exist for a continuum.

An indicator of the applicability of the approximate beam theories is obtained by comparing their wave dispersion relationships against similar quantities from the exact theory. Fung '65 and Crandall '68 discuss and analyze the dispersion relationships of beam theories and compare them to the exact theory. The so called dispersion equation can be derived by substituting a sinusoidal wave solution (a sinusoid is an exact solution only for an infinite beam but studies show it to produce adequate results for short beams) into the governing homogeneous differential equations of motion. The dispersion equation relates wave frequencies and velocities to physical parameters of the beam. Relationships like those shown in Figure 5.2 can also be derived between wave velocities and wave lengths. A discussion of Figure 5.2 (obtained from Fung '65) is instructive.

Figure 5.2 compares elastic waves for a uniform beam of circular cross-section for three different theories. These results are very similar to those of beams with other simple cross sections. As seen the elementary theory of Bernoulli-Euler is valid only for very large wavelengths. In the curves for the Timoshenko theory the lower curve corresponds to the flexure-shear waves and the upper curve corresponds to the thickness-shear waves. As seen, the Timoshenko theory agrees

very well with the exact theory for the flexure-shear waves, but the agreement for the thickness-shear waves becomes worse as the wavelength λ gets smaller than the thickness of the beam. This conclusion was also reached by Colton '73. As the wavelength approaches zero (i.e., very high frequencies) the velocity of the flexure-shear waves approaches the shear wave speed and the velocity of thickness-shear waves approaches the speed of longitudinal waves in a uniform bar. At the other extreme, as the wavelength approaches infinity, the flexure-shear wave velocity approaches zero and the thickness-shear wave velocity approaches infinity. These limiting conditions have physical interpretations which are shown in Figure 5.3.

Since the wavelength, wavespeed, and wave frequency all are related it is possible to find the frequency above which the Timoshenko theory no longer agrees closely with the exact theory. Figure 5.4 shows a plot of the frequency versus wavelength relationship for the two types of wave propagation. As mentioned earlier for wavelengths greater than approximately the thickness of the beam discrepancies develop between the Timoshenko and exact theories. Using the frequency relationship $\omega = 2\pi c/\lambda$ and the wave velocity of the exact theory at a wavelength equal to the beam thickness, as shown in Figure 5.2, the frequency corresponding to that wavelength is roughly $\omega = 2\pi c_0/\lambda$ where c_0 is the longitudinal wave speed. Again referring to Figure 5.4, the frequency corresponding to an infinite wavelength and the thickness-shear waves is called the first thickness-shear frequency.

The following Timoshenko beam model includes forced motions arising from a transverse load along the span and from applied moments arising from surface

shear tractions as reported in Herrmann '55. However, after deriving the solution the applied moments are neglected, i.e., set equal to zero, since only transverse loads are of interest in this dissertation.

The deformation of a Timoshenko beam is specified by two dependent variables: y , the transverse deflection and ϕ , the angle of rotation of the cross section due to bending. However, due to the presence of a shearing force, the total rotation of the cross section, denoted as y' , also includes a shear angle γ_{xy} . The total slope, shown in Figure 5.5a, is given by

$$y' = \phi + \gamma_{xy} \quad (5-1)$$

Figure 5.5b shows a free body diagram of an infinitesimal element of the beam under dynamic equilibrium with the D'Alembert inertial forces.

Forced motions of a Timoshenko beam can be described completely by the force-deformation relations

$$\begin{aligned} M &= -EI\phi' \\ V &= k'AG(y' - \phi) \end{aligned} \quad (5-2)$$

by the equations of motion (see Figure 5.5)

$$\frac{E}{\rho} \phi'' + \frac{k'G}{\rho r^2} (y' - \phi) + \frac{M_s}{\rho I} = \ddot{\phi} \quad (5-3)$$

$$\frac{k'G}{\rho} (y'' - \phi') + \frac{q}{\rho A} = \ddot{y}$$

by the boundary conditions

$$y(0, t) = 0$$

$$\phi(0, t) = \frac{M(0, t)}{R} \quad (5-4)$$

$$y(L, t) = 0$$

$$\phi(L, t) = \frac{M(L, t)}{R}$$

and by the initial conditions

$$y(x, 0) = \dot{y}(x, 0) = 0 \quad (5-5)$$

$$\phi(x, 0) = \dot{\phi}(x, 0) = 0$$

In the equations above and throughout the remainder of this dissertation differentiation of the dependent variables (y and ϕ) with respect to x , the distance along the beam, is denoted by (') and differentiation of the dependent variables with respect to time t , is denoted by ('). The symbols are defined in the List of Symbols.

Mindlin and Deresiewicz '54 pointed out that the shear force is a function of the shear coefficient, k' , where k' relates the average shear stress on a beam section to the product of the shear modulus and the shear strain at the neutral axis. This coefficient depends on the distribution of shear stress on a section and, hence, on

the shape of the cross section as Timoshenko '21 observed. Mindlin and Deresiewicz correctly observed that the distribution of shear stress on a section also depends on the mode shape of vibration and that, whereas the maximum shear stress occurs at the neutral axis for the low modes of motion, the shear stress is a minimum at the neutral axis for very high modes of vibration. Thus, k' is also strongly influenced by the frequency of vibration and, hence, should be varied as a function of frequency rather than be taken as a constant as is normally done in a conventional analysis.

Mindlin '51 has shown that the shear coefficient calculated from the first thickness-shear frequency provides good results for both low and high frequencies. This coefficient can be calculated by equating the first thickness-shear frequencies obtained from the Timoshenko beam equations and the exact three-dimensional equations of an elastic body. This was accomplished by Mindlin and results in the following relationship for a rectangular cross-section:

$$\omega' = \frac{c}{r} \sqrt{k'} = \frac{\pi c}{h} \quad (5-6)$$

where $c = (G/\rho)^{1/2}$ and h is the thickness of the beam. Equation (5-6) results in a value $k' = 0.822$ which compares closely to the shear coefficient used for the static case which is 0.833.

5.2.1.1 Flexure-Shear Modes

The normal modes and natural frequencies are determined from the homogeneous differential equations of motion and the boundary conditions, i.e. q and M_s are set to zero in Equations (5-3). The solution is in the form

$$\begin{aligned} y(x,t) &= Y(x) e^{j\omega t} \\ \phi(x,t) &= \Phi(x) e^{j\omega t} \end{aligned} \quad (5-7)$$

The equations of motion and boundary conditions are satisfied for an infinite set of discrete frequencies ω_n , each of which corresponds to a mode shape given by functions $Y_n(x)$ and $\Phi_n(x)$. Substituting Equations (5-7) into the homogeneous versions of Equations (5-3) yields

$$\begin{aligned} k'G (Y_n'' - \Phi_n') &= -\rho\omega_n^2 Y_n \\ \beta G \Phi_n'' + \frac{k'G}{r^2} (Y_n' - \Phi_n) &= -\rho\omega_n^2 \Phi_n \end{aligned} \quad (5-8)$$

where $\beta = 2(1+\nu)$. Here the constant β relates the Young's and Shear modulus for elastic behavior as a function of Poisson's ratio, ν , for the material.

The solution to Equations (5-8) can be found as

$$\begin{aligned} Y &= C_1 \cosh \xi x + C_2 \sinh \xi x + C_3 \cos \gamma x + C_4 \sin \gamma x \\ \Phi &= C_1' \sinh \xi x + C_2' \cosh \xi x + C_3' \sin \gamma x + C_4' \cos \gamma x \end{aligned} \quad (5-9)$$

where

$$\begin{aligned} \xi &= \left\{ -\frac{\pi_1 \pi_2}{2} + \frac{1}{2} \left\{ (\pi_1 \pi_3)^2 + \frac{4k' \pi_1}{r^2 \beta} \right\}^{1/2} \right\}^{1/2} \\ \gamma &= \left\{ \frac{\pi_1 \pi_2}{2} + \frac{1}{2} \left\{ (\pi_1 \pi_3)^2 + \frac{4k' \pi_1}{r^2 \beta} \right\}^{1/2} \right\}^{1/2} \end{aligned} \quad (5-10)$$

The parameters π_i in Equations (5-10) are given by

$$\begin{aligned}\pi_1 &= \frac{\rho \omega_n^2}{k'G} \\ \pi_2 &= 1 + \frac{k'}{\beta} \\ \pi_3 &= 1 - \frac{k'}{\beta}\end{aligned}\tag{5-11}$$

Only four of the eight constants in Equations (5-9) are independent. The relationship among the eight constants can be found from either of Equations (5-8) as follows:

$$\begin{aligned}C_1 &= K_1 C_1' \\ C_2 &= K_1 C_2' \\ C_3 &= -K_2 C_3' \\ C_4 &= K_2 C_4'\end{aligned}\tag{5-12}$$

where

$$\begin{aligned}K_1 &= \frac{1}{\xi} \left\{ 1 - r^2 \pi_1 - \frac{r^2 \beta}{k'} \xi^2 \right\} \\ K_2 &= \frac{1}{\delta} \left\{ 1 - r^2 \pi_1 + \frac{r^2 \beta}{k'} \delta^2 \right\}\end{aligned}\tag{5-13}$$

Application of the boundary conditions, Equations (5-4), and the relations of integration constants, Equations (5-12, 5-13), to Equations (5-9) yields a set of four homogeneous linear algebraic equations in four constants C_1' to C_4' . For solutions other than the trivial case to exist, the determinant of the coefficients of each of the four constants must equal zero. This results in the following characteristic equation, from which the natural frequencies ω_n can be determined:

$$2(1 - \cosh \xi L \cos \gamma L) + 2\theta \left(\gamma + \xi \frac{K_2}{K_1} \right) \cosh \xi L \sin \gamma L - 2\theta \left(\xi + \gamma \frac{K_1}{K_2} \right) \sinh \xi L \cos \gamma L + \quad (5-14)$$

$$\left\{ 2\theta^2 \gamma \xi + \frac{K_2}{K_1} (1 + \theta^2 \xi^2) + \frac{K_1}{K_2} (\theta^2 \gamma^2 - 1) \right\} \sinh \xi L \sin \gamma L = 0$$

where $\theta = EI/R$.

Note that when the beam-end restraint approaches infinity, $R \rightarrow \infty$, the frequency Equation (5-14) should decay to the case for a fixed-end beam. That it does can be verified in Huang '61.

The normal modes, Y_n and θ_n , for each natural frequency can be obtained, to within an arbitrary constant, from the same four homogeneous equations that determined the frequency equation. These modes are given as

$$\begin{aligned} Y_n(x) &= C_1 K_1 \left\{ \cosh \xi x + \mu \sinh \xi x + \psi \sin \gamma x - \cos \gamma x \right\} \\ \Phi_n(x) &= C_1 \left\{ \mu \cosh \xi x + \sinh \xi x + \frac{K_1}{K_2} \sin \gamma x + \delta \cos \gamma x \right\} \end{aligned} \quad (5-15)$$

where

$$\mu = \left\{ \frac{K_1 \cos \gamma L - K_1 \cosh \xi L - \theta K_2 \left(\xi + \gamma \frac{K_1}{K_2} \right) \sin \gamma L}{K_1 \sinh \xi L - K_2 \sin \gamma L} \right\}$$

$$\psi = \frac{K_2}{K_1} (\theta \xi - \mu) + \theta \gamma$$

$$\delta = \theta \left(\xi + \gamma \frac{K_1}{K_2} \right) - \mu$$

and the constant C_1 is arbitrary.

To solve Equations (5-3) for forced motions using the normal mode method, the applied actions (forces or moments) are expanded into a series involving the normal modes. To do this the property of orthogonality of the principal modes of free vibration must be established. This has been done by Herrmann '55 and is given by

$$\int_0^L (Y_n Y_m + r^2 \Phi_n \Phi_m) dx = 0, \quad m \neq n \quad (5-16)$$

The solution to the forced motion case is given in the form

$$y(x, t) = \sum_n Y_n(x) T_n(t) \quad (5-17)$$

$$\phi(x, t) = \sum_n \Phi_n(x) T_n(t)$$

where the normal modes form a complete set. Furthermore, the applied time-dependent actions can be expanded in the form

$$\frac{q}{\rho^2 A} = \sum_n Y_n(x) G_n(t) \quad (5-18)$$

$$\frac{M_s}{\rho I} = \sum_n \Phi_n(x) G_n(t)$$

Multiplying the first of Equations (5-18) by Y_n , multiplying the second of Equations (5-18) by $r^2 \Phi_n$, adding the equations term by term, integrating over the length of the beam, and using the property of orthogonality of normal modes (Equation 5-16) results in the determination of $G_n(t)$:

$$G_n(t) = \frac{\int_0^L \left(\frac{q}{\rho^2 A} Y_n + \frac{r^2 M_s}{\rho I} \Phi_n \right) dx}{\int_0^L (Y_n^2 + r^2 \Phi_n^2) dx} \quad (5-19)$$

Therefore, Equations (5-3) can be rewritten in terms of a series expansion in the normal modes. Substituting Equations (5-8), (5-17) and (5-18) into Equations (5-3) and equating the n^{th} term in the infinite series, produces the following equations:

$$\begin{aligned} -\omega_n^2 Y_n T_n + G_n Y_n &= Y_n \ddot{T}_n \\ -\omega_n^2 \Phi_n T_n + G_n \Phi_n &= \Phi_n \ddot{T}_n \end{aligned} \quad (5-20)$$

Two identical equations for T_n result from Equations (5-20):

$$\ddot{T}_n + \omega_n^2 T_n = G_n \quad (5-21)$$

the solution of which is given by

$$T_n = A_n \cos \omega_n t + B_n \sin \omega_n t + \frac{1}{\omega_n} \int_0^t G_n(\tau) \sin \omega_n (t-\tau) d\tau \quad (5-22)$$

Application of the initial conditions, given in Equations (5-5), determines the values of the constants of integration to be $A_n = 0$ and $B_n = 0$. Finally, the complete solution to the Timoshenko beam for forced vibrations with homogeneous initial conditions is

$$y(x,t) = \sum_n \frac{Y_n(x)}{\omega_n} \int_0^t G_n(\tau) \sin \omega_n (t-\tau) d\tau \quad (5-23)$$

$$\phi(x,t) = \sum_n \frac{\Phi_n(x)}{\omega_n} \int_0^t G_n(\tau) \sin \omega_n (t-\tau) d\tau$$

It is now a simple matter to go back to Equation (5-19) and let $M_s = 0$ for the case to be studied in this dissertation.

5.2.1.2 Thickness-Shear Modes

The natural frequency spectrum of a beam changes at the first thickness-shear mode. This frequency, denoted as ω' and shown in Figure 5.4, is the lowest frequency at which an infinite beam can vibrate with no transverse deflection, the displacement being entirely parallel to the axis of the beam, i.e. an inplane shear mode as seen in Figure 5.3. The change in the frequency spectrum at ω' occurs

when the frequencies of the first thickness-shear mode become strongly coupled with the flexure-shear mode of motion.

Mindlin '51 points out that the thickness-shear modes do not physically exist in finite length supported beams. The resonances in the bounded beam, referred to as thickness-shear and its overtones, are actually local regions in the spectrum of flexural resonances over which the frequency does not change as quickly as other regions in the spectrum with change in beam dimensions. Furthermore, since shearing deformation is always present in flexural motion, these flexural resonances can be developed by forcing shearing deformations in the beam at the resonant flexural frequencies.

This change in the frequency spectrum occurs when the expression inside the outer brackets of the first of Equations (5-10) becomes negative, or when

$$\left\{ (\pi_1, \pi_3)^2 + \frac{4k'\pi_1}{r^2\beta} \right\}^{1/2} > \pi_1, \pi_2 \quad (5-24)$$

The condition expressed by Equation (5-24) occurs at the first thickness-shear frequency.

For frequencies higher than the first thickness-shear frequency the solution of Equations (5-3) changes and Equations (5-9) become

$$\begin{aligned} Y &= C_1 \cos \xi'x + jC_2 \sin \xi'x + C_3 \cos \gamma x + C_4 \sin \gamma x \\ \Phi &= jC_1' \sin \xi'x + C_2' \cos \xi'x + C_3' \sin \gamma x + C_4' \cos \gamma x \end{aligned} \quad (5-25)$$

where

$$\xi' = \left\{ \frac{\pi_1 \pi_2}{2} - \frac{1}{2} \left\{ (\pi_1 \pi_3)^2 + \frac{4k' \pi_1}{r^2 \beta} \right\}^{1/2} \right\}^{1/2} = \frac{\xi}{j} \quad (5-26)$$

$$j = \sqrt{-1}$$

Equations (5-11) and (5-12) remain unchanged. The first of Equations (5-13) becomes

$$K_i' = \frac{1}{\xi'} \left\{ 1 - r^2 \pi_1 + \frac{r^2 \beta}{K_i'} \xi'^2 \right\} \quad (5-27)$$

and the frequency Equation (5-14) changes to

$$2 \left(1 - \cos \xi' L \cos \gamma L \right) + 2 \theta \left(\gamma - \xi' \frac{K_2}{K_1'} \right) \cos \xi' L \sin \gamma L \\ + 2 \theta \left(\xi' - \gamma \frac{K_1'}{K_2} \right) \sin \xi' L \cos \gamma L - \quad (5-28)$$

$$\left\{ 2 \theta^2 \gamma \xi' + \frac{K_2}{K_1'} (1 - \theta^2 \xi'^2) + \frac{K_1'}{K_2} (1 - \theta^2 \gamma^2) \right\} \sin \xi' L \sin \gamma L = 0$$

The normal modes, Y_n and Φ_n , also change at frequencies higher than the first thickness-shear mode. Equations (5-15) become

$$Y_n(x) = C_1 \left\{ \cos \xi' x + \mu' \sin \xi' x + \psi' \sin \gamma x - \cos \gamma x \right\} \\ \Phi_n(x) = \frac{C_1}{K_1'} \left\{ \mu' \cos \xi' x - \sin \xi' x + \frac{K_1'}{K_2} \sin \gamma x + \delta' \cos \gamma x \right\} \quad (5-29)$$

where

$$\mu' = \left\{ \frac{\cos \gamma L - \cos \xi' L - \theta \left(\gamma - \xi' \frac{K_2}{K_1'} \right) \sin \gamma L}{\sin \xi' L - \frac{K_2}{K_1'} \sin \gamma L} \right\}$$

$$\psi' = \theta \left\{ \gamma - \xi' \frac{K_2}{K_1'} \right\} - \mu' \frac{K_2}{K_1'}$$

$$\delta' = \theta \left\{ \gamma \frac{K_1'}{K_2} - \xi' \right\} - \mu'$$

and again the constant C_1 is arbitrary. The process now remains unchanged for Equations (5-16) through (5-23).

5.2.1.3 Convergence

Inasmuch as Equations (5-23) are normal mode representations of the beam response, a very important issue in numerical calculations is the issue of convergence. An exact analysis would include an infinite number of normal modes as denoted by the summation sign in Equations (5-23). Practically, however, the analysis has to be truncated at some mode to be numerically feasible. This truncation usually occurs when the differences in y or ϕ at two consecutive modes is acceptably small or when their values approach some convergent value with the inclusion of ever-higher modal contributions.

Since Equations (5-23) also involve the loading function $q(t)$, any issues involving convergence must consider the frequency content of the loading. Obviously, load pulses with short rise times will excite higher frequency modes than pulses with long rise times. To show the influence of load pulse shape on frequency, the Fourier transform is used to determine the frequency content of the loading. The Fourier amplitude spectrum shows the relative energy in the frequencies inherent in the load pulse. Figures 5.6 and 5.7 are normalized spectra in which all amplitudes are normalized with respect to the Fourier amplitude at zero frequency. The Fourier amplitude $|X(\omega)|$ is determined by the following relationship (see Newland '75)

$$|X(\omega)| = \left\{ A^2(\omega) + B^2(\omega) \right\}^{1/2} \quad (5-30)$$

$$\text{where } A(\omega) = \frac{1}{2\pi} \int_{-\infty}^{\infty} q(t) \cos \omega t dt$$

$$B(\omega) = \frac{1}{2\pi} \int_{-\infty}^{\infty} q(t) \sin \omega t dt$$

Figure 5.6 shows the amplitude spectrum for a triangular load pulse with a duration of 0.6 msec, and different rise times. For the frequency range shown the curves are identical for peak pressures above 1,000 psi. Figure 5.7 shows the same information for a load duration 2 msec. The range of load durations from 0.6 msec to 2 msec encompasses all the interface pressure data presented in Chapter 4. Figures 5.6 and 5.7 show that frequencies above 100,000 rad/sec generally have less than a 5% contribution to the frequency content of the load.

Computer studies of the convergence issue show that frequencies beyond that associated with the 21st mode (generally less than 90,000 rad/sec for all cases studied here) have negligible influence on the shear force at the support. For the remainder of the normal mode section, therefore, the 21st mode is presumed to represent convergence. Convergence for the bending moment at the support generally is attained at a much lower mode.

5.2.1.4 Shear and Moment Analysis

To compare the bending moment M and the transverse shear force V in the beam at the support, where direct shear failures likely take place, Equations (5-2) and (5-23) are combined and evaluated at $x = 0$, resulting in the following equations for M and V :

$$M(0,t) = -EI \sum_n \frac{\Phi_n'(0)}{\omega_n} \int_0^t G_n(\tau) \sin \omega_n(t-\tau) d\tau \quad (5-31)$$

$$V(0,t) = k'AG \sum_n \frac{Y_n'(0) - \Phi_n'(0)}{\omega_n} \int_0^t G_n(\tau) \sin \omega_n(t-\tau) d\tau$$

Values of M and V can be computed using the results of the previously discussed normal mode solution. In order to identify the likelihood of a direct shear failure, a comparison is made between normalized shear and moment as a function of time. The moment and shear are normalized to their respective strength capacities, M_U and V_U as defined by the failure criteria given by Equations (3-2) and (3-8). It is then possible to determine whether the beam is expected to fail in direct shear before it fails in flexure (i.e., the normalized shear exceeds a value of 1 before the normalized moment exceeds 1).

For purposes of shear and moment comparisons in all of Section 5.2, a beam similar to the roof element of the Group III test structures is used as a model. The nominal mechanical and geometric properties of this example beam are given in Table 5.1.

The following paragraphs discuss results obtained from Equations (5-31) on the relationship between the normalized shear and the normalized moment at the support for different parameters of the loading applied to the Timoshenko beam model and for different beam-end restraints.

Figures 5.8 and 5.9 show plots of normalized support shear (V/V_U) and normalized support bending moment (M/M_U) versus time for two different peak pressures for

the example elastic beam. The plots are for a fixed beam-end condition and for a given rise time and load duration as shown.

The curves in Figures 5.8 and 5.9 are theoretical because as soon as either ratio V/V_u or M/M_u exceeds a value of 1 the beam is presumed to have reached its ultimate capacity and is no longer elastic. Several interesting aspects of theoretical beam behavior can be seen in these plots. In these figures the time at which $V/V_u = 1$ is denoted as t' and the time at which $M/M_u = 1$ is denoted as t'' . At early times the normalized shear curves increase at a higher rate than the normalized moment curves. However, at later times the normalized moment curves increase faster than the normalized shear curves. Therefore, the occurrence of failure in either direct shear or bending depends on whether the failure threshold (V/V_u and M/M_u equals one) intersects these curves at an early or a later time, respectively. For example, Figure 5.8 shows a condition where an early time direct shear failure is indicated ($t' < t''$) and Figure 5.9 shows a condition where a bending failure is indicated ($t' > t''$). Figure 5.9 shows that for some peak pressure (generally less than about 2000 psi for the rise time and duration shown here) the ultimate shear capacity will not be attained before the ultimate moment capacity is reached, or $t'' < t'$.

The influence of peak pressure, rise time, and pulse duration on the times t' and t'' can be seen in Figures 5.10 and 5.11, respectively. Figure 5.10 shows the relationship of t' versus peak pressure for different rise times for a fixed beam-end condition. The figure shows that, for a given peak pressure, t' increases as rise time increases. Moreover, for a constant rise time, t' decreases as the peak pressure increases. Also, as the peak pressure drops below about 1200 psi the time

t' gets exceedingly large, indicating that a shear failure will not occur because of the lack of sufficient loading to cause the condition $V = V_u$. Figure 5.11 shows similar information for the parameter t'' . Both Figures 5.10 and 5.11 are for a load duration of 1 millisecond (1 msec). However, the plots show little variation for load pulse durations greater than about 0.5 msec. These relationships are developed into direct shear failure curves in Section 5.2.3.

The degree of the restraint at the beam-ends, shown schematically in Figure 5.1, is another important parameter regarding the possibility of achieving a direct shear failure. Figure 5.12 shows a plot of normalized support shear and moment versus time for the example beam for a beam-end restraint stiffness of $R = 4EI/L$. This restraint corresponds to the rotational resistance offered by a wall with the same properties and length as the beam as shown in the schematic in Figure 5.12. The curves in Figure 5.12 show the influence of end restraint on the time parameters t' and t'' . Both these parameters increase when compared to the values associated with a fixed beam-end condition (see Figure 5.8). Figure 5.12 also shows that in early time, shear forces become more dominant over bending moments at the support as the beam-end restraint decreases.

5.2.2 Rate Effects on Response

Under the rapid rates of loading and strain that occur in impulsive tests, the material strengths and elastic properties of reinforcing steel and concrete are greater than they are under static load tests. Bazant and Byung '82 provide an excellent bibliography on basic data regarding the dynamic properties of concrete and steel (like the uniaxial compressive strength, the tensile yield strength, and the

modulus of elasticity) as a function of strain rate. Information on load rate effects on elastic and strength properties is given by Watstein and Borezi '52.

Two approaches are outlined here for modeling rate effects on beam response. The first approach models strain rate effects by using viscoelastic constitutive relationships in the Timoshenko beam equations of motion. The viscoelastic relation used is that of a Voight (also called Kelvin) solid, and is schematically shown along with the stress-strain characteristics in Figure 5.13. This approach, although intuitively plausible, has limitations because the viscous parameter (shown in the figure as η) is not constant over a large range of strain rates. The second approach, based on load rate, simply employs the results of Section 5.2.1 and alters the beam material properties to account for rate influence.

5.2.1 Strain Rate

No previous study or analysis has been found on the forced or free vibration of a Timoshenko beam with linear viscoelastic constitutive properties. In developing the viscoelastic Timoshenko beam it is assumed that the proportionality parameter for the strain rate terms is a constant during the time domain of interest. Since the analytic time span of interest is a very short time (less than 0.2 msec) this assumption should be acceptable. Certainly, strain rate is a function of the response history and when the strain rate changes, so too should the viscous proportionality constant. However, the general trends showing strain rate influence on shear and moment should be apparent even with the assumption of a constant rate parameter. Moreover, it is also assumed that the rate effects in shear and moment are linearly related by the same constant, β , as is the relationship between Young's modulus and the shear modulus. In particular, if α ' is

the viscous coefficient for a compressive strain rate, then $\eta = \alpha'/\beta$ is the viscous coefficient for a shear-strain rate. This should be valid for the linear elastic case.

For the Timoshenko beam the viscoelastic counterparts of Equations (5-2) are,

$$M = -I \{ E \phi' + \alpha' \dot{\phi}' \} = -Ar^2\beta \{ G \phi' + \eta \dot{\phi}' \} \quad (5-32)$$

$$V = k'A \{ G (y' - \phi) + \eta (\dot{y}' - \dot{\phi}') \}$$

where $\dot{\phi}$, $\dot{\phi}'$, and \dot{y}' are generalized strain rate terms. Equations (5-32) contain an elastic part and a viscous part for both shear and moment. Since strain rate is always a positive quantity these equations show that the viscoelastic stiffness is always greater than or equal to (for zero strain rate) the elastic case. This condition is seen in rate application tests for both concrete and steel. Hence, the viscous term accounts for an increase in stiffness due to rate effects.

The viscoelastic form of Equations (5-3) is now (for the case $M_s = 0$),

$$k'AG (y' - \phi) + k'A\eta (\dot{y}' - \dot{\phi}') + Ar^2\beta (G\phi'' + \eta \dot{\phi}'') = 0 \quad (5-33)$$

$$k'AG (y'' - \phi') + k'A\eta (\dot{y}'' - \dot{\phi}') - \rho A \ddot{y} = -q$$

In order to make Equations (5-33) mathematically tractable, the rotary inertia term has been neglected. This makes the first of Equations (5-33) approximate. But considering the fact that the effects due to shear deformations are three to

four times as large as the effects due to rotary inertia (see Timoshenko, et al '74) it is felt the approximation is valid in order for a solution to be obtained. In fact Mindlin '51 found that the transverse shear deformation accounted almost entirely for the discrepancy between the simple (Bernoulli-Euler) theory and the exact three-dimensional theory.

The solution of Equations (5-33), along with the boundary conditions (for this case assumed to be those for a fixed-end beam) and initial conditions (5-5), is quite difficult. A convergent series solution for small time (i.e., a nondimensionalized time parameter such as Gt/η being less than 1) is not possible because of the poor coupling between the two Equations (5-33). For example, second derivatives in space or time on ϕ appear only in the first of Equations (5-33) and second derivatives on y appear only in the second of Equations (5-33).

A self-similar solution (for a semi-infinite beam) is not possible for inhomogeneous equations, unless the loading term is an implicit function of space and time and can be expressed in terms of the similarity variable. A separation of variables technique is also not possible since the equations are clearly not separable because of the strain rate terms.

The method of characteristics is a possible technique if one can show that the equations are hyperbolic (the elastic Equations 5-3 are hyperbolic as shown by Colton '73). This is difficult to do for these equations, but even if the equations are hyperbolic the solution procedure become lengthy. In order to reduce the simultaneous third order equations to a system of first order equations and then to transform the independent variables to the characteristic coordinates would

require the analytic evaluation of a determinant of rank six. The characteristics also would not be straight lines, resulting in the evaluation of simultaneous ordinary differential equations with variable coefficients.

The theory finally adopted as a solution technique is the Laplace transform method in both space and time coordinates; that is, a double Laplace transformation with a subsequent double inversion. Anderson '71 successfully employed this technique in his analysis of an elastic Timoshenko beam under forced motions. He pointed out that the advantage of the transform method is that a series solution can be obtained by using the theory of residues. Here, the inversions in space and time are obtained by summing the residues about the poles of the resulting characteristic equations in the Laplacian domain (see Wylie '75). This residue principle replaces the usual integration associated with the orthogonality condition when solving the equations in normal modes.

5.2.2.1.1 Laplace Transform Solution

Since orthogonality is not valid (i.e., a harmonic solution is not possible) for the Timoshenko beam with viscoelastic properties, a Laplace transform method is used in conjunction with an asymptotic approximation in time to achieve a solution valid only for very small times. In order to simplify the solution, a fixed-end beam under the influence of a step-loading is studied.

The Laplace Transform method, as applied here, transforms the dependent variables, y and ϕ , using

$$\bar{y}(x,s) = \int_0^{\infty} e^{-st} y(x,t) dt \quad (5-34)$$

$$\bar{\bar{y}}(p,s) = \int_0^{\infty} e^{-px} \bar{y}(x,s) dx$$

with similar linear operators applying to ϕ , i.e., $\bar{\phi}(x,s)$ and $\bar{\bar{\phi}}(p,s)$. A single bar above a variable indicates a transform in time and a double bar designates a double transform in both time and space.

In order to satisfy the conditions of transformation in time and space all initial conditions must be specified at a single time (usually $t = 0$) and all boundary conditions must be specified at a single location (usually $x = 0$). This condition is satisfied for the time domain using Equations (5-5). However, for the space domain two additional boundary conditions at $x = 0$ are required (the first and second of Equations (5-4) where $R = \infty$ are the other two). These four transformed boundary conditions are found by taking the time Laplace transform of both Equations (5-32) and the first two of Equations (5-4). This results in

$$\begin{aligned} \bar{y}(0,s) &= 0 \\ \bar{\phi}(0,s) &= 0 \\ \bar{y}'(0,s) &= -\frac{\bar{V}(0,s)}{\zeta} + \bar{\phi}(0,s) \\ \bar{\phi}'(0,s) &= \frac{\bar{M}(0,s)k'}{r^2 \beta \zeta} \end{aligned} \quad (5-35)$$

where $\zeta = k'A(G + \eta s)$ and $\bar{V}(0,s)$, $\bar{M}(0,s)$ are the time Laplace transforms of the support shear and support bending moment, respectively.

Transforming Equations (5-33) first in time and then in space results in the following simultaneous linear algebraic equations in the Laplace functions $\bar{\bar{y}}$ and $\bar{\bar{\phi}}$

$$p\bar{\bar{y}} + \left(\frac{r^2 \rho}{k'} p^2 - 1\right) \bar{\bar{\phi}} = \frac{\bar{M}(0,s)}{\zeta} \quad (5-36)$$

$$\left(\frac{\rho A s^2}{\zeta} - p^2\right) \bar{\bar{y}} + p \bar{\bar{\phi}} = \frac{-\bar{q} + \bar{V}(0,s)}{\zeta}$$

Solution of Equations (5-36) gives

$$\bar{\bar{y}}(p,s) = \left\{ \frac{pk' \bar{M}}{r^2 \rho \zeta} + \left(\frac{k'}{r^2 \rho \zeta} - \frac{p^2}{\zeta}\right) (-\bar{q} + \bar{V}) \right\} / D(p) \quad (5-37)$$

$$\bar{\bar{\phi}}(p,s) = \left\{ \frac{k'}{r^2 \rho \zeta} \left(p^2 - \frac{\rho A s^2}{\zeta}\right) \bar{M} + \frac{pk'}{r^2 \rho \zeta} (-\bar{q} + \bar{V}) \right\} / D(p)$$

where

$$D(p) = p^4 - \frac{\rho A s^2}{\zeta} p^2 + \frac{k' \rho A s^2}{r^2 \rho \zeta} = (p^2 - p_1^2)(p^2 - p_2^2)$$

The roots of $D(p)$ are given as

$$p_1(s) = \left\{ \frac{\rho A s^2}{2\zeta} \pm \frac{\rho A s^2}{2\zeta} \left\{ 1 - \frac{4k'\zeta}{r^2 \rho A s^2} \right\}^{1/2} \right\}^{1/2} \quad (5-38)$$

The inversion of Equations (5-37) is accomplished in two sequential steps: the first inversion in p and the second in s . Inverting first with respect to p is accomplished using the inversion theorem or the residue theorem

$$\bar{y}(x,s) = \frac{1}{2\pi j} \int_{g-j\infty}^{g+j\infty} e^{px} \bar{y}(p,s) dp \quad (5-39)$$

$$= \sum \text{residues of } e^{px} \bar{y}(p,s) \text{ at } \pm p_1 \text{ and } \pm p_2$$

where "g" is chosen so that all the singular points of $\bar{y}(p,s)$ lie to the left of "g" on the real line in the complex p plane. A similar operation is also accomplished for $\bar{\phi}(x,s)$.

Anderson '71 has shown that the residue theorem results in

$$L_p^{-1} \frac{p^{n-1}}{D(p)} = G_n(x,s) \quad (5-40)$$

and

$$G_n(x,s) = \frac{1}{(p_1^2 - p_2^2)} \frac{d^{n-1}}{dx^{n-1}} \left\{ \frac{\sinh p_1 x}{p_1} - \frac{\sinh p_2 x}{p_2} \right\}$$

where L_p^{-1} is a symbol denoting the inversion operator in the variable p and (n-1) is the power of p in Equations (5-37). Hence, Equations (5-40) are used to invert all terms on the right-hand sides of Equations (5-37) except those terms associated with the distributed load $q(x,t)$. For terms involving $\bar{q}(p,s)$ the convolution theorem is used in the inversion process. Applying this theorem to the pertinent terms in Equations (5-37) results in

$$\begin{aligned} A_0(x,s) &= -L_p^{-1} \left\{ \frac{k'}{r\beta\zeta} - \frac{p^2}{\zeta} \right\} \frac{\bar{q}(p,s)}{D(p)} \\ &= - \int_0^x \bar{q}(x-u,s) \left\{ \frac{k'}{r\beta\zeta} G_1(u,s) - \frac{G_3(u,s)}{\zeta} \right\} du \end{aligned} \quad (5-41)$$

and similarly

$$\begin{aligned}
 B_0(x,s) &= -L_p^{-1} \left\{ \frac{pk'}{r^2 \beta \zeta} \right\} \frac{\bar{q}(p,s)}{D(p)} \\
 &= - \int_0^x \bar{q}(x-u,s) \left\{ \frac{k'}{r^2 \beta \zeta} G_2(u,s) \right\} du
 \end{aligned}
 \tag{5-42}$$

For this analysis a simple step function in time and space is an adequate load function to show the relationship between shear and moment. The load function and its double Laplace transform is given by

$$\begin{aligned}
 q(x,t) &= P_0 H(t) \{ H(x) - H(x-L) \} \\
 \bar{q}(p,s) &= \frac{P_0}{s} \{ 1 - e^{-Lp} \}
 \end{aligned}
 \tag{5-43}$$

where $H(u) = 1, u > 0$ is the unit step function
 $= 0, u \leq 0$
 $P_0 =$ peak load (see Figure 5.14)

Finally, using the results from Equations (5-40) through (5-43) produces

$$\begin{aligned}
 \bar{y}(x,s) &= A_0(x,s) + A_3(x,s)\bar{V} + A_4(x,s)\bar{M} \\
 \bar{\phi}(x,s) &= B_0(x,s) + B_3(x,s)\bar{V} + B_4(x,s)\bar{M}
 \end{aligned}
 \tag{5-44}$$

where

$$\begin{aligned}
 A_3(x,s) &= k'G_1(x,s)/r^2 \beta \zeta - G_3(x,s)/\zeta \\
 A_4(x,s) &= k'G_2(x,s)/r^2 \beta \zeta \\
 B_3(x,s) &= A_4(x,s) \\
 B_4(x,s) &= k'G_3(x,s)/r^2 \beta \zeta - k' \rho A s^2 G_1(x,s)/r^2 \beta \zeta
 \end{aligned}$$

The two unknown constants \bar{V} and \bar{M} are determined by using Equation (5-44) and the boundary conditions shown as the third and fourth of Equations (5-4) where $R = \infty$ for a fixed-end beam, and by evaluating these at $x = L$. Solving simultaneously for \bar{V} and \bar{M} results in

$$\bar{V}(0,s) = \frac{B_0 A_4 - A_0 B_4}{A_3 B_4 - A_4 B_3} \quad (5-45)$$

$$\bar{M}(0,s) = \frac{A_0 B_3 - B_0 A_3}{A_3 B_4 - A_4 B_3}$$

where

$$A_i = A_i(L,s) \quad i = 0,3,4$$

$$B_i = B_i(L,s) \quad i = 0,3,4$$

Since only the ratio of $V(0,t)/M(0,t)$ is of interest here, this ratio is obtained once \bar{V} and \bar{M} are inverted in the variable s . However, the expressions (5-45) are very complicated, involving products of hyperbolic functions. Since the interest is in achieving a solution for only a small time beyond $t = 0$ it is possible to use an asymptotic approximation on s , thereby simplifying Equations (5-45) prior to inversion. If the Laplace variable s is allowed to grow very large (corresponding to a small time) the roots given in Equation (5-38) and the expressions in (5-45) are simplified to

$$P_1^2(s) = \frac{\rho s}{k \eta} \quad (5-46)$$

$$P_2^2(s) = 0$$

and

$$\bar{V}(0, s) = \frac{P_0 \sinh p_1 L}{s p_1 (\cosh p_1 L - 1)} \quad (5-47)$$

$$\bar{M}(0, s) = \frac{P_0 r^2 \beta}{s k' (\cosh p_1 L - 1)}$$

The inversion of Equations (5-47) is now accomplished using the theory of residues. In both Equations (5-47) all singularities occur at the pole $s = 0$. However, because both Equations (5-47) involve hyperbolic functions the order of the poles are unknown. This is overcome by replacing the hyperbolic functions by their Maclaurin expansions, which results in

$$\bar{V}(0, s) = \frac{P_0}{s^2} \left\{ \frac{a_0 + a_1 s + a_2 s^2 + \dots}{b_0 + b_1 s + b_2 s^2 + \dots} \right\}$$

$$\bar{M}(0, s) = \frac{P_0 r^2 \beta}{k' s^2} \left\{ \frac{1}{b_0 + b_1 s + b_2 s^2 + \dots} \right\} \quad (5-48)$$

where

$$a_0 = L \qquad b_0 = \rho L^2 / 2k'\eta$$

$$a_1 = \rho L^3 / 6k'\eta \qquad b_1 = \rho^2 L^4 / 24k'^2 \eta^2$$

and so forth for higher order terms of the series.

The denominators in Equations (5-48) identify the poles as being of second order.

Using the residue theorem the inversions are found as

$$V(0, t) = \lim_{s \rightarrow 0} \frac{d}{ds} \left\{ \frac{s^2 P_0 e^{st}}{s^2} \left[\frac{a_0 + a_1 s + \dots}{b_0 + b_1 s + \dots} \right] \right\}$$

$$= P_0 \left\{ \frac{a_0 t + a_1 - a_0 b_1 / b_0}{b_0} \right\} \quad (5-49)$$

$$\begin{aligned}
 M(0,t) &= \lim_{s \rightarrow 0} \frac{d}{ds} \left\{ \frac{s^2 P_0 r^2 \beta e^{st}}{k' s^2} \left[\frac{1}{b_0 + b_1 s + \dots} \right] \right\} & (5-50) \\
 &= \frac{P_0 r^2 \beta}{k''} \left\{ \frac{t - b_1/b_0}{b_0} \right\}
 \end{aligned}$$

The ratio V/M , at the support ($x = 0$), including rate effects (denoted by a subscript z), is obtained as

$$\left\{ \frac{V(0,t)}{M(0,t)} \right\}_z = \frac{k' L}{r^2 \beta} \left\{ \frac{t + \frac{\rho L^2}{12 k' \eta}}{t - \frac{\rho L^2}{12 k' \eta}} \right\} \quad (5-51)$$

In an effort to determine whether shearing forces are enhanced more than bending moments by the presence of rate effects, Equation (5-51) must be compared to the same ratio determined for a fixed-end Timoshenko beam without rate effects.

Proceeding in the same manner as before, Equations (5-33) are simplified when rate effects are ignored. These equations become

$$\begin{aligned}
 y' - \phi + \frac{r^2 \beta}{k'} \phi'' &= 0 & (5-52) \\
 y'' - \phi' - \frac{\rho}{k' G} \ddot{y} &= \frac{-q}{k' A G}
 \end{aligned}$$

Using the same boundary conditions, Equations (5-4) with $R = \infty$, and the same initial conditions (5-5), Equations (5-34) through (5-45) remain exactly the same except for the following change

$$\zeta = k' A G \quad (5-53)$$

This change (5-53) then results in a change of the roots (5-46) after an asymptotic approximation on s ($s \rightarrow \infty$) as follows

$$\begin{aligned} P_1^2(s) &= \frac{\rho s^2}{k'G} \\ P_2^2(s) &= 0 \end{aligned} \tag{5-54}$$

Again proceeding as before, Equation (5-47) remains unchanged and, after Maclaurin expansions are performed on the hyperbolic functions, Equations (5-48) become

$$\begin{aligned} \bar{V}(0,s) &= \frac{P_0}{s^3} \left\{ \frac{a_0 + a_1 s^2 + a_2 s^4 + \dots}{b_0 + b_1 s^2 + b_2 s^4 + \dots} \right\} \\ \bar{M}(0,s) &= \frac{P_0 r^2 \beta}{k' s^3} \left\{ \frac{1}{b_0 + b_1 s^2 + b_2 s^4 + \dots} \right\} \end{aligned} \tag{5-55}$$

where

$$\begin{aligned} a_0 &= L & b_0 &= \rho L^2 / 2k'G \\ a_1 &= \rho L^3 / 6k'G & b_1 &= \rho^2 L^4 / 24k'^2 G^2 \end{aligned}$$

and so forth for the higher order terms.

The poles at $s = 0$ in Equations (5-55) are now identified as being of order three. Now, using the residue theorem for the inversion, Equations (5-49) and (5-50) become

$$\begin{aligned}
 V(0,t) &= \frac{1}{2} \lim_{s \rightarrow 0} \frac{d^2}{ds^2} \left\{ \frac{s^3 P_0 e^{st}}{s^3} \left[\frac{a_0 + a_1 s^2 + \dots}{b_0 + b_1 s^2 + \dots} \right] \right\} \quad (5-56) \\
 &= \frac{P_0}{2} \left\{ \frac{a_0 t^2 + 2a_1 - 2a_0 b_1 / b_0}{b_0} \right\}
 \end{aligned}$$

$$\begin{aligned}
 M(0,t) &= \frac{1}{2} \lim_{s \rightarrow 0} \frac{d^2}{ds^2} \left\{ \frac{s^3 P_0 r^2 \beta e^{st}}{k' s^3} \left[\frac{1}{b_0 + b_1 s^2 + \dots} \right] \right\} \quad (5-57) \\
 &= \frac{P_0 r^2 \beta}{2k'} \left\{ \frac{t^2 - 2b_1 / b_0}{b_0} \right\}
 \end{aligned}$$

Substituting for the appropriate constants in Equations (5-56) and (5-57), the V/M ratio at the support, neglecting rate effects, becomes

$$\left\{ \frac{V(0,t)}{M(0,t)} \right\} = \frac{k' L}{r^2 \beta} \left\{ \frac{t^2 + \frac{\rho L^2}{6k'G}}{t^2 - \frac{\rho L^2}{6k'G}} \right\} \quad (5-58)$$

5.2.2.1.2 Elastic and Strength Effects

The purpose for obtaining the solution of the viscoelastic Timoshenko beam is to show that, initially, rate effects have a more pronounced impact on shear than bending moment, thereby enhancing the dominance of shear over bending moment under rapidly applied load conditions. This dominance of shear over moment is shown if the following ratio is greater than one:

$$\text{RER} = \left| \frac{\left(\frac{V}{M} \right)_{\epsilon}}{\left(\frac{V}{M} \right)} \right| \geq 1 \quad (5-59)$$

where RER is the "rate effect ratio" and the numerator and denominator of Equation (5-59) are given by Equations (5-51) and (5-58), respectively.

Obviously, before the value of $(V/M)_2$ can be computed an estimate for the shear viscosity coefficient, η , must be available. Impact data from Watstein and Boresi '53 relating the elastic properties of concrete to strain rate and load rate and shown in Figures 3.2 and 3.3, is used to estimate the shear viscosity coefficient (which has units of psi-sec). The concrete dynamic modulus of elasticity, shown in Figures 3.2 and 3.3, corresponds to a secant modulus through a strain of 0.001.

Since these data are for samples in uniaxial compression the slope of the curve represents the viscosity coefficient for compression, α' . The shear viscosity is simply computed from the relation, $\alpha' = \eta\delta$. For example a value of $\eta = 100$ corresponds to a strain rate of about 5/sec and an elastic modulus enhancement factor, Ψ , of approximately 1.25. Since the analysis described in this chapter relies on a discrete value of η , selected values of this coefficient are valid only over a short range of strain rates and load rates. This limitation presents no barrier at this point since the RER computed by Equation (5-59) is only valid for a small interval of time.

Figure 5.14 shows a plot of the RER versus time. The time scale has been truncated at about 0.2 msec. This is about the time at which the denominator in the ratio (V/M) becomes nonanalytic. This time is equivalent to the time it takes a shear wave to travel a distance of about 40% of the beam length and is taken to be the maximum time over which Equation (5-59) is valid.

The curves shown in Figure 5.14 correspond to three different values of the shear viscosity. Generally, the smaller the shear viscosity coefficient the shorter is the time during which the RER is greater than one. This is intuitive because the asymptotic approximation used to derive the RER is based on the Laplace variable "s" approaching infinity. In the time domain this corresponds to a solution near $t = 0$. Since the Laplacian parameter s appears as a product ηs the lower the value η the higher the value s required to let ηs get large. Hence, a small shear viscosity corresponds to a much shorter time where the RER exceeds one.

The plot in Figure 5.14 clearly shows the main conclusion of this section of the dissertation. Rate effects have a more pronounced effect on shear than on moment during an early time in the loading history comparable to the times of interest in this dissertation.

Figures 5.15 and 5.16 show another feature of the effect of strain rate. These are a plot of the time parameter t' (see Section 5.2.1.4) versus peak pressure from a step loading. In each plot one curve is for an elastic beam without rate effects and the other is for a viscoelastic beam with $\eta = 200$ (strain rate = 1.5/sec). The curves showing rate effects differ according to whether the ultimate shear capacity V_u was increased to account for rate effects i.e., $V = V_u$ in Figure 5.15 versus $V = 1.5 V_u$ in Figure 5.16. The value for the strength enhancement factor, shown as 1.5 in Figure 5.16, corresponds to a strain rate of 1.5/sec as seen from the curve for a 6500 psi concrete in Figure 3.2. As shown, the viscoelastic curve is always lower than the elastic curve indicating that the support shear force will reach its failure level sooner when considering elastic rate effects than when rate effects are not considered. In addition, the parameter t' increases when the influence of

rate effects on the strength capacity is included through the use of a strength enhancement factor. It is important to remark that the information provided in Figures 5.14 through 5.16 is only qualitative owing to the approximations involved in the Laplace solution procedure.

5.2.2.2 Load Rate

It is simpler to include load rate effects rather than strain rate effects in the elastic analysis, because Equations (5-2) and (5-3) remain unaltered when load rates are considered. There are two factors associated with load rate effects, and these have been addressed in Chapter 3. The first is the modulus enhancement factor and the second is the strength enhancement factor. Both these factors for load rate are only approximations to the true enhancements due to rate influences. The use of load rate as an indicator of the true rate of response (stress rate) is not precise. Nevertheless, its use can be justified when one considers that most available test data on dynamic material properties is based on average load rate. Furthermore the load rate is probably an upper bound to the true rate of response during the first quarter-cycle of vibration (generally the response period for impulsive loads).

By assuming load rate to be equivalent to stress rate, enhancement factors for both elastic and strength properties can be obtained from the curves shown in Figure 3.3. When these enhancement factors are used to increase the elastic modulus of the beam and to increase the strength capacities, in accordance with Equations (3-2) and (3-8), curves similar to those shown in Figures 5.8 and 5.9 can be developed. Figures 5.17 and 5.18 show the separate influence of the strength enhancement factor $\Omega = 1.6$ and the elastic modulus enhancement factor $\Psi = 1.2$,

respectively, on the normalized support shear for a load rate of approximately 1×10^7 psi/sec (the associated strain rate is approximately 4/sec). In Figure 5.17 the effect of the strength enhancement factor is to reduce V/V_u by the quantity $1/\Omega$. In Figure 5.18 the effect of the elastic modulus enhancement factor is to alter the frequency content of the beam making it slightly stiffer and, hence, quicker to respond. Although not shown here, the load rate effects on the normalized bending moment M/M_u are the same as those just described for V/V_u .

A conclusion reached in this section on load rate is the same as that drawn in Section 5.2.2.1 on strain rate. The parameter t' increases as the strength enhancement factor increases and it decreases as the elastic modulus enhancement factor increases.

On the basis of this limited study on load rate effects, it is concluded that the major influences on t' and t'' come from strength enhancement. The effect of modulus enhancement on time to failure is very small. The results from the analysis including strain rate (Section 5.2.2.1) show a larger decrease in time to failure due to viscoelastic enhancement, and also show that the support shear force is influenced more than the support bending moment.

Thus, the effect of viscous or elastic modulus enhancement is to amplify the dominance of shear force over bending moment. In the subsequent development of failure curves, these effects are neglected which results in conservative estimates on the domain of direct shear failure. However, enhancement of both shear and bending strength due to rate effects is considered in the construction of failure curves since this effect is to restrict the domain of direct shear failure.

5.2.3 Failure Curves

Referring to Figure 5.19a, a direct shear failure is indicated if the parameter t' is less than the parameter t'' . On the other hand, direct shear failure is not indicated when t' is larger than t'' , as shown in Figure 5.19b. Therefore the transition from a predicted direct shear failure to no shear failure occurs when $t' = t''$.

If Figures 5.10 and 5.11 are superposed, the intersection of the t' and t'' curves for each constant rise time will result in a series of points which describe a failure "curve" separating the direct shear failure domain from the domain of bending failures and no failure. Figure 5.20 shows the concept of this construction of failure curves.

These failure curves can be plotted in a different domain from that shown in Figure 5.20. In particular, the domain relating peak pressure P_0 to rise time t_r is of interest because these are the essential parameters of the impulsive loading. Figure 5.21 is an actual plot of the failure curve for the example beam described in Table 5.1. This curve pertains to a fixed beam-end condition, and strength enhancement due to rate effects is neglected. The curve in this figure separates the peak pressure versus rise time domain into two regions. Combinations of peak pressure and rise time which lie in the region above the curve define a loading for which analysis indicates a direct shear failure. Points that lie in the region below the failure curve describe load parameter combinations which will cause either a bending failure or no failure in the beam.

Figures 5.22 and 5.23 reveal two interesting results regarding the influence of beam-end restraint and strength enhancement, respectively, on direct shear

failure. Figure 5.22 shows that, for a given strength enhancement factor, the influence of beam-end restraint is small for very short load rise times. For larger rise times the influence becomes more pronounced, and for a given rise time direct shear failures are predicted for lower peak pressures as the degree of beam-end restraint is reduced from the fixed-end case. In Figure 5.23, for a given end restraint condition, the influence of strength enhancement is to restrict the domain for direct shear failure by moving the failure curves up. The failure curves shown in Figures 5.21 through 5.23 correspond to one particular beam geometry. Similar curves for different beams are shown and compared to experimental data in Section 5.4 in order to assess the accuracy of this elastic approach in predicting direct shear failures.

An examination of the failure curves developed to this point, and shown in Figures 5.20 through 5.23, has revealed that the curves are obviously sensitive to certain load parameters and to certain structural parameters. Regarding load parameters the two most obvious and pertinent are the peak pressure and rise time. Load duration has been shown to be a parameter which does not significantly affect the direct shear failure curves. In terms of structural parameters the degree of beam-end restraint and the particular values chosen for the strength capacity in shear V_u and moment M_u have been seen to have a tremendous impact on the failure curves. Other structural parameters such as the L/d ratio, the reinforcement ratio, and the beam frequency content should also significantly influence the failure curves. Examples of the influence of two of these structural parameters are shown in Figures 5.24 and 5.25. Figure 5.24 shows the influence of reinforcement ratio ρ_s for a given L/d ratio and a given strength enhancement factor Ω . As seen the direct shear failure domain is restricted, in general, as ρ_s increases. This is

because the increased amount of steel in a beam influences the moment capacity more than the direct shear capacity, thereby making it less likely that a direct shear failure will precede a flexural failure. Figure 5.25 shows the influence of L/d ratio for a given ρ_s and Ω . As the L/d ratio increases, the direct shear failure domain decreases because of the increase in the M/V ratio.

Since this dissertation represents an initial attempt at describing the conditions necessary for a direct shear failure in reinforced concrete beams, an extensive parametric study is not conducted here. This study does specify, however, the pertinent parameters influencing the development of failure curves based on an elastic beam model.

5.3 Shear Beam

The equations of motion and resulting solution for the Timoshenko beam theory, described in Section 5.2, involve a complicated process for the determination of the support shear force. A model which is more simple mathematically than the Timoshenko beam and which can also describe shear forces is represented by the classical shear beam. Obviously, solutions derived for a shear beam cannot be used to distinguish between a direct shear failure and a flexural failure because of the lack of a bending moment influence in the shear beam theory. But the simpler shear beam theory can be exploited to develop comparisons with the Timoshenko beam theory in terms of the support shear forces. Therefore, the objectives of this section are to: 1) determine the "domain of equivalence", represented by load parameters, between the Timoshenko beam and shear beam theories; 2) estimate the time to direct shear failure (t') within the domain of equivalence; and 3) verify the strain rate solution for support shear force for a viscoelastic Timoshenko beam.

The first two objectives will be met by solving the shear beam equations using the normal mode method and the third objective is met by using Laplace transform methods.

5.3.1 Normal Mode Method

The forced motion of an elastic shear beam is described by the force deformation relation

$$V = k'AGy' \quad (5-60)$$

by the equation of motion

$$k'AGy'' + q = \rho A\ddot{y} \quad (5-61)$$

by the boundary conditions

$$y(0,t) = y(L,t) = 0 \quad (5-62)$$

and by the initial conditions

$$y(x,0) = \dot{y}(x,0) = 0 \quad (5-63)$$

The normal mode method again is employed to solve Equations (5-60) to (5-63). Equation (5-61) is a linear second order partial differential equation with constant coefficients. Therefore, only two boundary conditions and two initial conditions, as shown in Equations (5-62) and (5-63), are required for a complete unique solution.

This equation represents the classic wave equation with an input source term $(q/\rho A)$, which can be solved by a variety of techniques. Without repeating the rigor of Section 5.2.1, the solution in terms of the normal modes $Y_n(x)$ and natural frequencies ω_n is given by

$$y(x, t) = \sum_n \frac{Y_n(x)}{\omega_n} \int_0^t G_n(\tau) \sin \omega_n(t - \tau) d\tau \quad (5-64)$$

where ω_n is determined from the frequency equation

$$\omega_n = \frac{n\pi}{L} \left(\frac{k'G}{\rho} \right)^{1/2} \quad (5-65)$$

and the n^{th} mode shape is given by

$$Y_n(x) = C_1 \sin \frac{n\pi x}{L} \quad (5-66)$$

where C_1 is an arbitrary constant. The function $G_n(\tau)$ is determined from the property of orthogonality of the normal modes and is given by

$$G_n(t) = \frac{\int_0^L \frac{q(x, t)}{\rho A} Y_n dx}{\int_0^L Y_n^2 dx} \quad (5-67)$$

For the case where $q(x,t)$ is a uniformly distributed load along the span length (i.e., constant with x), the shear force at the support ($x = 0$) is represented by the expression

$$V(0,t) = \sum_n \frac{2}{n\pi} \left(\frac{k'G}{\rho} \right)^{1/2} (1 - \cos n\pi) \int_0^t q(\tau) \sin \omega_n(t-\tau) d\tau \quad (5-68)$$

where $q(\tau)$ is the temporal forcing function. Inspection of Equation (5-68) shows that the shear force is only a function of the odd-numbered modes. This is as it should be for a symmetric loading which excites only antisymmetric shear forces.

Plots of V/V_u versus time, obtained from Equation (5-68), are shown in Figure 5.26 for three different rise times for the example beam of Section 5.2. The results for the shear beam are compared to the shear results of the Timoshenko beam, obtained from the second of Equations (5-31), for the support shear force where rate effects are not considered. The support shear force from a shear beam reasonably approximates that from the Timoshenko beam for early times. The early time support shear force of the shear beam builds up quicker than the shear force of the Timoshenko beam because the frequency content of the first few modes is higher in the shear beam than the Timoshenko beam. At the shear level of interest ($V/V_u < 1$), the agreement in shear forces is quite good for a limited range of rise times for the peak pressure and beam-end restraint shown for this case. The combinations of load parameters for which this agreement is specified in terms of a percentage difference in V/V_u for a given time are used to determine the domain of equivalence between the Timoshenko beam and shear beam theories for the support shear force. Figure 5.26 also shows the comparison of approximate time to failure ($V/V_u = 1$) between the two theories.

Once an allowable percentage difference between the two theories is chosen, an approximate equivalence in the peak pressure versus rise time domain (domain of equivalence) can be established. The construction of an approximate domain of equivalence can be described by reviewing Figure 5.26. The dots on the shear beam curves in this figure show where V/V_u for the two theories differ by 10 percent for a peak pressure of 5000 psi. Each of the pairs of curves are for a specified rise time, as shown. Of interest is the peak pressure P_0 which will create an intersection between the threshold failure level ($V = V_u$) and the dots on the shear beam curves for each rise time. Since the curves are a linear function of peak pressure, the failure threshold level in Figure 5.26 will rise with a decrease in P_0 and, conversely, will drop with an increase in P_0 . This procedure will produce rise time and peak pressure combinations corresponding to a predicted direct shear failure for both theories to within a 10 percent difference.

Figure 5.27 shows this domain for the example beam in Table 5.1 with fixed beam-end and for the particular case of a 10 percent difference in V/V_u between the two theories where rate effects are not included. Peak pressure and rise time combinations of the external load that fall above the equivalence curve in Figure 5.27 indicate that the shear beam solution approximates the Timoshenko beam solution to within a maximum error of 10 percent. Curves similar to those in Figures 5.26 and 5.27 can be constructed for cases where load rate effects are considered.

5.3.2 Strain Rate Effects

In order to verify the strain rate solution for the support shear force for a viscoelastic Timoshenko beam, a similar solution for the support shear force

resulting from an analysis of a viscoelastic shear beam is developed. The governing equation of motion for a viscoelastic shear beam is given as

$$k'AGy'' + k'A\eta\dot{y}'' - \rho A\ddot{y} = -q \quad (5-69)$$

and the constitutive relationship for shear is given by the second of Equations (5-32). Equation (5-69) is solved using the same Laplace transform methods as described in Section 5.2.2.1.1.

Applying a Laplace transform to the time variable in Equation (5-69) and the initial conditions (5-63) results in the following linear ordinary differential equation in x

$$\bar{y}'' - \frac{\rho As^2}{\zeta} \bar{y} = \frac{-\bar{q}}{\zeta} \quad (5-70)$$

where $\zeta = k'A(G + \eta s)$ and all symbols are as previously defined in Section 5.2.2.1.1.

The solution to Equation (5-70) is straightforward and is given by

$$\bar{y}(x,s) = C_1 e^{px} + C_2 e^{-px} + \frac{\bar{q}(x,s)}{\rho As^2} \quad (5-71)$$

where

$$p^2 = \frac{\rho As^2}{\zeta}$$

The constants C_1 and C_2 are determined from the boundary conditions (5-62). The Laplace transform of the shear force at the left support ($x = 0$) is provided as the third relation in Equations (5-35) and is given here for the shear beam

$$\bar{V}(0,s) = -\zeta \bar{y}'(0,s) \quad (5-72)$$

Equation (5-72) is determined for a step-load condition (see Equation 5-43) by evaluating the first derivative of Equation (5-71) at $x = 0$, and is given by

$$\bar{V}(0,s) = \frac{P_0 \sinh pL}{sp(\cosh pL + 1)} \quad (5-73)$$

For early time (i.e., as s gets large) the expression for \bar{V} in (5-73) and the analogous expression in Equations (5-47) for a Timoshenko beam are equivalent since $p = p_1$ and $\cosh pL \gg 1$.

These results show that the support shear for a viscoelastic shear beam approximates the support shear for a viscoelastic Timoshenko beam for a short time period. Again, this time is the time it takes a shear wave to traverse a distance of about $0.4L$ along the beam length.

5.4 Comparisons to Data

The results of Section 5.2.3 on the construction of failure curves for direct shear failures show that a family of curves associated with different strength enhancement factors (which are functions of load rate) can be produced for a particular beam geometry. The experimental data outlined in Chapter 4 describes twelve tests which are categorized by beam geometry into three groups. While it is possible to construct a failure curve for each of the twelve tests it would not be very instructive. Instead, a failure curve is produced for each of the three groups of structures as this should be sufficient to show the information of interest in this

dissertation. This can be done because the strength enhancement factors vary among the tests by only a few percentage points and the beams within each group were all designed the same. The major variations among the tests are in the actual strength of the concrete and steel and the in peak pressure which was applied during the test. The latter will be studied here while the former will not.

Table 5.2 shows the beam geometry, reinforcement ratio, and average concrete and steel strength for each of the three test groups outlined in Chapter 4. Also shown in the table are the average load rate and strength enhancement factor Ω for each test group. The load rate for each test is determined by dividing the average peak pressure by the approximate rise time of the interface pressure measurements. The strength enhancement factor is then obtained by using the average test group load rate (assumed equal to the stress-rate) on the strength enhancement curves in Figure 3.3 for a 6500 psi concrete. A failure curve for each of these test groups could be constructed for various beam-end restraints. However, since no information is available to estimate the degree of support restraint, the most conservative assumption of a fixed beam-end condition is used here.

Figures 5.28, 5.29, and 5.30 show the direct shear failure curves for test Groups I, II, and III, respectively. Plotted with these curves are the various peak pressure and rise time pairs corresponding to each of the specific tests within each test group. The individual measured average peak pressures and rise times are listed in Table 4.3. Points that fall above these curves indicate direct shear failure as determined by elastic analysis. The observed failure modes, according to test data records, are listed in Table 5.3. Also shown in Table 5.3 for each test is an indication of whether analysis predicted a direct shear failure.

The results shown in Figures 5.28 through 5.30 and Table 5.3 show that the methods developed in this dissertation provide an adequate assessment of the likelihood of direct shear failure. Five of the six tests in Groups II and III are correctly predicted to fail in direct shear when compared to test data. In Group I tests the failure mode of four tests is correctly predicted while that of the other two tests is not correctly predicted. However, all three cases where the analytic predictions are wrong are very close to the failure curve, as seen in Figures 5.28 and 5.29. Using a model with a beam-end restraint less than the assumed fixed-end condition or a slightly lower strength enhancement factor would bring all these cases within the direct shear failure region and the predictions would match the data.

5.5 Summary

An elastic model based on the well known Timoshenko beam theory is used to develop a methodology which permits an identification of conditions necessary for the occurrence of direct shear failure prior to bending failure for different combinations of load parameters and beam-end restraint and for various beam geometries. The normal mode method is used to describe the response of an elastic beam subjected to an idealized triangular load pulse which is uniformly distributed along the span of the beam. The response in the transient region is shown to be very sensitive to higher frequencies which involve both flexure-shear and thickness-shear considerations. The Timoshenko theory is shown to be very accurate in comparison to the exact three-dimensional vibration theory for the frequency domain of interest in this study. For all cases studied, the normalized shear force is greater than the normalized bending moment at the support for a fixed-end condition, but only for the very early transient stages (less than 0.1 msec). The same is true for beam-end restraints less than fixed, except that the

time during which the normalized shear exceeds the normalized bending moment is longer.

The elastic Timoshenko equations are extended to account for viscoelastic material properties in order to model strain rate effects. Results from a Laplace solution show that strain rate amplifies shear more than bending moment in the early transient response regime. The simplified modeling of load rate indicates that both material strengths and elastic moduli are enhanced, and that the domain within which a direct shear failure will precede a flexural failure is reduced. Analysis shows that failure predictions are much more sensitive to load rate effects on strength than on elastic moduli.

A simple shear beam is shown to be an adequate substitute for a Timoshenko beam in determining the support shear force for a restricted range of load parameters. Furthermore, a Laplace solution to viscoelastic shear beam equations, which result from the influence of strain rate, verifies the Laplace solution for the support shear force of a viscoelastic Timoshenko beam, over a time domain where the solution procedure is applicable.

Failure curves developed from the elastic Timoshenko beam theory and load rate enhanced failure criteria are shown to be an adequate means for predicting the occurrence of early time transient direct shear failures in reinforced concrete beams. Failure curves developed for three groups of beams show good agreement with test data. Strength enhancement due to load rate is shown to be a very important parameter in determining the threshold between direct shear failures and flexural failures.

Chapter 6

Post Failure Models

6.1 Introduction

A brief description of the modeling of the post failure regime (see discussion in Chapter 1 and Figure 1.1) of beam response is provided here. This description includes only the basic development of deterministic and stochastic models that may be useful for an evaluation of the beam response after a direct shear failure has taken place at the support.

In reality, the actual response of a beam after it has failed in direct shear involves a mix of rigid-body motion and vibrational motion. This has been verified by experimental data of the type described in Chapter 4. In fact, roof slab deflection profiles, shown in Figures 4.21b and 4.22b for two separate tests, clearly show that the post failure (beyond 1 msec) response of beams (as models of one-way slabs) is depicted by a combination of rigid-body, flexural, and membrane modes. However, this data also shows that the predominant early time post failure response (1 msec to about 3 msec) is described primarily by rigid-body motion, resulting from a vertical translation of the roof slab at the direct shear zone near the supports. Therefore, for purposes of simplification the complex post failure behavior of beams and one-way slabs for early times is assumed to be adequately defined by rigid-body motion. These models are valid only for the early time before flexural and membrane influences become important.

Under the assumption of rigid-body vertical translation, the deterministic post failure models are described by ordinary homogeneous differential equations in

time, where motion is developed by an initial velocity and the engineering model involves only one degree of freedom -- the vertical translation. Furthermore, the deterministic models developed here serve only as an introduction to a physical problem, which is best elaborated and solved with stochastic (probabilistic) processes because of inherent uncertainties.

6.2 Simplistic Deterministic Models

As discussed in Chapter 4, the interface pressure loading near the support decays very rapidly after peak pressure is attained when a direct shear failure is realized. This drop in pressure results when the beam moves down away from the soil overburden along a "slip" surface provided by a shear zone at the time of direct shear failure. Just after this slip takes place the beam behaves as a rigid body undergoing a vertical translation as shown in Figure 6.1. In this figure the shear zone, which in reality has some non-zero width (see Figure 2.1b), has been reduced to an infinitesimal width for modeling purposes. The beam will not have an interface pressure on its surface just after failure, as described previously in Chapter 4, but it will have an initial velocity, $\dot{y}(0)$.

As shown in Figure 6.1, equilibrium of forces along the crack planes produces the following equation of motion

$$m\ddot{y}(t) + V_e(y, t) = 0 \quad (6-1)$$

where $m = \rho LA$

$V_e(y, t)$ = total shear resistance along the crack planes

The resistance term $V_e(t)$ is a function of the slip along the crack plane and its derivatives. A simple interpretation of $V_e(t)$ is to assume that the beam resists downward movement by a rate dependent force which is linearly proportional to the slip and its first time derivative. This relation can be expressed as

$$V_e(y, t) = c'(y, t) \dot{y}(t) + k(y, t) y(t) \quad (6-2)$$

where

$c'(y, t)$ = shear viscosity (pounds-seconds per inch)

$k(y, t)$ = shear stiffness (pounds per inch)

Equation (6-1) can be rewritten in the more classical form

$$m \ddot{y}(t) + c'(y, t) \dot{y}(t) + k(y, t) y(t) = 0 \quad (6-3)$$

The model described by Equation (6-3) and shown in Figure 6.1 will have general initial conditions

$$\begin{aligned} y(0) &= x_0 \\ \dot{y}(0) &= v_0 \end{aligned} \quad (6-4)$$

where x_0 and v_0 are the initial slip and beam velocity, respectively, at the instant of a direct shear failure.

Equation (6-3) describes a simple model of the phenomenon taking place along the shear plane shown in Figure 6.1, assuming rigid-body motion. An implicit assumption of the model is that identical behavior is taking place at both supports. Equation (6-3) can be a nonlinear equation, or a linear equation with either

constant or variable coefficients depending on the form of $c'(y,t)$ and $k(y,t)$. The shear stiffness k , as a function of the slip y , can be found from the shear resistance versus slip relationships developed by Hawkins '81. In fact, Hawkins' relationships have been used in a recent finite element investigation by Murtha and Holland '82.

Equation (6-3) can be simplified under certain limiting conditions. For cases where the rate effects are small, $c'(y,t)y(t)$ can be neglected. For conditions where the initial resistance to slip is small and the relative velocity is high, the term $k(y,t)y(t)$ may be negligible compared to the term $c'(y,t)y(t)$. This can be the case for a precracked shear plane as shown in Figure 6.2. This phenomenon occurs when the initial slip is related to the crack width and is associated with little resistance. Figure 6.2b shows a single crack in concrete whose surface asperities are idealized by a sawtooth pattern. The initial crack width is w_0 and the crack faces are inclined at an angle θ' as shown. Application of shear force after a crack has formed will at first cause a slip of magnitude $\delta_0 = w_0 \cot \theta'$ until contact is made between opposing faces of the crack. During this stage only the reinforcing bars crossing the crack provide restraint by dowel action and the crack stiffness is equal to the dowel stiffness. After aggregate interlock is mobilized when the crack faces contact, the crack stiffness is the sum of the interface shear stiffness and the dowel stiffness, as shown in Figure 6.2a (Buyukozturk '79).

For the case where rate effects dominate shear resistance, the equation of motion is

$$m\ddot{y}(t) + c'(y,t)\dot{y}(t) = 0 \quad (6-5)$$

In this case the term $c'(y,t)\dot{y}(t)$ can be thought of as an equivalent resistance due to dynamic friction between two surfaces undergoing a relative velocity $\dot{y}(t)$. Unfortunately, little or no data exists to empirically establish the value of $c'(y,t)$ for cracked concrete. A testing program on pushoff specimens under static and dynamic loads is needed for this purpose.

The solution to Equations (6-1) to (6-5) is straightforward and is not presented here. It is necessary to reiterate that these beam models are described by rigid-body motion and that the solution $y(t)$ is only valid until the beam experiences flexural and membrane influences. Then the models are described by partial differential equations and may become inhomogeneous with a reloading term and they must also include the displacement $y(t)$ and velocity $\dot{y}(t)$ as initial conditions at the point of reloading.

6.3 Stochastic Models

Continuous time, continuous state Markov processes (also termed diffusion models) are fashioned from the deterministic models developed in Section 6.2 of this chapter. These Markov processes are formulated through the stochastic analogs of equations such as (6-3) and (6-5). These equations are known as stochastic differential equations.

In the deterministic world Equation (6-3) represents an ideal balance between inertial forces and resistive forces. However, in the real world, hereafter called the stochastic world, an error term results from our inability to define an adequate

model of reality. For example, the actual force balance may involve terms with nonlinear coefficients or terms with higher order derivatives of $y(t)$. Hence, the error expresses the difference between reality and the model represented by Equation (6-3).

This error term expresses the uncertainty in the equilibrium arising from an inexact choice of coefficients or from neglecting other features of the real model. In the time domain this error is expected to fluctuate randomly back and forth about the true equilibrium value of zero. And although the expected value of this error is zero under conditions where the true inertial forces and resistive forces are known "a priori", its general bounds are diffuse. Such an error term has been successfully modeled by white noise in electrical and mechanical systems where the "noise" is actually a random fluctuation of the system about its equilibrium state.

Because white noise is the derivative of the Wiener process, it provides for independent increments between perturbations of the forcing function. The Wiener process is the only continuous path, stationary independent increment process. The Poisson process has these characteristics for discrete time but its derivative is zero. If the independence requirement is dropped, other random forcing functions can be used to describe the error term.

If Equation (6-1) is rewritten to consider a random error source $\dot{W}(t)$ and random initial conditions on the actual response $y(t)$, the following stochastic differential equation results,

$$m\ddot{X}(t) + V_e(X(t), t) = \dot{W}(t), \quad t \geq 0 \quad (6-6)$$

where $X(t)$ is a transverse displacement stochastic process and $\dot{W}(t)$ is a white noise random process that is the derivative of the Wiener process (which is a diffusion process) with mean 0 and variance σ^2 .

The assumption of a white noise error term $\dot{W}(t)$ actually can be envisioned from a more heuristic and intuitive approach. In the stochastic world the difference between the inertial forces and the shear resistive forces is expected to fluctuate randomly about the current equilibrium position as the process evolves in time, much in the same way as particles suspended in a fluid randomly fluctuate under the influence of a disturbing force. This fluctuation is known as Brownian motion (Brownian motion was first observed by R. Brown in 1828, was later studied by A. Einstein in 1905 and was formulated mathematically by Norbert Wiener in 1930). If the initial position of the error term is zero, and if the magnitude and sign of the error from time step to time step is random and not influenced by any physical perturbation, and if the error at successive times is not influenced by the magnitude or sign of any previous error terms, then the equilibrium process is modeled by a Wiener process, $W(t)$.

The Wiener process has the following properties (see Hoel, Port and Stone '72)

- (i) $W(0) = 0$
- (ii) $W(t) - W(u)$ is normally distributed with mean 0 and variance $\sigma^2(t-u)$
for $u < t$
- (iii) $W(t_2) - W(t_1), W(t_3) - W(t_2) \dots W(t_n) - W(t_{n-1})$ are independent increments for $t_1 < t_2 < \dots < t_n$

The first property simply results from the choice of coordinate systems and is arbitrary. The second property follows from the central limit theorem. In addition, the Wiener process is a continuous path process which is nowhere differentiable (i.e., $\dot{W}(t)$ does not exist). This means that white noise $\dot{W}(t)$, although physically an abstraction arising from the chaotic path structure of the Wiener process, is only mathematically useful when it is integrated in time as it is in the solution of stochastic differential equations. Hence, white noise arises from the Wiener process which has several nice features for modeling purposes. It is a Markov process, it is a Gaussian process, it has stationary independent increments (but is not stationary itself), and has a continuous state or path function.

Before finishing this specific area of stochastic differential equations it is beneficial to look at a process that is a simple transformation of the Wiener and that arises from the stochastic equivalent of Equation (6-5). This process, called the Ornstein-Uhlenbeck process (see Uhlenbeck and Ornstein '30), is an exponentially damped Wiener process with a scaled time domain. The Ornstein-Uhlenbeck process, denoted $U(t)$, is actually a nicer model in that it has all the properties of the Wiener plus it has a limiting stationary distribution with a constant variance σ^2 . For special initial conditions this process can be stationary at all times. Both the Wiener and Ornstein-Uhlenbeck processes are shown in Figure 6.3. Two example problems are discussed to show the possible applications of these two stochastic processes on the models posed in Section 6.2 of this chapter.

6.3.1 Shear Slip Model: Wiener Process

6.3.1.1 Moments

If Equation (6-2) is simplified by neglecting rate effects and by assuming a constant shear stiffness the resulting stochastic differential equation has the form of Equation (6-6) and is given by

$$m\ddot{X}(t) + kX(t) = \dot{W}(t), \quad t \geq 0 \quad (6-7)$$

The general solution $X(t)$ of the second order Equation (6-7) on the time interval (t_0, ∞) involves the use of stochastic integration and is given by the relation

$$X(t) = X(t_0)\phi_1(t-t_0) + \dot{X}(t_0)\phi_2(t-t_0) + \int_{t_0}^t h(t-u)dW(u), \quad t \geq t_0 \quad (6-8)$$

where $X(t_0)$ and $\dot{X}(t_0)$ are general random initial conditions at time t_0 , $\phi_1(t-t_0)$ are differentiable solutions to the homogeneous version of Equation of (6-7), and the integral in Equation (6-8) represents the particular solution to Equation (6-7) which involves the impulse response function $h(t-u)$.

The impulse response function is specified as

$$h(t-u) = \begin{cases} \frac{\phi_2(t-u)}{m} & , t \geq u \\ 0 & , t < u \end{cases} \quad (6-9)$$

Another feature in the particular integral of Equation (6-8) is the substitution

$$dW(u) = \dot{W}(u)du \quad (6-10)$$

Since the derivative of the Wiener process, white noise, is not a stochastic process in the probabilistic sense, $dW(u)$ is a functional that assigns values to the integral in Equation (6-8).

The specific solution to Equation (6-7) for the case $t_0 = 0$ is found to be

$$X(t) = X(0)\cos\omega t + \frac{\dot{X}(0)}{\omega}\sin\omega t + \frac{1}{m\omega} \int_0^t \sin\omega(t-u)dW(u), \quad (6-11)$$

$t \geq 0$

where $\omega^2 = k/m$. Equation (6-11) represents a stochastic process whose uncertainty comes from the randomness of both the white noise term and the initial conditions. The equation is still valid for the special case of deterministic initial conditions.

The problem is further developed by looking at the probabilistic structure of $X(t)$. The mean or expected value, denoted as $E\{\cdot\}$, is given by

$$E\{X(t)\} = \cos\omega t E\{X(0)\} + \frac{\sin\omega t}{\omega} E\{\dot{X}(0)\} \quad (6-12)$$

Since the mean of the Wiener process is zero the expected value of the stochastic integral in Equation (6-11) vanishes. The mean square of the solution process, denoted $E\{x^2\}$, is

$$E\{X^2(t)\} = \cos^2\omega t E\{X^2(0)\} + \frac{\sin^2\omega t}{\omega^2} E\{\dot{X}^2(0)\} + \frac{\sigma^2}{mk} \left\{ \frac{t}{2} - \frac{\sin 2\omega t}{4\omega} \right\} \quad (6-13)$$

where σ^2 is the variance of the Wiener process. The left-hand side of Equation (6-7) is not stable since the solution (6-11) does not vanish as $t \rightarrow \infty$. Because this system does not have a convergent solution as $t \rightarrow \infty$ the covariance function is not defined for the stationary case. However, the process $X(t)$ is a Gaussian process because of the Gaussian structure of the Wiener process.

For the special case where the initial conditions are deterministic and are specified as $X(0) = 0$ and $\dot{X}(0) = v_0$, the mean and variance of $X(t)$ are

$$E\{X(t)\} = \frac{v_0 \sin \omega t}{\omega} \quad (6-14)$$

$$\text{Var}\{X(t)\} = \frac{\sigma^2}{mk} \left\{ \frac{t}{2} - \frac{\sin 2\omega t}{4\omega} \right\} - \frac{v_0^2 \sin^2 \omega t}{\omega^2}$$

The initial velocity v_0 is estimated from a deterministic analysis or from experimental data. An example of the latter is given in Figure 6.4 for three different tests. The asterisk on the curves in Figure 6.4 corresponds to the point of incipient direct shear failure.

Before leaving the formulation of this particular problem, it is also possible to model a situation where the slab is reloaded while still in a rigid-body mode. In this case Equation (6-7) is altered to account for another term on the right hand side

$$m\ddot{X}(t) + kX(t) = q(t) + \dot{W}(t), \quad t \geq 0 \quad (6-15)$$

where $q(t)$ represents an interface pressure on the beam at the reload condition. Closed form solutions to the stochastic differential Equation (6-15) are available if $q(t)$ is either deterministic or is a second order stationary process.

6.3.1.2 First Passage Probability

The strong Markov property of the Wiener process allows for the determination of first passage (also termed first crossing, first hitting, and absorption) statistics of the stochastic process $X(t)$. It is often useful to determine the probabilistic structure of the time at which the process $X(t)$ first exceeds a given barrier or threshold. In the particular example of a post failure model it is interesting to estimate the time at which the vertical translation along the shear plane, $X(t)$, first reaches a yield displacement. This displacement has been determined in tests (see Hawkins '81).

In accordance with the strong Markov property the only condition needed to determine this probability is that the process has not exceeded the threshold at any time prior to the time of interest. In statistical notation the definition of the first passage probability to a barrier of magnitude "a" is given by

$$\Pr\{T_a < t\} = \Pr\left\{\max_{0 \leq u \leq t} X(u) > a \mid X(0) = 0\right\} \quad (6-16)$$

The expression (6-16) is equivalent to saying: the probability of the first passage time T_a being less than time t , is equal to the probability that the maximum value of the process $X(t)$ exceeds the barrier "a" at some time in the interval $(0,t)$, given

that the process starts at zero at $t = 0$. Using the reflection principle adopted in Karlin and Taylor '75 for second order processes, this probability is expressed as

$$Pr \{T_a < t\} = 2 \int_a^{\infty} f_x(u) du \quad (6-17)$$

where $f_x(u)$ is the probability density function of the process $X(t)$, which is determined from the probability structure given by the second order moments in (6-12) and (6-13). Since $X(t)$ is Gaussian, Equation (6-17) is further simplified to

$$Pr \{T_a < t\} = 2 \left\{ 1 - \Gamma \left(\frac{a - m_x(t)}{\sigma_x(t)} \right) \right\} \quad (6-18)$$

where $m_x(t) = E \{X(t)\}$

$$\sigma_x^2(t) = \text{Var} \{X(t)\}$$

Γ = standardized normal distribution

Finally, the probability density function of T_a is obtained by differentiating the right hand side of Equation (6-18) with respect to time. The resulting density function is a second order process but is not, in general, Gaussian.

6.3.2 Shear Slip Rate Model: Ornstein-Uhlenbeck Process

6.3.2.1 Moments

As mentioned earlier, Equation (6-5) has a stochastic analog represented by the Ornstein-Uhlenbeck process, $U(t)$, under the condition that the coefficient $c'(y,t)$ is a constant. The resulting stochastic differential equation describing the

uncertainty in the force balance along a shear plane between beam inertia and the viscous resistance is given as

$$m\ddot{X}(t) + c'\dot{X}(t) = \dot{W}(t), \quad t \geq 0 \quad (6-19)$$

with initial conditions where

$$X(0) = x_0$$

$$\dot{X}(0) = v_0$$

The solution to this equation is well documented (see Hoel, Port and Sone '72 and Karlin and Taylor '75) in the literature and is shown to be

$$X(t) = x_0 - \frac{v_0}{2} (e^{-\alpha t} - 1) - \frac{1}{m\alpha} \int_0^t \left\{ e^{-\alpha(t-u)} - 1 \right\} dW(u), \quad t \geq 0 \quad (6-20)$$

with $\alpha = c'/m$

The mean and variance of $X(t)$ are computed to be

$$E\{X(t)\} = x_0 - \frac{v_0}{2} (e^{-\alpha t} - 1) \quad (6-21)$$

$$\text{Var}\{X(t)\} = \frac{\sigma^2 m}{2c'^3} (4e^{-\alpha t} - e^{-2\alpha t} + 2\alpha t - 3)$$

The process $X(t)$ is Gaussian and is actually the integral of the Ornstein-Uhlenbeck process. The constant α is sometimes referred to as the damping factor. As the

process evolves in time, α tends to constantly damp or pull the position of the process back to its initial value.

Because of the special nature of Equation (6-19), a complete closed form probabilistic description of the velocity process $X(t)$ is available. Equation (6-19) is written as

$$\dot{U}(t) + \alpha U(t) = \dot{W}(t), \quad t \geq 0 \quad (6-22)$$

where $U(t) = \dot{X}(t)$.

The solution to this equation is described in the literature as the Ornstein-Uhlenbeck process (Hoel, Port and Stone '75 refer to it as Langevins' velocity process). This process is a diffusion process which, in the limit, is stationary Gaussian with the following moments

$$E\{U(t)\} = v_0 e^{-\alpha t} \quad (6-23)$$

$$\text{Var}\{U(t)\} = \frac{\sigma^2}{2c'm} \{1 - e^{-2\alpha t}\}$$

If v_0 has a zero mean and a variance equal to $\sigma^2/2c'm$, then $U(t)$ is normally distributed with mean zero and variance σ^2 . The $X(t)$ and $U(t)$ processes are related by the following relationship

$$X(t) = x_0 + \int_0^t U(u) du \quad (6-24)$$

6.3.2.2 First Passage Probability

Absorption probabilities for $U(t)$ are not available in closed form, because in the computation of these probabilities natural logarithms must be evaluated at zero. To overcome these problems Dirake '75 proposed an asymptotic approximation to the first passage probabilities of a special standardized $U(t)$ process which was later corrected by Jennen '81. This asymptotic approximation is actually developed from the "tied-down Wiener" process (this process is also called a Brownian Bridge). The approximation becomes less accurate near the probabilities of zero and one for the case where the absorption barrier approaches infinity.

For a standardized Ornstein-Uhlenbeck process $U(t)$, with mean zero and variance one, the first passage probability as $a \rightarrow \infty$ is approximated by

$$Pr \left\{ \max_{0 \leq t \leq \epsilon} |U(t)| \geq a \right\} \approx \sqrt{\frac{2}{\pi}} e^{-\frac{a^2}{2}} \left\{ \epsilon a - \frac{\epsilon}{a} + \frac{2}{a} \right\} \quad (6-25)$$

where

$$\epsilon = \frac{1}{2} \log_e \left\{ \frac{t_2(1-t_1)}{t_1(1-t_2)} \right\}; \quad 0 < t_1 < t_2 < 1$$

In the expression above, the times t_1 and t_2 are the upper and lower bounds, respectively, for determining the absorption probabilities of the associated tied-down Wiener process. All times are nondimensionalized to a characteristic time of the problem such that the time domain of interest is $0 < t < 1$.

6.4 Summary

Simple linear deterministic and stochastic models are introduced to simulate the rigid-body behavior of a beam just after a direct shear failure has occurred. This

motion is created when vertical translation occurs at a shear zone near the supports. The models account for the stiffness effects due to dowel action and aggregate interlock and the viscous effects associated with the rate of response. Stochastic differential equations are developed from analogous deterministic models in an effort to account for random uncertainties inherent in a linear model and randomness in initial conditions at the time of a direct shear failure. Solutions for first passage probabilities are provided for two cases of simple stochastic models based on Markovian diffusion processes.

Chapter 7

Summary and Conclusions

7.1 Summary

Most previous studies dealing with direct shear failures in reinforced concrete have been associated with static loads, where failure mechanisms were postulated in terms of static equilibrium. In these studies parameters such as dowel action, reinforcement ratio, and shear span were found to have an important influence on direct shear behavior. In two dynamic test programs reported on direct shear failure in reinforced concrete specimens, the relevant findings were that the dynamic strength in direct shear generally is 30 to 90 percent greater than the static strength and that the presence of dowel steel improves the ductility at the crack plane. These findings modestly improved our knowledge of the strength of reinforced concrete in direct shear due to dynamic loads.

Recent tests conducted on reinforced concrete slabs under high explosive distributed impulsive pressures have provided additional information on the strength of members in a presumed direct shear mode, but relatively little understanding about the actual dynamic mechanism in direct shear and about the influence of moment on failure. For this reason the analytic effort described in this dissertation was undertaken for the purpose of understanding the transient influences occurring at the support of an impulsively loaded beam and for the purpose of developing a procedure to predict the conditions necessary for a dynamic direct shear failure.

To understand the conditions necessary for a direct shear failure, an elastic Timoshenko beam model is used to ascertain whether the support shear or the support bending moment attains its respective failure threshold first. These threshold levels are specified in terms of the maximum capacity of the reinforced concrete section in either a direct shear or a flexure failure mode. The Timoshenko theory is extended to account for the effects of rotational beam-end restraint and strain rate on the conditions necessary for direct shear failure. Failure curves, developed from an elastic Timoshenko beam and augmented to account for strength enhancement due to load rate, are compared to experimental evidence to determine the adequacy of the model in predicting direct shear failure.

Simple diffusion processes (continuous time and continuous state Markov processes) are proposed as adequate models for the early-time rigid-body motion of a beam after an initial elastic direct shear failure occurs. These stochastic models are linear and can treat random uncertainties in the loading and initial conditions. Shear-slip data from static tests, and slip displacement versus time and beam velocity data from dynamic tests are available to assess the adequacy of these post failure models.

7.2 Conclusions

Analytic results based on the five major assumptions outlined in Chapter 1 have revealed several conclusions regarding dynamic direct shear failure issues. These conclusions are based on an elastic analysis of a uniform beam subjected to idealized distributed loadings where failure is defined by the shear force or bending moment at the support exceeding prescribed threshold levels.

The first, and perhaps most fundamental, conclusion is that an elastic Timoshenko beam model gives a clear picture of the transient influences of shear and bending moment and is an accurate substitute for the exact three dimensional elastic theory for the frequencies of interest in this work.

Second, based on the elastic model used in this study, direct shear failures precede flexural failures in the early transient response regime for certain combinations of load parameters and beam-end restraint conditons.

Third, strain rate effects enhance support shear forces more than support bending moments for impulsive loads applied normal to the axis of the beam. This conclusion reinforces both the issues of early stage dominance of shear over bending moment and early time occurrence of direct shear failure.

Fourth, strength enhancement due to load rate effects increases failure levels and hence restricts the domain of load parameters over which direct shear failures are predicted. Load rate effects on elastic properties have the opposite influence on the domain of load parameters but this influence is small in comparison to rate effects on strength.

Fifth, the influence of beam-end restraint is to alter the magnitude of the support bending moment much more than it alters the support shear force. Thus, a decrease in the beam-end restraint increases the domain of predicted direct shear failures.

Sixth, a simple shear beam is found to reasonably approximate a Timoshenko beam in terms of the support shear force for a restricted set of conditions on load parameters.

Seventh, direct shear failure curves developed from elastic Timoshenko beam theory are found to be in good agreement with experimental data when strength enhancement due to load rate is taken into account. The comparison between analysis and experiment is made in the peak pressure versus rise time domain of idealized triangular loadings on fixed-end beams with the same properties as one-way slabs actually tested.

7.3 Recommendations for Future Work

No research area is fully exhausted in terms of additional enlightenment. Such is the case for this research. The work of this dissertation has revealed several areas where additional research can be focused in the future. A list of some of these additional considerations is provided here in the event that future research in the area of direct shear failures is attempted by other investigators. It is hoped that the results presented in this dissertation can be helpful in providing a base on which to expand or alter further investigations.

Recommendations for improving the work outlined here will involve assessing the impact of the five major assumptions on the conclusions of this dissertation. For example, concerning the first major assumption (see Section 1.2), a three dimensional finite element study of the support region would help reveal the influence of waves propagating through the thickness of the beam. A finite

element study should also incorporate inelastic features such as cracking and loss of bond and yielding in the longitudinal steel.

Perhaps the most crucial need for increased effort is in the area of failure criteria. This work considered only two failure modes — direct shear and flexure. There are actually two other possibilities for failure between the cases of direct shear and flexure. These transition modes, termed deep beam response and diagonal tension, need to be studied more fully to determine the expected failure mode. This is especially true for failure predictions which fall very close to the failure curves developed here.

It is recommended that more dynamic shear tests on plain concrete and reinforced concrete elements be performed in an effort to ascertain whether shear transfer mechanisms under impulsive loads relate to those seen in static tests. Active instrumentation should be used to allow for the interpretation of cracking on element response. These tests could be conducted on push off specimens so that as many parameters as possible can be controlled and replicated. It is also recommended that static experiments of shear and moment interaction be extended to dynamic loads.

Another area requiring effort is the influence of in-plane loads on direct shear failures. Many static studies, including those by Mattock '74, have shown that in-plane compression substantially increases direct shear resistance. This effect was neglected in this study because experiments show that in-plane loads occur at times later (greater than 1 msec) than the time to presumed failure.

The presence of confining steel stirrups in reinforced concrete beams has a very beneficial influence on strength and ductility in a diagonal tension failure mode. Stirrups do not have much effect on direct shear failures, except that they do provide confinement which improves concrete shear strength, and they do increase the effects of dowel action at cracks near a stirrup. Studies on stirrup influences on shear resistance under dynamic conditions would be helpful.

This work has presented an analysis procedure for beams and one-way slabs. The theory can be extended to two-way slabs by using the two-dimensional equivalent of the Timoshenko beam, the Mindlin plate theory. Analyses of this nature can verify the anomalous behavior of slabs near corners where box walls intersect.

Results acquired in this dissertation show that beam-end restraints have pronounced influences on the time to direct shear failure. However, no studies could be found for the case of impulsive loading where the true degree of restraint could be estimated. Because of this, a conservative assumption based on a fixed beam-end condition was used in this study. The results presented here can be enhanced considerably with an analytic or experimental study of beam-end restraint effects on direct shear failure.

Rate effects on response and failure criteria requires significant study and advancement. Rate effects have been found to be very important on time to failure and on failure criteria. The models used here to characterize rate effects are simple, and much more work is needed to assess the influence of these effects on direct shear failures. An initial step in this direction would be to evaluate the

effect of different strength enhancement factors on the direct shear and moment failure criteria.

Stochastic modeling efforts need to be pursued more vigorously. This is especially apparent when the large uncertainties in concrete properties, failure modes, and load transfer mechanisms are to be adequately accounted for in an engineering model. A simple preliminary assessment of uncertainty in the support shear force could be achieved by analyzing a shear beam with random properties. The shear beam has been shown in this study to be a good model under limited conditions, and it has the added advantage of being associated with a simple mathematical composition.

The field of direct shear failure in reinforced concrete under dynamic loads largely has been neglected analytically because these failures can be avoided judiciously through conservative designs. However, rising construction costs portend an emphasis on understanding the behavior of reinforced concrete elements near joints and supports where failures typically occur. Direct shear is important at these locations and hence requires much more study.

References

Air Force Systems Command (AFSC), Space and Missile Systems Organization, "Construction Joint Test Program", Karagozian and Case Structural Engineers Final Report, January 1973.

American Concrete Institute, ACI 318-77. Building Code Requirements for Reinforced Concrete, Chapter 11, Shear and Torsion, December 1977.

American Society of Civil Engineers, Report, Finite Element Analysis of Reinforced Concrete, 1982.

Anderson, G.M., "Timoshenko Beam Dynamics", ASME Journal of Applied Mechanics, September 1971, pp. 591-594.

Bazant, Z.P. and Byung H.O., "Strain Rate Effect in Rapid Triaxial Loading of Concrete", ASCE Journal of Engineering Mechanics, Vol. 108, No. EM5, October 1982, pp. 764-782.

Birkeland, P.W., and Birkeland, H.W., "Connection in Precast Concrete Construction", Journal of the American Concrete Institute, Proceedings, Volume 63, No. 3, March 1966.

Bleich, H.H. and Shaw, R., "Dominance of Shear Stresses in Early Stages of Impulsive Motion of Beams", Transactions of the ASME, Journal of Applied Mechanics, March 1960, pp. 132-138.

Bresse, M. "Cours de Mechanique Applique", Mallet Bachelier, Paris, 1859, p. 126.

Bresler, B., "Reinforced Concrete Engineering - volume I", John Wiley & Sons, 1974.

Brown, R., Philosophy Magazine, Second Ser., Vol. 4, 1828, p. 161.

Buyukozturk, O., et. al., "Research on Modeling Shear Transfer in Reinforced Concrete Nuclear Structures", Nuclear Engineering and Design, Vol. 59, No. 1, August 1979, pp. 67-84.

Chen, W.F., "Plasticity in Reinforced Concrete", McGraw-Hill, 1982.

Chung, H.W., "Shear Strength of Concrete Joints Under Dynamic Loads", Journal of the Concrete Society, Vol. 12, No. 3, March 1978, pp. 27-29.

Colton, J.D., "Multiple Fracture of Beams and Plates Under Localized Impulsive Loading", Ph.D. Dissertation, Stanford University, November 1973.

Cowell, W.L., "Dynamic Tests of Reinforcing Steels", US Navy Civil Engineering Laboratory, AD622554, Sept., 1965.

Crandall, S.H., et. al., "Dynamics of Mechanical and Electro-Mechanical Systems", McGraw-Hill, 1968.

- Cruni, R.G., "Tensile Impact Tests for Concrete Reinforcing Steels", *ACI Journal*, Vol. 56, No. 1, p. 59, July 1959.
- Davies, I., "Studies on the Response of Reinforced Concrete Structures to Short Duration Dynamic Loads", ISE/BRE International Seminar, Garston, Watford, England, Nov., 1981.
- Dirkse, J.P., "An Absorption Probability for the Ornstein-Uhlenbeck Process", *Journal of Applied Probability*, Vol. 12, 1975, pp. 595-599.
- Dulacska, H., "Dowel Action of Reinforcement Crossing Cracks in Concrete", *Journal of the American Concrete Institute*, Volume 69, No. 12, December 1972.
- Einstein, A., *Ann. der Physik*, Vol. 17, 1905, p. 549.
- Fenwick, R.C., and Paulay, T., "Mechanisms of Shear Resistance of Concrete Beams", *Journal of the Structural Division, ASCE*, Volume 94, No. ST10, October 1968, pp. 2325-2350.
- Fung, Y.C., "Foundations of Solid Mechanics", Prentice-Hall, 1965.
- Gerstle, K.H. et al., "Behavior of Concrete Under Multiaxial Stress States", *Journal of Engineering Mechanics Division, ASCE*, 1980.
- Hansen, R.J., Nawy, E.G. and Shah, J.M., "Response of Concrete Shear Keys to Dynamic Loading", *Journal of the ACI*, Vol. 57, May 1961, pp. 1475-1490.
- Hawkins, N., "Dynamic Shear Resistance of Reinforced Concrete" Letter report to U.S. Navy, 28 August 1981.
- Herrmann, G., "Forced Motions of Timoshenko Beams", *ASME Journal of Applied Mechanics*, March 1955, pp. 53-56.
- Hermansen, B.R., "Shear Failure in Reinforced Concrete Brackets", MS Thesis, Civil Engineering Dept., Heriot-Watt University, Edinburgh, Scotland, Sept., 1972.
- Hoel, Port and Stone, "Introduction to Stochastic Processes", Houghton-Mifflin, 1972.
- Houde, J. and Mirza, M.S., "A Finite Element Analysis of Shear Strength of Reinforced Concrete Beams", *ACI Publication SP-42*, 1974.
- Huang, T.C., "The Effect of Rotary Inertia and of Shear Deformation on the Frequency and Normal Mode Equations of Uniform Beams With Simple End Conditions", *ASME Journal of Applied Mechanics*, December 1961, pp. 579-584.
- Jennen, C., "Asymptotische Bestimmung von Kenngrößen Sequentieller Verfahren", University of Heidelberg Dissertation, 1981.
- Jimenez, R., Gergely, P., and White, R.N., "Bond and Dowel Capacities of Reinforced Concrete", *Journal of the American Concrete Institute*, Volume 76, No. 1, January 1979, pp. 73-92.

Karlin and Taylor, "A First Course in Stochastic Processes", Academic Press, Second Edition, 1975.

Kemp, E.L., and Wilhelm, W.J., "An Investigation of the Parameters Influencing Bond Behavior with a View Towards Establishing Design Criteria", Report No. WVDOH 46-2, Department of Civil Engineering, West Virginia University, 1977.

Kiger, S.A. and Getchell, J.V., "Vulnerability of Shallow-Buried Flat-Roof Structures, FOAM HEST 1 and 2", US Army Waterways Experiment Station Report SL-80-7, Sept., 1979.

Kiger, S.A. and Slawson, T.R. "Data Reports For Dynamic Shear Tests" Two reports, FY81 and FY82, September 1981 and July 1982, U.S. Army Corps of Engineers, Waterways Experiment Station.

Krefeld, W.J., and Thurston, C.W., "Contribution of Longitudinal Steel to Shear Resistance of Reinforced Concrete Beams", Journal of the American Concrete Institute, Volume 63, No. 3, March 1966.

Kriz, L.B. and Raths, C.H., "Connections in Precast concrete Structures: Strength of Corbel Brackets", PCI Journal, Vol. 10, No. 1, 1965, pp. 16-61.

Lamb, H., "On Waves in an Elastic Plate", Proceedings of the Royal Society, Series A, Vol. 93, 1917, pp. 223-251.

Mattock, A.H., "Effect of Moment and Tension Across the Shear Plane on Single Direction Shear Transfer Strength in Monolithic Concrete", Report No. SM-74-3. Department of Civil Engineering, University of Washington, October 1974.

Mattock, A.H., "Shear Transfer Under Monotonic Loadings Across an Interface Between Concrete Cast at Different Times", Report SM-76-3, Dept. of Civil Engineering, University of Washington, September, 1976.

Mattock, A.H. and Hawkins, N.M., "Shear Transfer in Reinforced Concrete -Recent Research", Journal of the Prestressed Concrete Institute, Volume 17, No. 2, March-April, 1972, pp. 55-75.

Mast, R.F., "Auxiliary Reinforcement in Concrete Connections", ASCE Journal of the Structural Division, Proceedings, Volume 94, ST6, June 1968.

Mindlin, R.D., "Influence of Rotary Inertia and Shear on Flexural Motions of Isotropic Elastic Plates", Journal of Applied Mechanics, Vol. 18, 1951, pp. 31-38.

Mindlin, R.D. and Deresiewicz, H., "Timoshenko's Shear Coefficient for Flexural Vibrations of Beams", Proceedings of the Second U.S. Congress of Applied Mechanics, June 1954, Ann Arbor, Michigan, pp. 175-178.

Murtha, R.N. and Holland, T.J., "Analyses of WES FY82 Dynamic Shear Test Structures", US Navy Civil Engineering Laboratory Report No. 51-83-02, December 1982.

Newland, D.E., "An Introduction to Random Vibrations and Spectral Analysis", Longman, 1975.

Nichols, R., "Composite Construction Materials Handbook", Prentice Hall, 1976.

Park R. and Paulay T., "Reinforced Concrete Structures", Wiley, 1975.

Paulay, T. and Loeber, P.S., "Shear Transfer by Aggregate Interlock", Shear in Reinforced Concrete, Volume 1, Special Publication SP-42, American Concrete Institute, 1974.

Paulay, T., Park, R., and Phillips, M.H., "Horizontal Construction Joints in Cast-in-Place Reinforced Concrete", Shear in Reinforced Concrete, Volume 2, Special Publication SP-42, American Concrete Institute, 1974.

Rayleigh, Lord, "Theory of Sound", first edition, Cambridge, England, 1877. Current Second edition, MacMillan Company, New York, 1945, p. 293-294.

Reinhardt, H.W., and Walraven, J.C., "Shear Transfer in Reinforced Concrete with Small Crack Widths", Preprint 80-012, ASCE Convention, Portland, April, 1980.

Rinehart, J.S. "Fracturing Under Impulsive Loads", Seminar to the Air Force Weapons Laboratory, Albuquerque, New Mexico, July 1979.

Sharma, N.K., "Splitting Failures in Reinforced Concrete Members", Ph.D. Thesis, Department of Structural Engineering, Cornell University, Ithaca, New York, 1969.

Somerville, G., "The Behavior and Design of Reinforced Concrete Corbels", ACI Special Publication SP-42, Vol. 2, 1974.

Taylor, H.P., "The Fundamental Behavior of Reinforced Concrete Beams in Bending and Shear", Shear in Reinforced Concrete, Volume 1, Special Publication SP-42, American Concrete Institute, 1974.

Timoshenko, S.P., "On the Correction for Shear of the Differential Equation for Transverse Vibrations of Prismatic Bars," Philosophical Magazine, series 6, Vol. 41, 1921, pp. 744-746.

Timoshenko S., Young D.A., Weaver, W., "Vibration Problems in Engineering" Fourth Edition, Wiley, 1974, pp. 432-435.

Uhlenback, G.D. and Ornstein, L.S., Phys. Rev., Vol. 36, 1930, p. 823.

Watstein, D. and Boresi, A.P., "The Effect of Loading Rate on the Compressive Strength and Elastic Properties of Plain Concrete", National Bureau of Standards Report 1523, 1001-22-4703, March 1952 and ACI Journal, Volume 24, 1953 page 729.

Wiener, N., "Generalized Harmonic Analysis", Acta. Math., Vol. 55, 1930, p. 117.

Wong, F.S. "A Study of the Effect of Structure/Medium Interaction on the Loading on a Buried Structure", Technical Report R7864, Weidlinger Associates, Nov 1978, Menlo Park, California.

Wylie, C.R., "Advanced Engineering Mathematics", Fourth Edition, McGraw-Hill, 1975.

Tables

Table 4.1
Test Groups and Test Designations

<u>Group I</u>	<u>Group II</u>	<u>Group III</u>
FH1	DS2-1	DS2-4
DS1-1	DS2-2	DS2-5
DS1-2	DS2-3	DS2-6
DS1-3		
DS1-4		
DS1-5		

Table 4.2
Physical Parameters For Each Test Group

<u>Group I</u>	<u>Group II</u>	<u>Group III</u>
$L/d = 10$	$L/d = 7$	$L/d = 7$
$L/t = 8.6$	$L/t = 6.1$	$L/t = 6.1$
$3710 < f'_c(\text{psi}) < 5840$	$6955 < f'_c(\text{psi}) < 7328$	$6955 < f'_c(\text{psi}) < 7328$
$62750 < f_y(\text{psi}) < 74700$	$f_y \approx 79,500 \text{ psi}$	$f_y \approx 67,340 \text{ psi}$
$\rho_s = 0.01 \text{ (each face)}$	$\rho_s = 0.0075 \text{ (each face)}$	$\rho_s = 0.012 \text{ (each face)}$

Table 4.3
Summary of Test Results

<u>Test</u>	<u>Average Peak Pressure (psi)</u>	<u>Rise Time (msec)</u>
Group I		
FH1	1500	0.05
DS1-1	4000	0.05
DS1-2	4700	0.07
DS1-3	3300	0.05
DS1-4	3500	0.05
DS1-5	5000	0.10
Group II		
DS2-1	6000	0.05
DS2-2	6000	0.10
DS2-3	3200	0.05
Group III		
DS2-4	6000	0.05
DS2-5	5500	0.10
DS2-6	4000	0.05

Table 5.1

Example Reinforced Concrete Beam Properties

Length (L) = 44.75 inches

Width (b) = Unit

Thickness (h) = 7.25 inches

Effective Depth (d') = 6.44 inches

Steel Percentage (ρ_s) = 0.012 (each face)

Concrete Compressive Strength (f'_c) = 7000 psi

Steel Yield Strength (f_y) = 70000 psi

Beam Density (ρ) = 0.0002247 $\frac{\text{#-sec}^2}{\text{in}^4}$

Shear Modulus (G) = 2 x 10⁶ psi

Poisson's ratio (ν) = 0.20

Table 5.2**Test Group Beam Parameters**

<u>Parameter</u>	<u>Group I</u>	<u>Group II</u>	<u>Group III</u>
Length (in)	48	44.75	44.75
Thickness (in)	5.6	7.25	7.25
Effective Depth (in)	4.8	6.44	6.44
Reinforcement Ratio (each face)	0.01	0.0075	0.012
Concrete Strength (psi)	5000	7000	7000
Steel Strength (psi)	70000	70000	70000
Shear Modulus (psi)	1.7×10^6	2×10^6	2×10^6
Beam Density (#-sec ² /in ⁴)	2.247×10^{-4}	2.247×10^{-4}	2.247×10^{-4}
Poissons Ratio	0.2	0.2	0.2
End Restraint	Fixed	Fixed	Fixed
Strength Enhancement Factor	1.50	1.55	1.60
Average Load Rate (psi/sec)	0.6×10^7	0.9×10^7	1.1×10^7

Table 5.3

Comparison of Analysis Prediction and Experimental Data

	<u>Test</u>	<u>Does Analysis Predict Direct Shear Failure?</u>	<u>Does Data Show a Direct Shear Failure</u>
Group I			
	FH1	No	No
	DS1-1	Yes	Yes
	DS1-2	Yes	Yes
	DS1-3	No	Yes
	DS1-4	Yes	Yes
	DS1-5	No	Yes
Group II			
	DS2-1	Yes	Yes
	DS2-2	Yes	Yes
	DS2-3	No	Yes
Group III			
	DS2-4	Yes	Yes
	DS2-5	Yes	Yes
	DS2-6	Yes	Yes

Figures

DIRECT SHEAR FAILURE REGIMES

1) Elastic Response Leading to Incipient Failure

2) Actual Failure Process

3) Post Failure Conditions

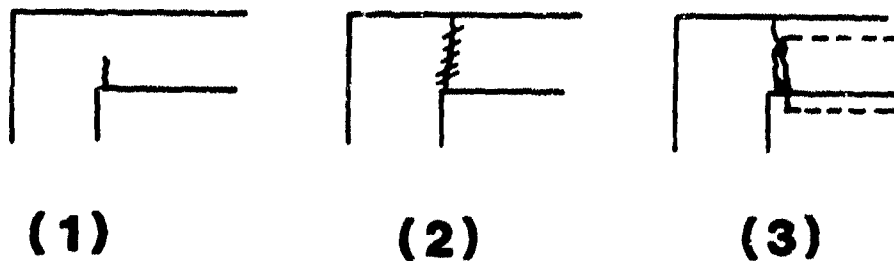
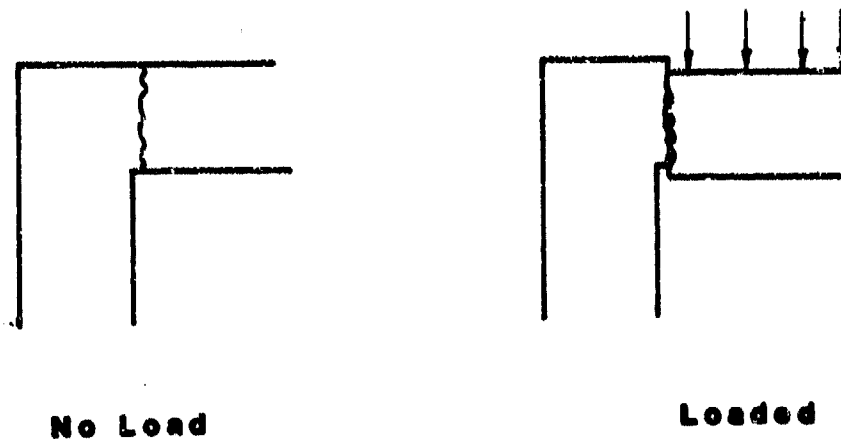
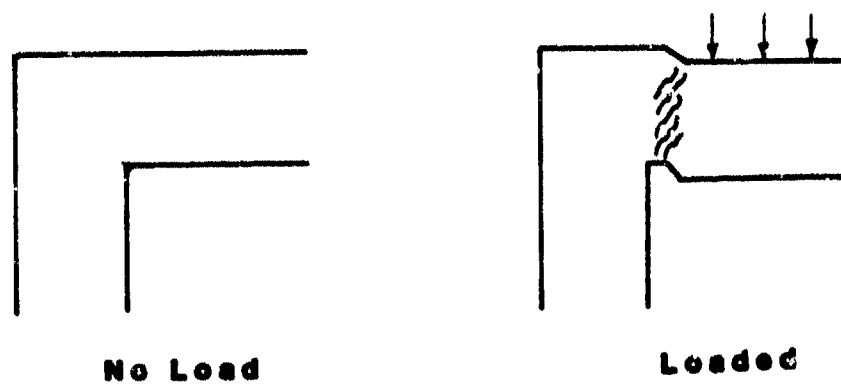


Figure 1.1 Classification of Direct Shear Failures into Three Regimes

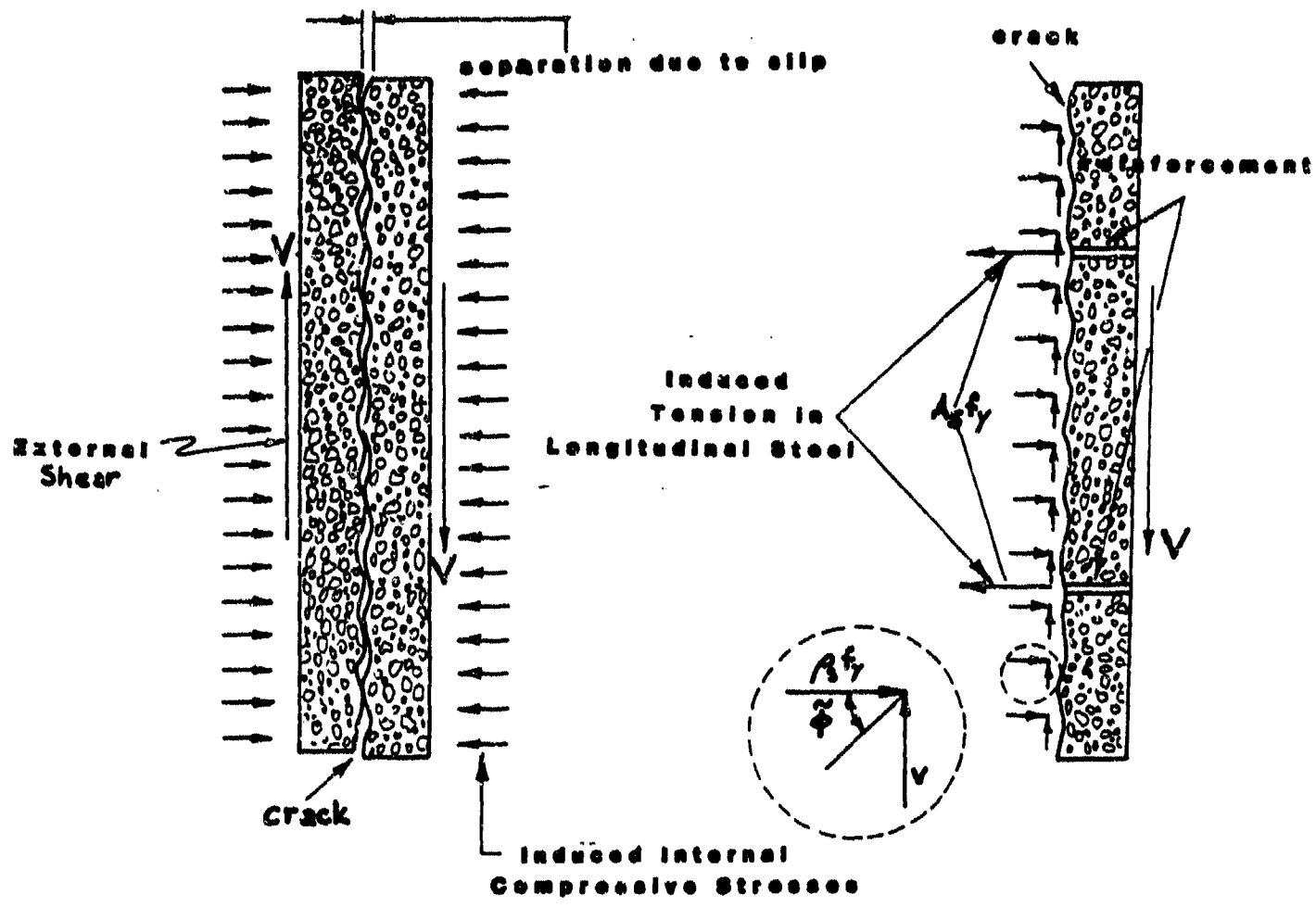


a) Initially Cracked



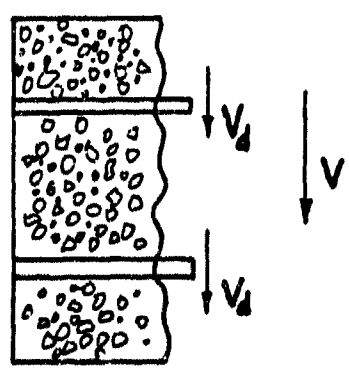
b) Initially Uncracked

Figure 2.1 Initially Cracked and Initially Uncracked Concrete Beams



a) External Shear and Induced Compressive Forces

b) Equilibrium of Forces



c) Dowel Forces, V_d

Figure 2.2 Force Transfer Mechanisms in Direct Shear for an Initially Cracked Concrete Section

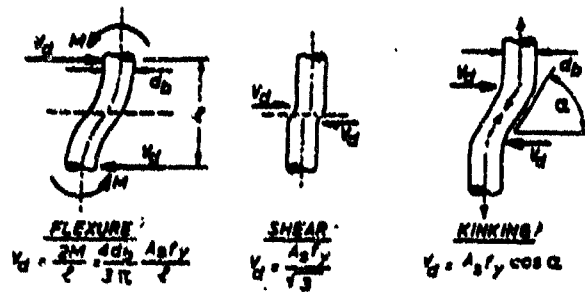


Figure 2.3 Dowel Reinforcement Patterns Across a Crack Plane (Bresler '74)

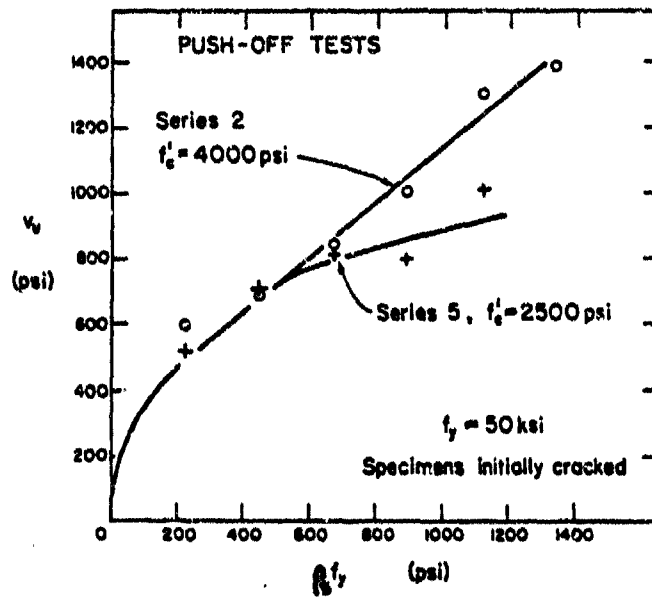


Figure 2.4 Effect of Concrete Strength on Shear Transfer Strength of Initially Cracked Specimens (Mattock & Hawkins '72)

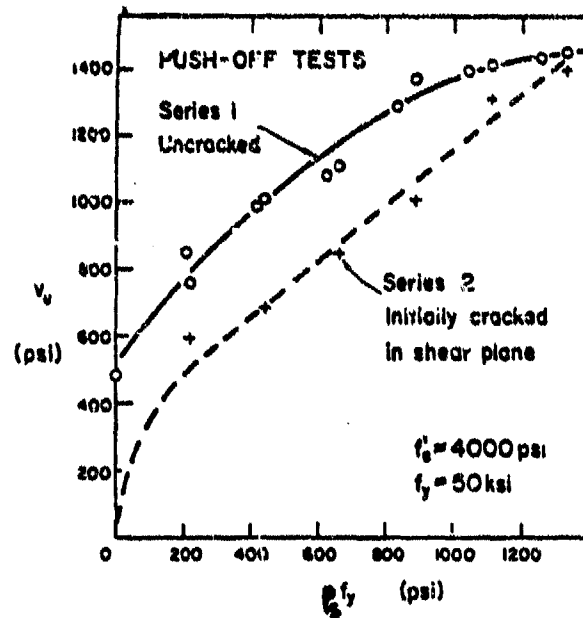


Figure 2.5 Shear Transfer Strength vs. Reinforcement Parameter $\rho_s f_y$ for Specimens With and Without an Initial Crack Along the Shear Plane (Mattock & Hawkins '72)

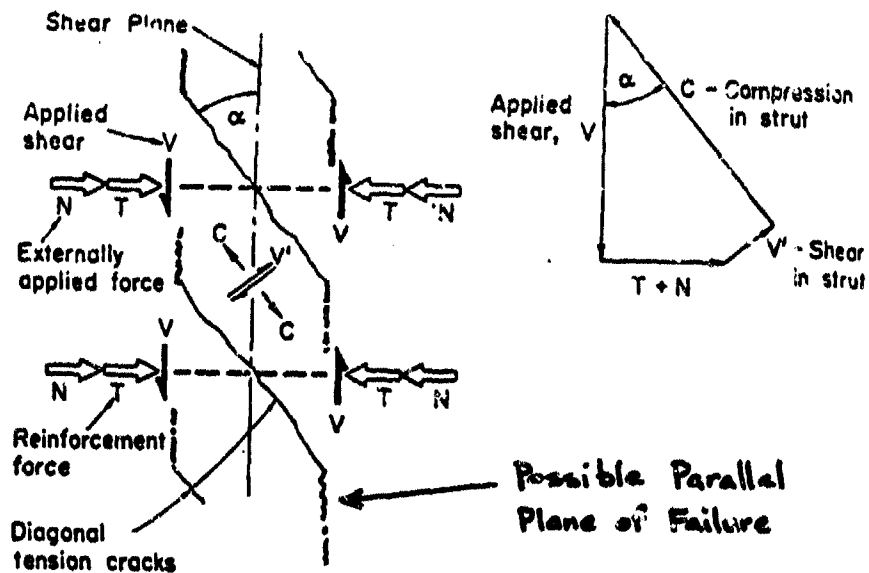


Figure 2.6 Shear Transfer in Initially Uncracked Concrete (Mattock & Hawkins '72)

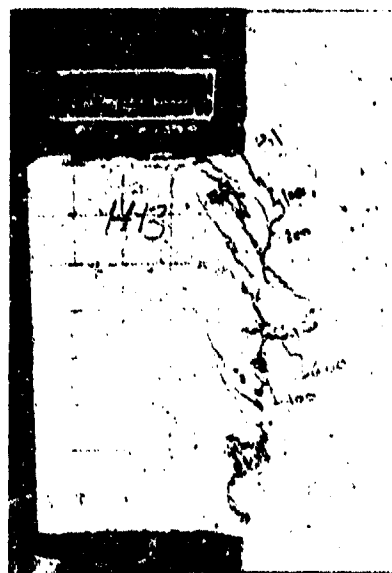


Figure 2.7 Typical Shear Failure for a Corbel (Somerville '74)

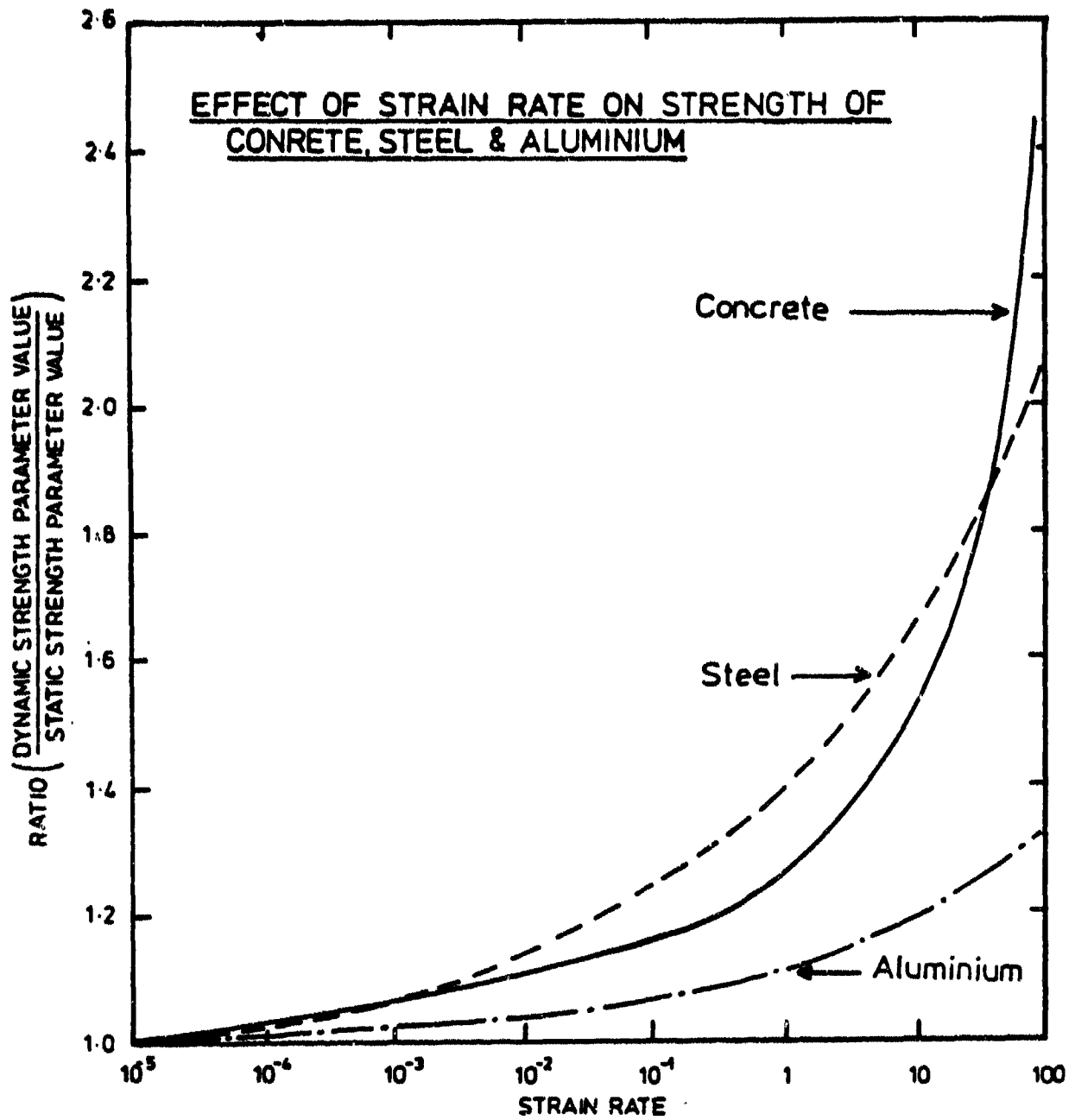


Figure 3.1 Effect of Strain Rate on Strength of Concrete, Steel, and Aluminium (Davies '81)

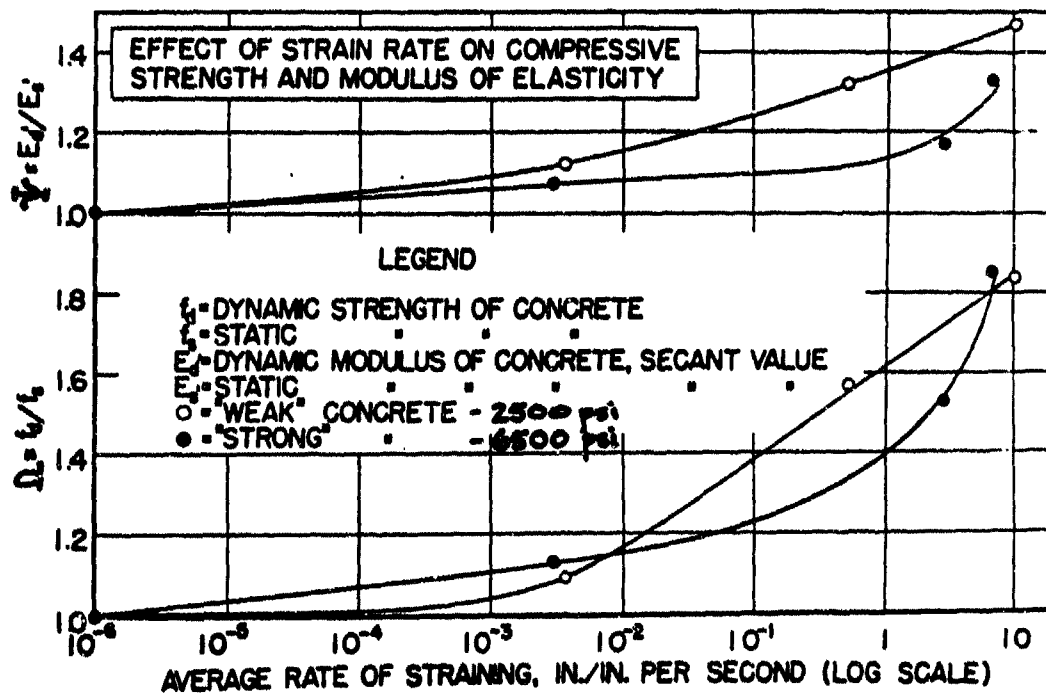


Figure 3.2 Strength Enhancement and Modulus Enhancement Factors for Concrete vs. Strain Rate (Watstein & Boresi'52)

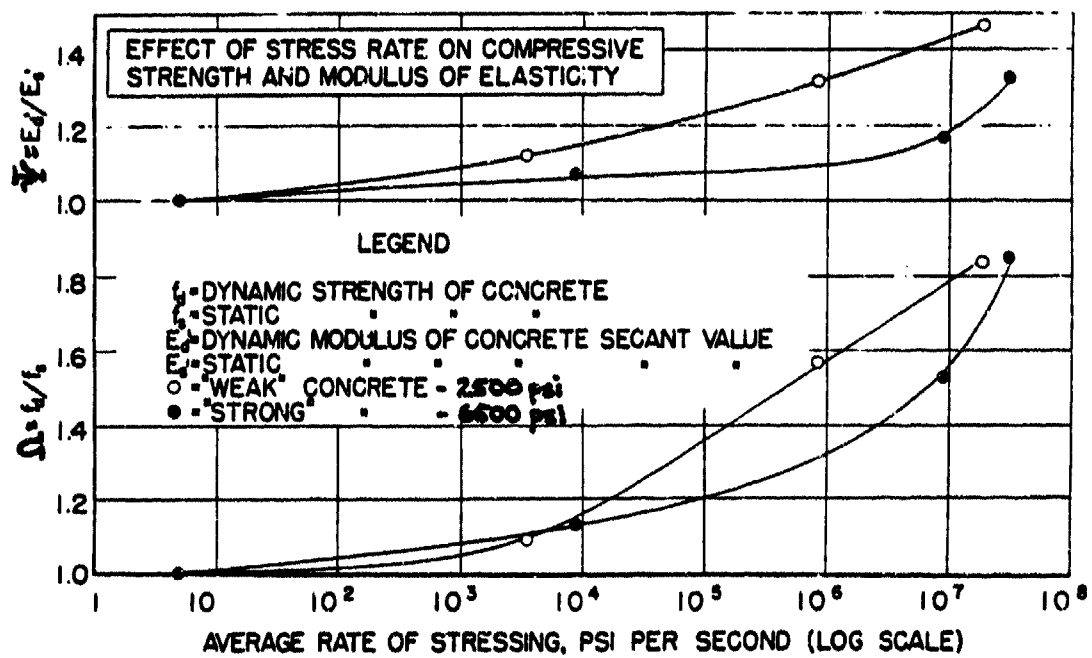


Figure 3.3 Strength Enhancement and Modulus Enhancement Factors for Concrete vs. Load Rate (Stress Rate) (Watstein & Boresi '52)

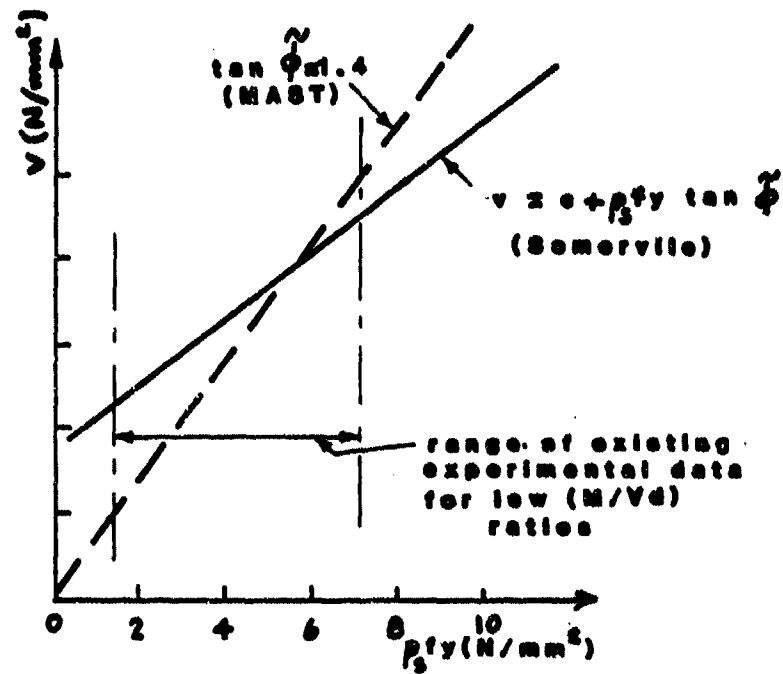


Figure 3.4 Shear Friction Plus Cohesion Approach (Somerville '74)

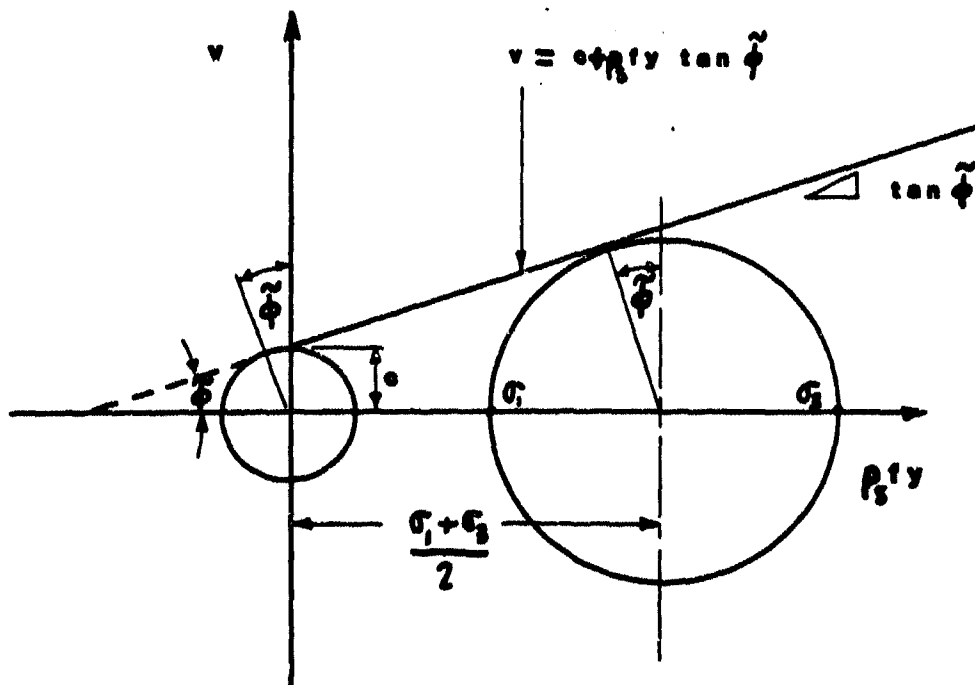
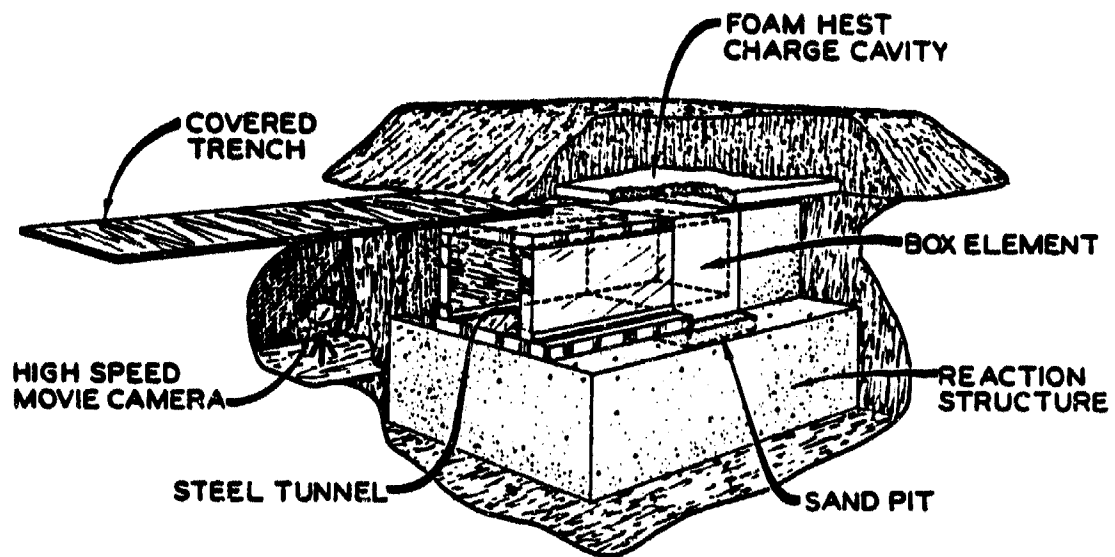


Figure 3.5 Relationship of Principal Stresses ($\sigma_3 > \sigma_1$) for Mohr-Coulomb Criterion



TEST CONFIGURATION

Figure 4.1 Test Configuration for the WES Tests (Kiger'82)

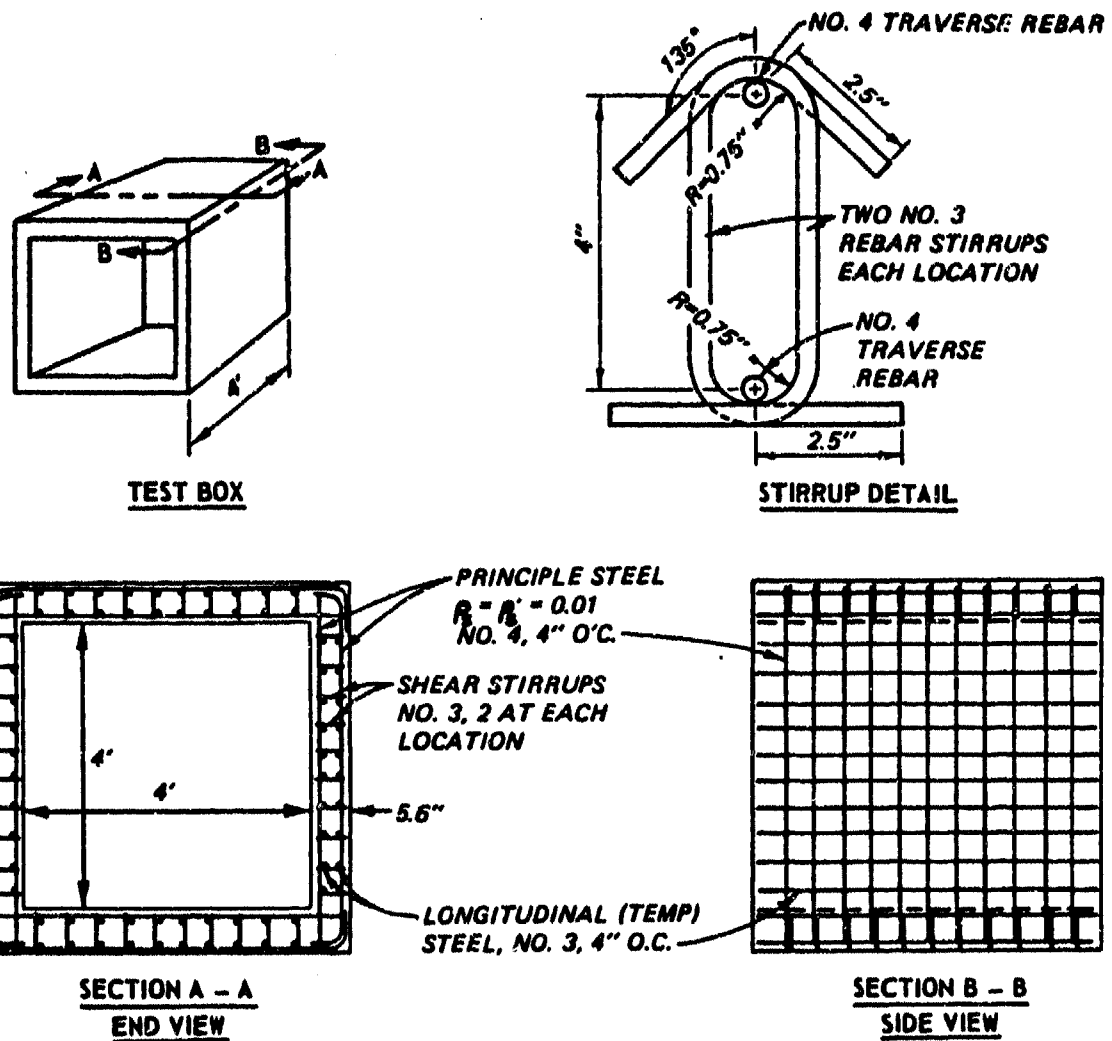


Figure 4.2 Test Element Construction Details, Test Group I (Kiger'82)

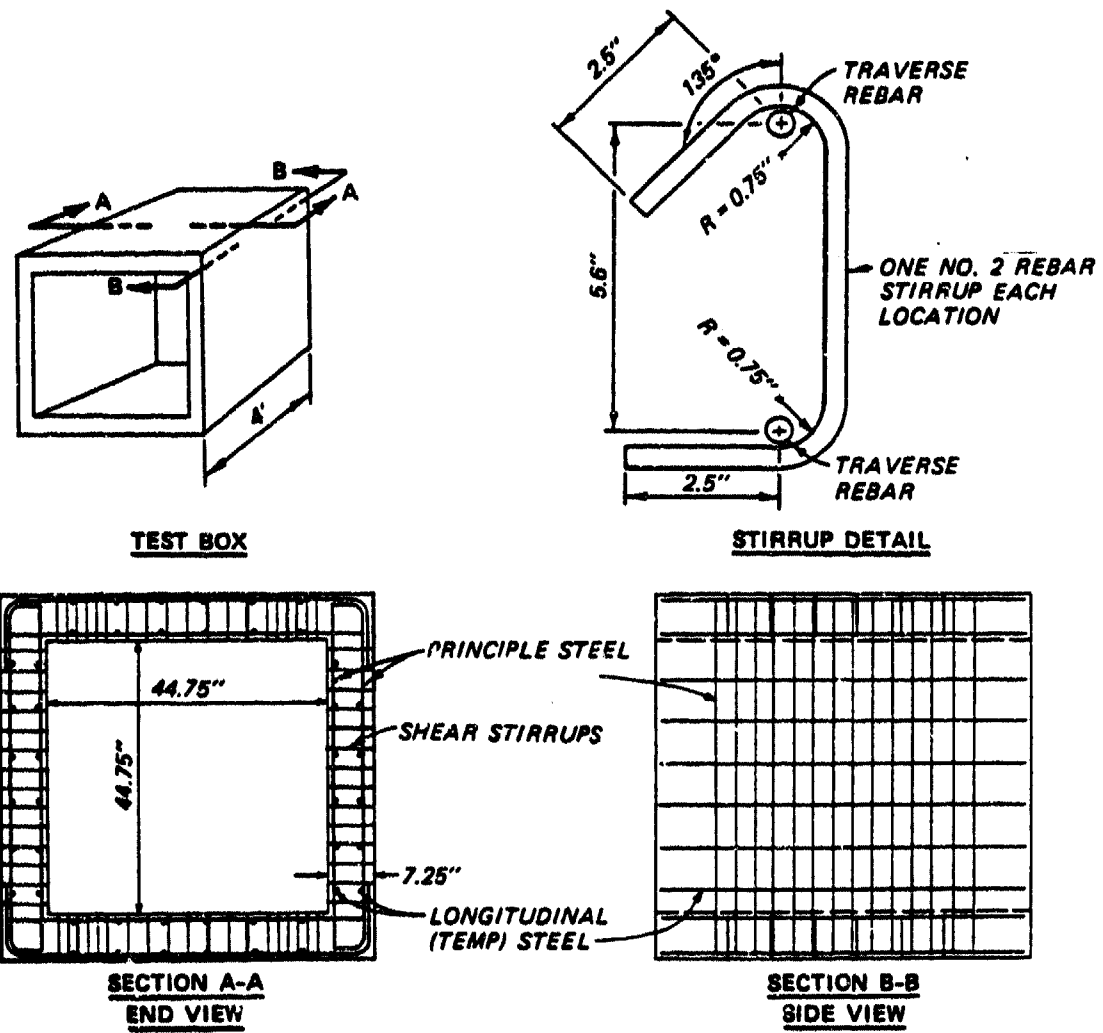


Figure 4.3 Test Element Construction Details, Test Groups II & III (Kiger'82)

NOTATION

IF = Interface Pressure
 EO = Steel Strain on outside face
 EI = Steel Strain on inside face

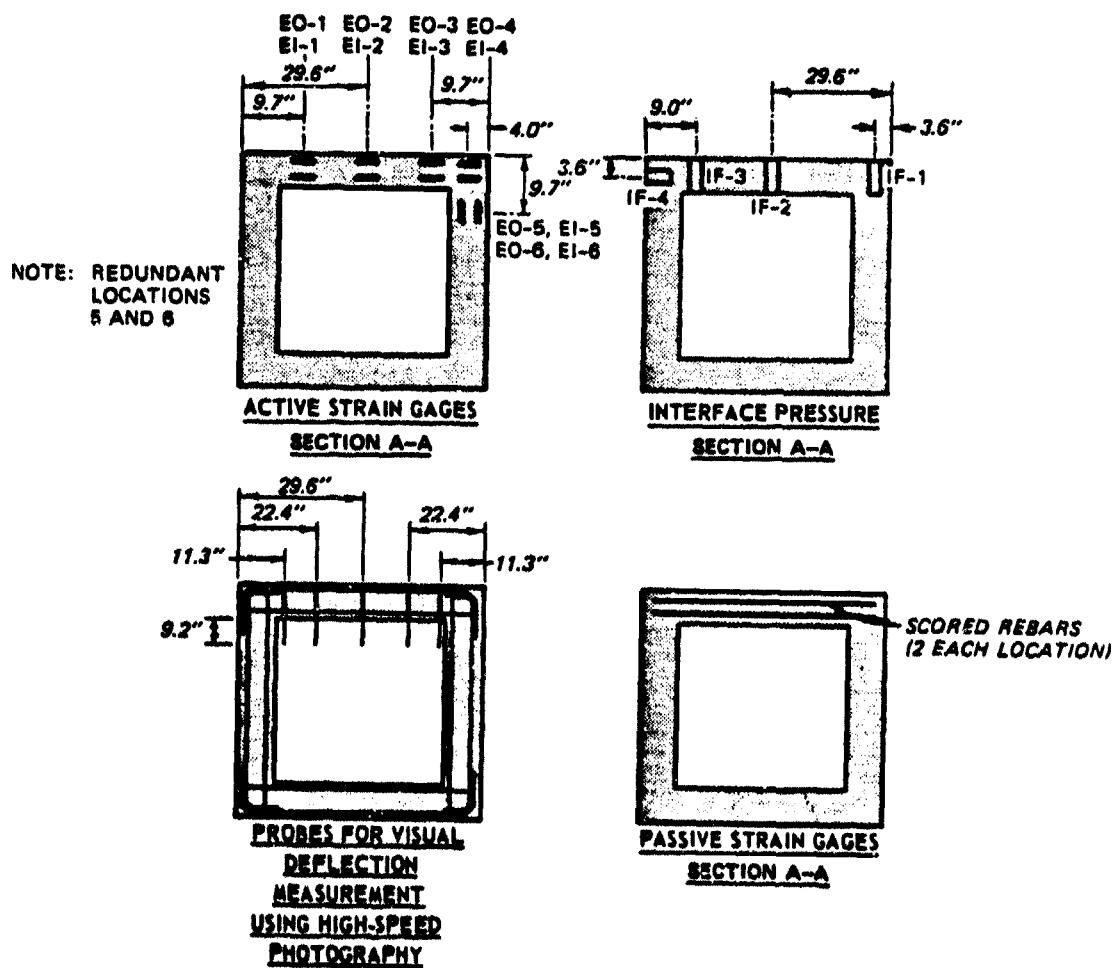


Figure 4.4 Example Test Instrumentation Layout, Test Groups II & III (Kiger'82)

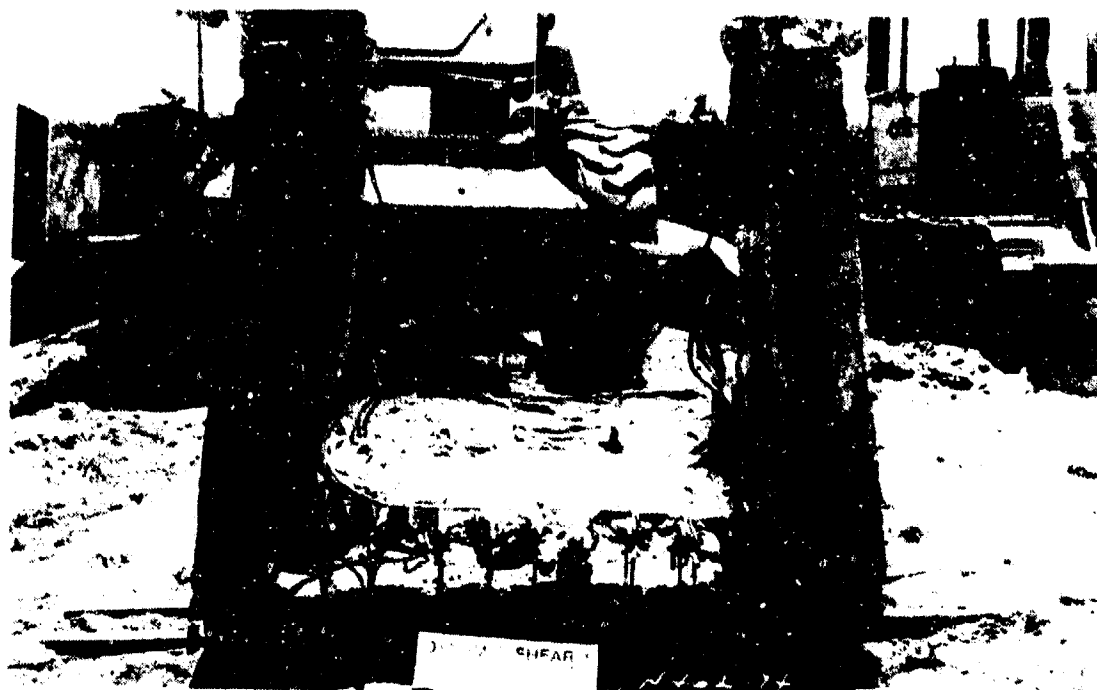


Figure 4.5 Post Test View of Test Element DS1-1 (Kiger'82)



Figure 4.6 Post Test View of Test Element DS1-2 (Kiger'82)



Figure 4.7 Post Test View of Test Element DS1-4 (Kiger'82)

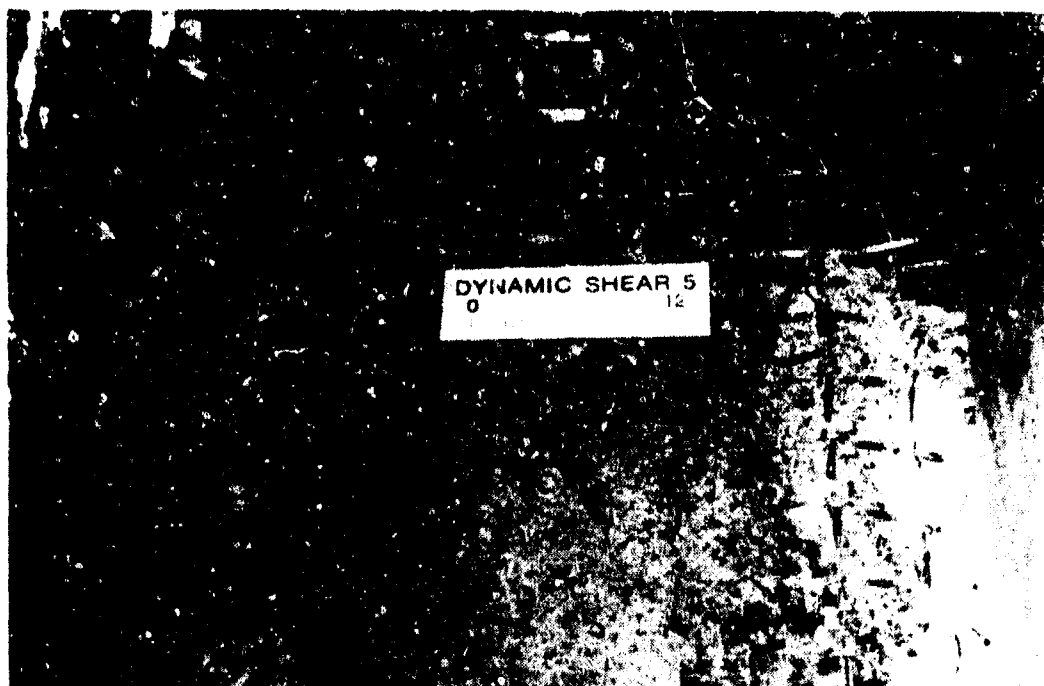


Figure 4.8 Post Test View of Test Element DS1-5 (Kiger'82)

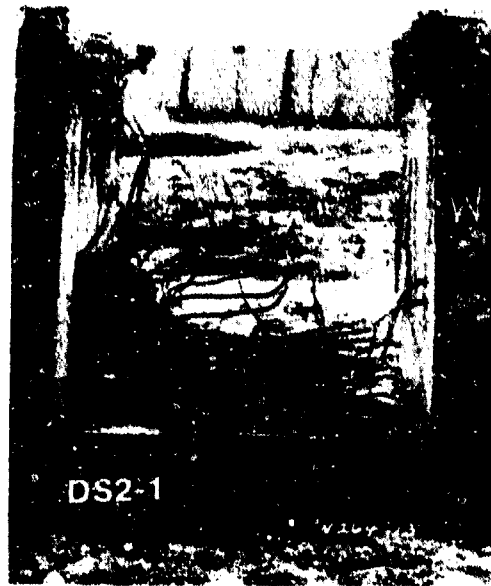


Figure 4.9 Post Test View of Test Element DS2-1 (Kiger'82)



Figure 4.10 Post Test View of Test Element DS2-2 (Kiger'82)



Figure 4.11 Post Test View of Test Element DS2-4 (Kiger'82)



Figure 4.12 Post Test View of Test Element DS1-3 (Kiger'82)

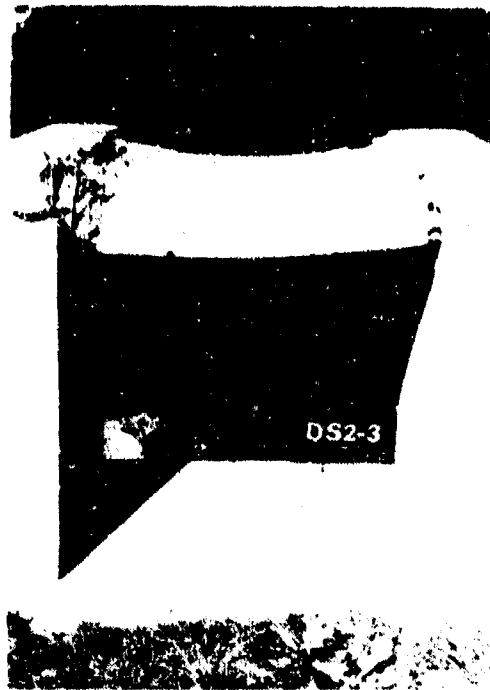


Figure 4.13 Post Test View of Test Element DS2-3 (Kiger'82)

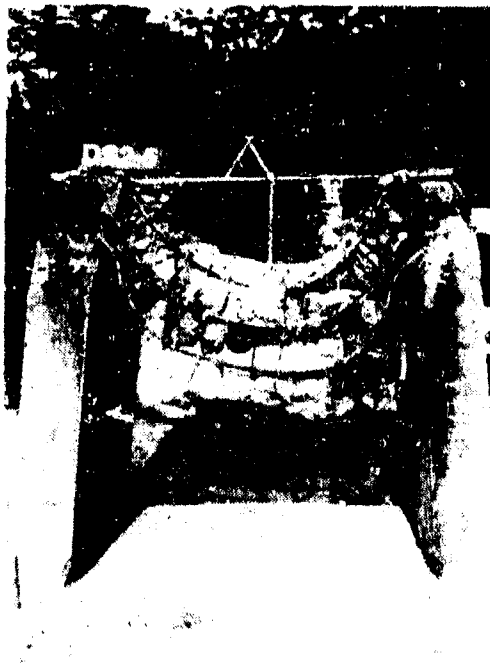


Figure 4.14 Post Test View of Test Element DS2-5 (Kiger'82)

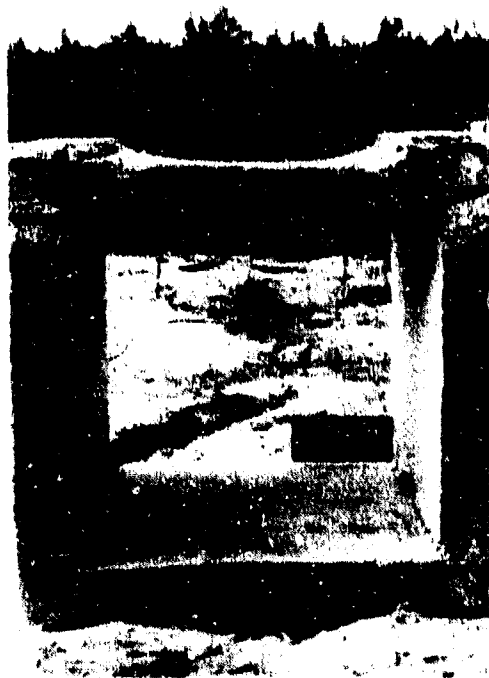


Figure 4.15 Post Test View of Test Element DS2-6 (Kiger'82)

Foam Nest I

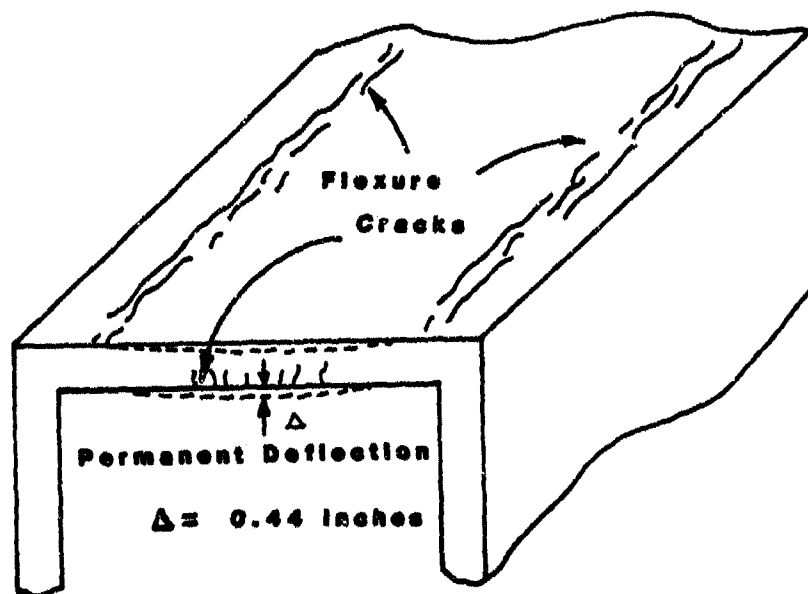


Figure 4.16 Post Test Schematic of Test Element FH1 (Kiger'79)

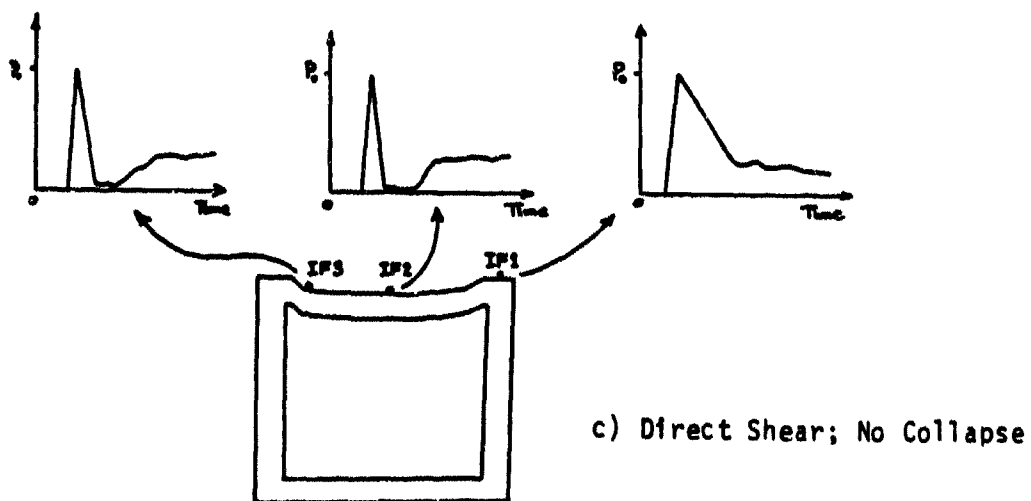
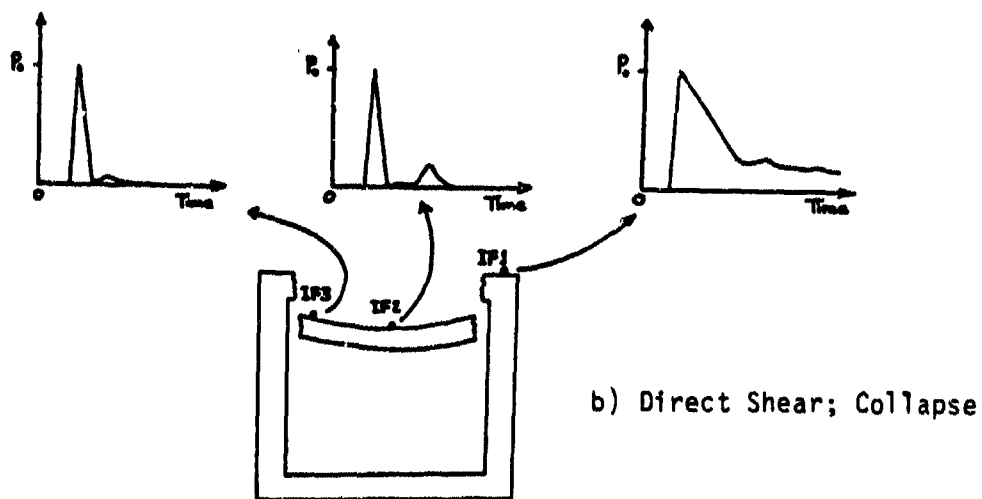
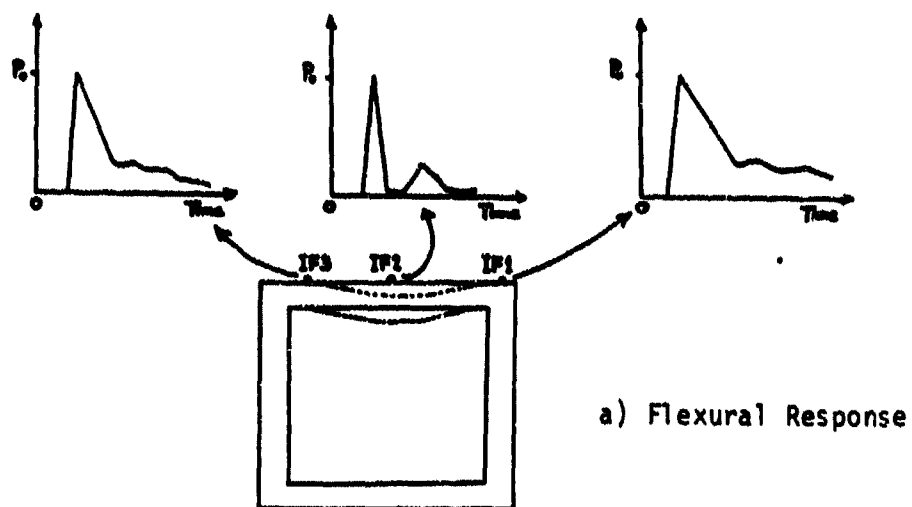


Figure 4.17 Failure Mode Determination Using Interface Pressure Measurements

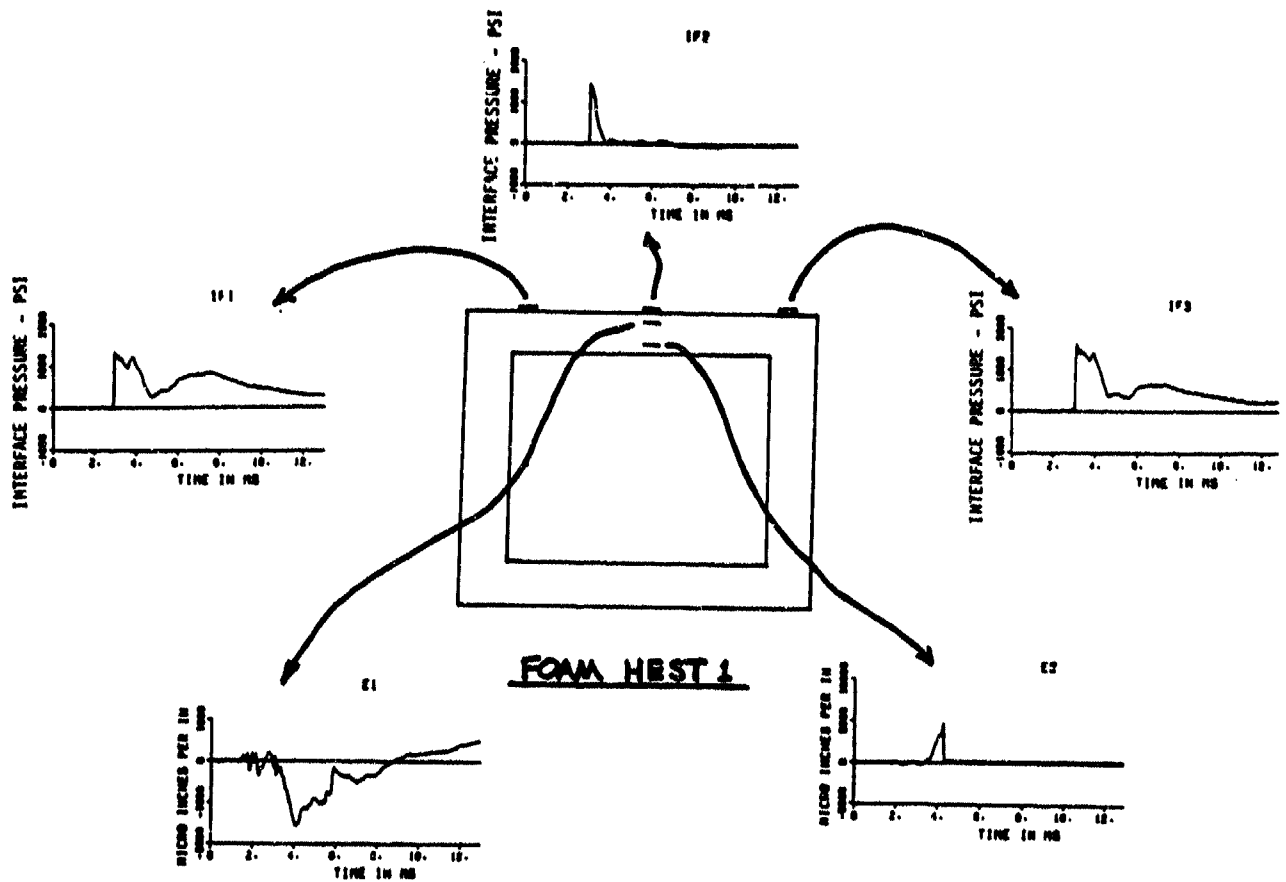


Figure 4.18 Active Measurements for FH1: Flexural Failure (Kiger '79)

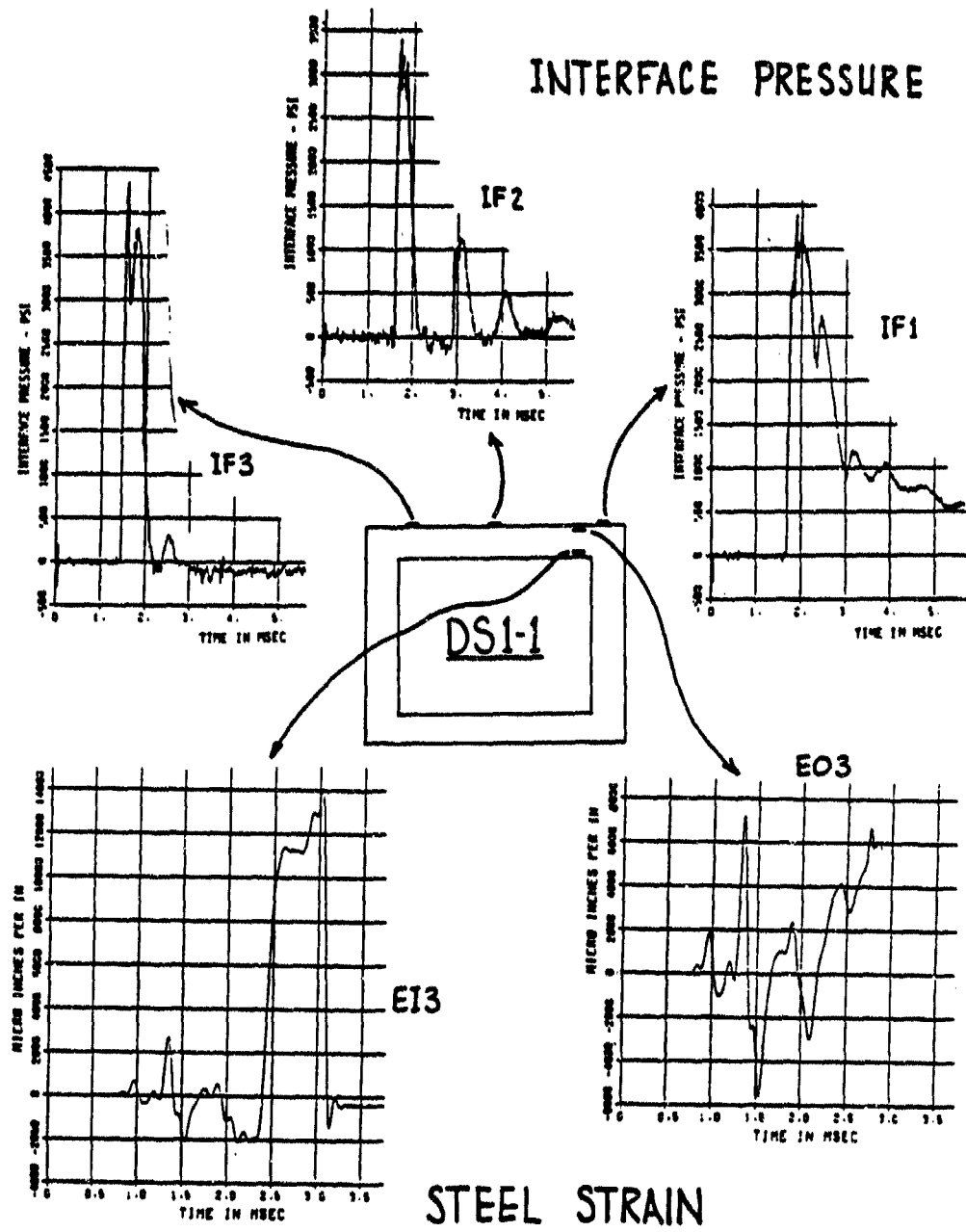


Figure 4.19 Active Measurements for DS1-1: Direct Shear Failure (Kiger'82)

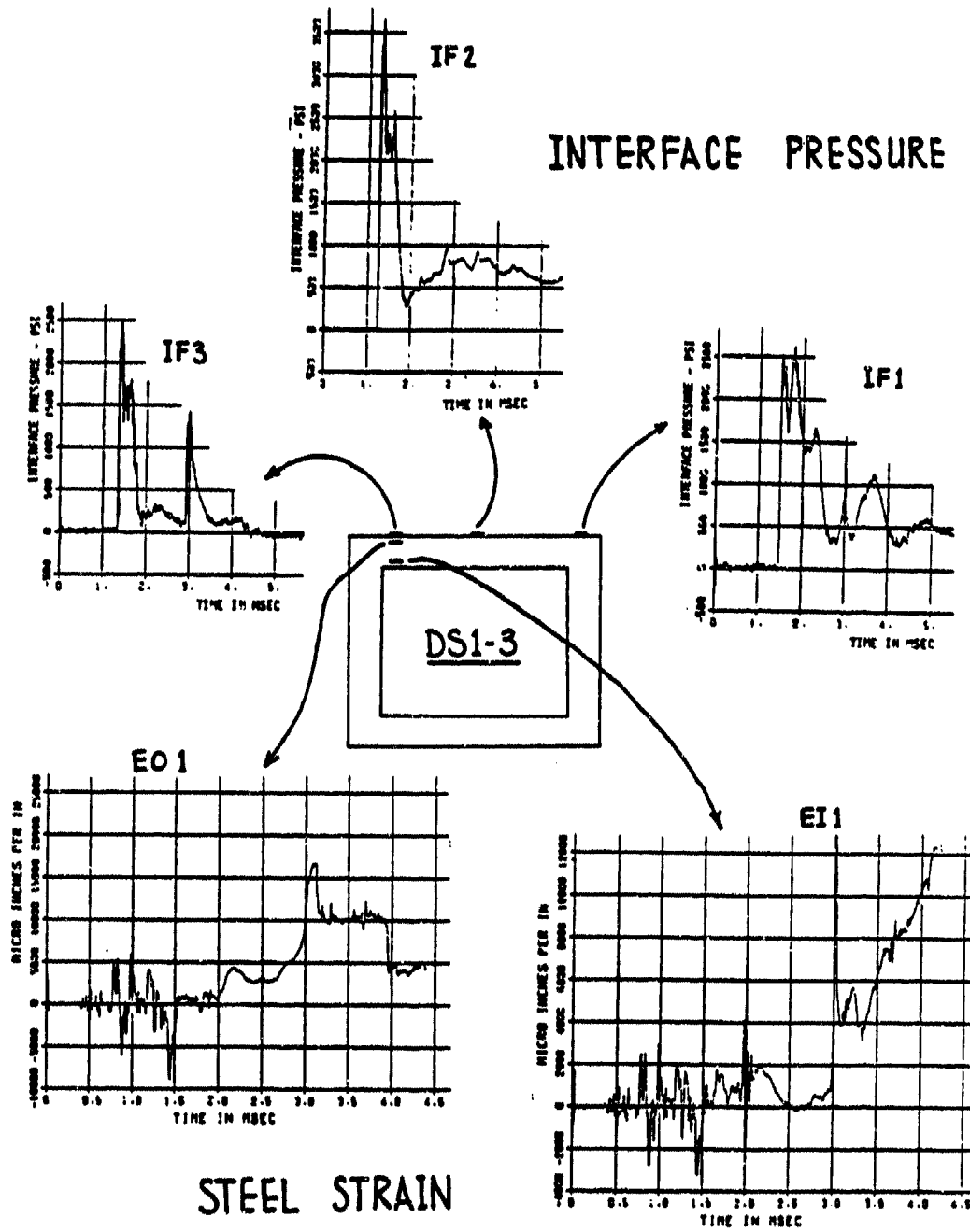
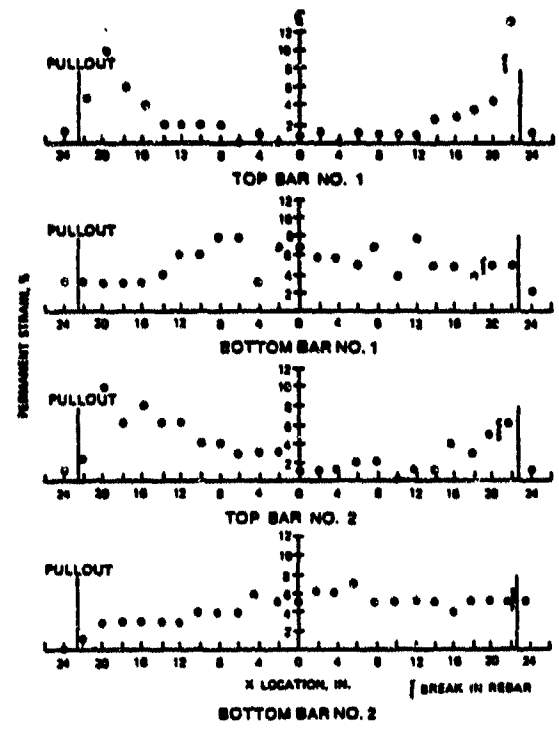
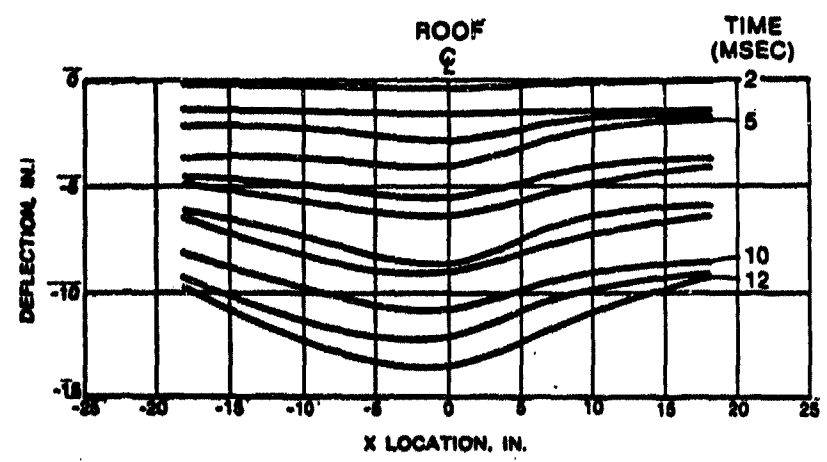


Figure 4.20 Active Measurements for DS1-3: Direct Shear Failure (Kiger'82)

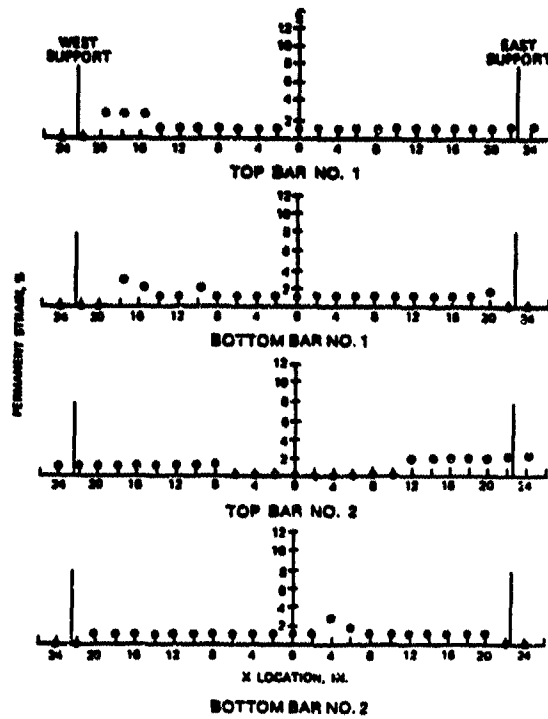


a) PERMANENT STRAIN OF REBAR FOR DS2-1

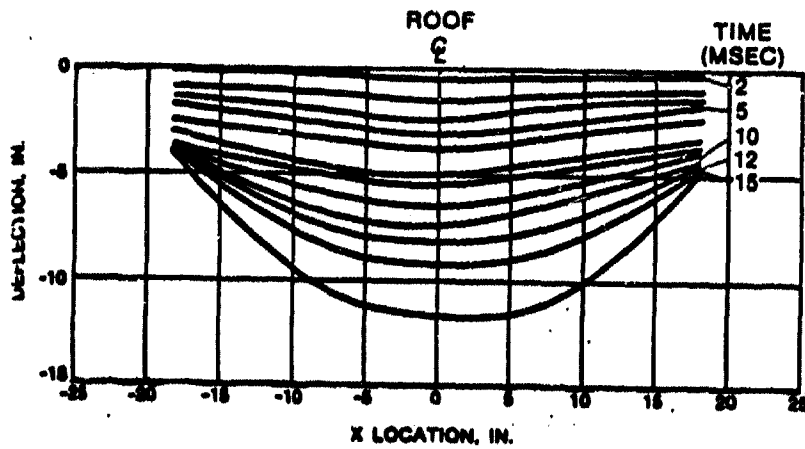


b) DS2-1 ROOF DEFLECTION PROFILES

Figure 4.21 Post Failure Measurements for DS2-1: Direct Shear Failure (Kiger'82)



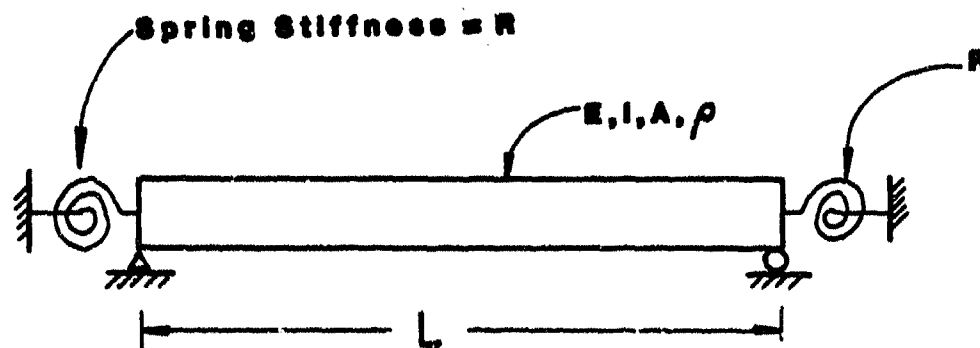
a) PERMANENT STRAIN OF REBAR FOR DS-5



b) DS2-5 ROOF DEFLECTION PROFILES

Figure 4.22 Post Failure Measurements for DS2-5: Direct Shear Failure (Kiger'82)

TIMOSHENKO BEAM WITH ELASTIC END SPRINGS



UNIFORMLY DISTRIBUTED PRESSURE

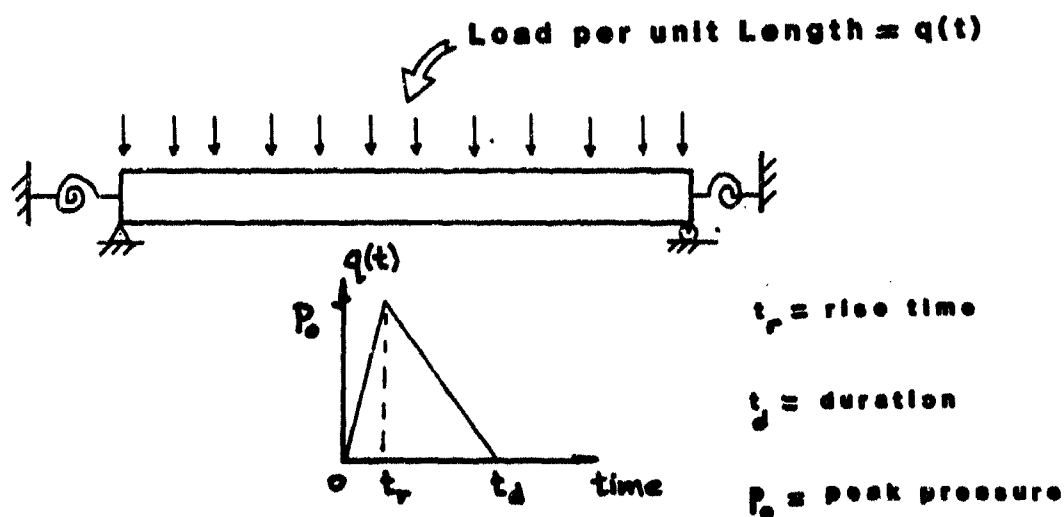
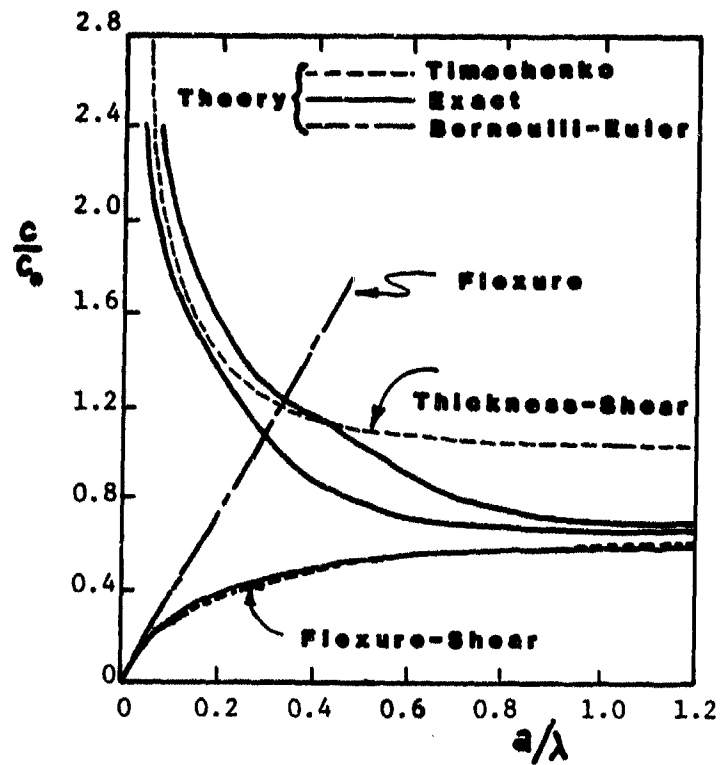


Figure 5.1 Timoshenko Beam Model and Idealized Interface Pressure Loading



$c_0 \cong$ Longitudinal Wave Velocity

$c \cong$ Wave Velocity

$a \cong$ Cylinder Radius

$\lambda \cong$ Wavelength

Figure 5.2 Elastic Wave Velocity Curves for a Solid Circular Cylinder of Radius a (Fung '65)

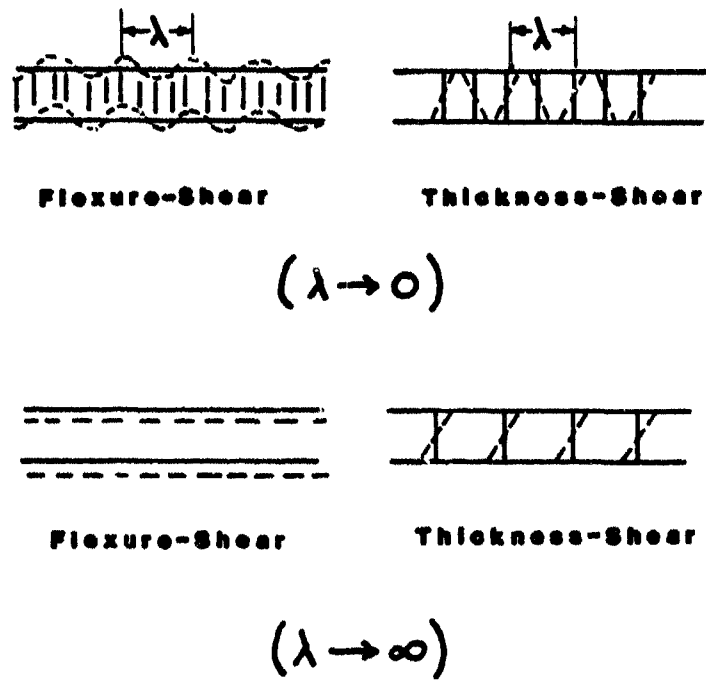


Figure 5.3 Timoshenko Beam Wave Configurations (Crandall '68)

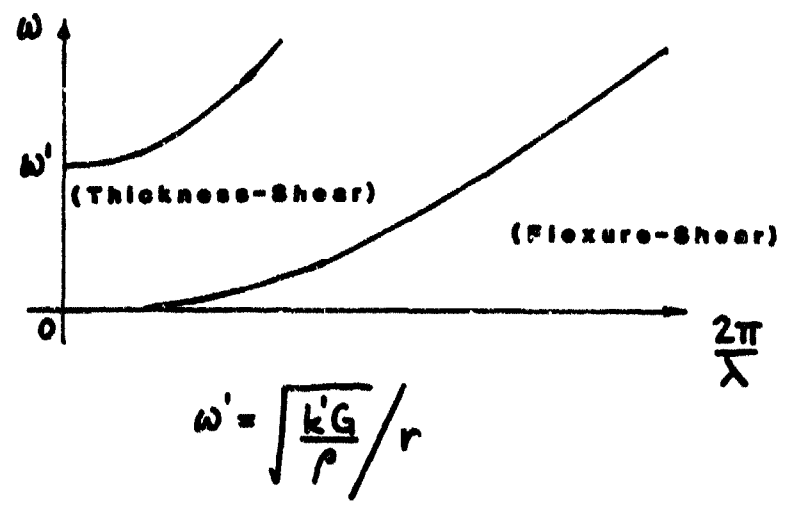
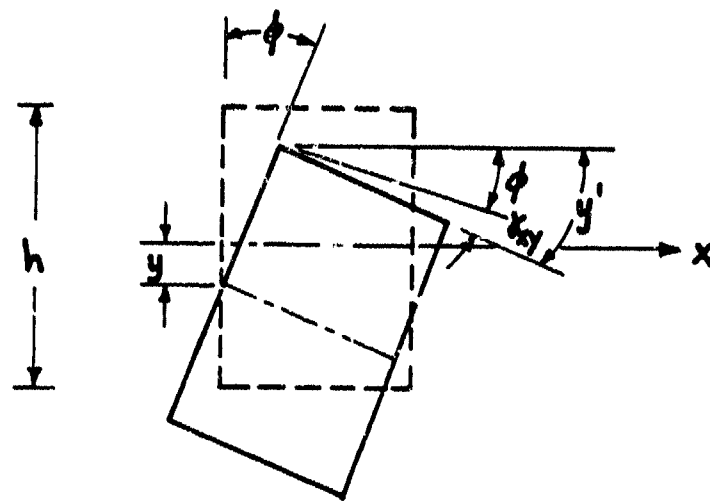
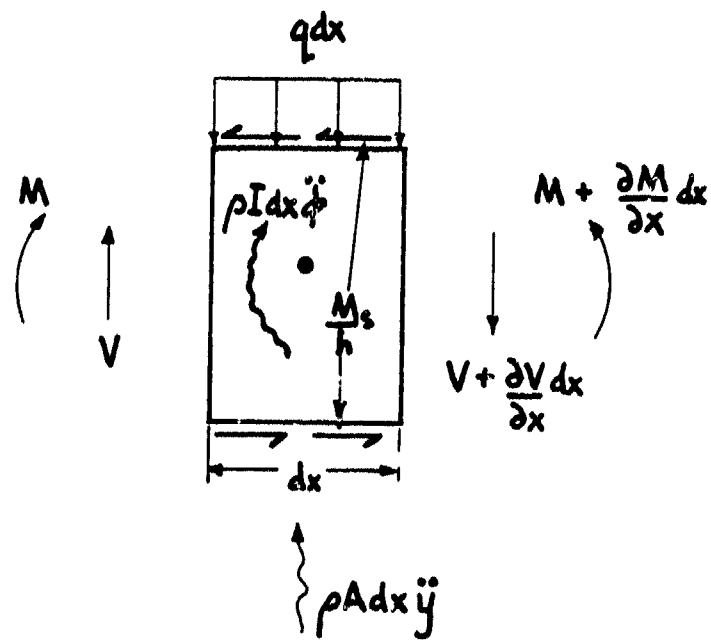


Figure 5.4 Dispersion Relations for a Timoshenko Beam (Crandall '68)



a) Element Deformation



b) Dynamic Equilibrium

Figure 5.5 Timoshenko Beam Element

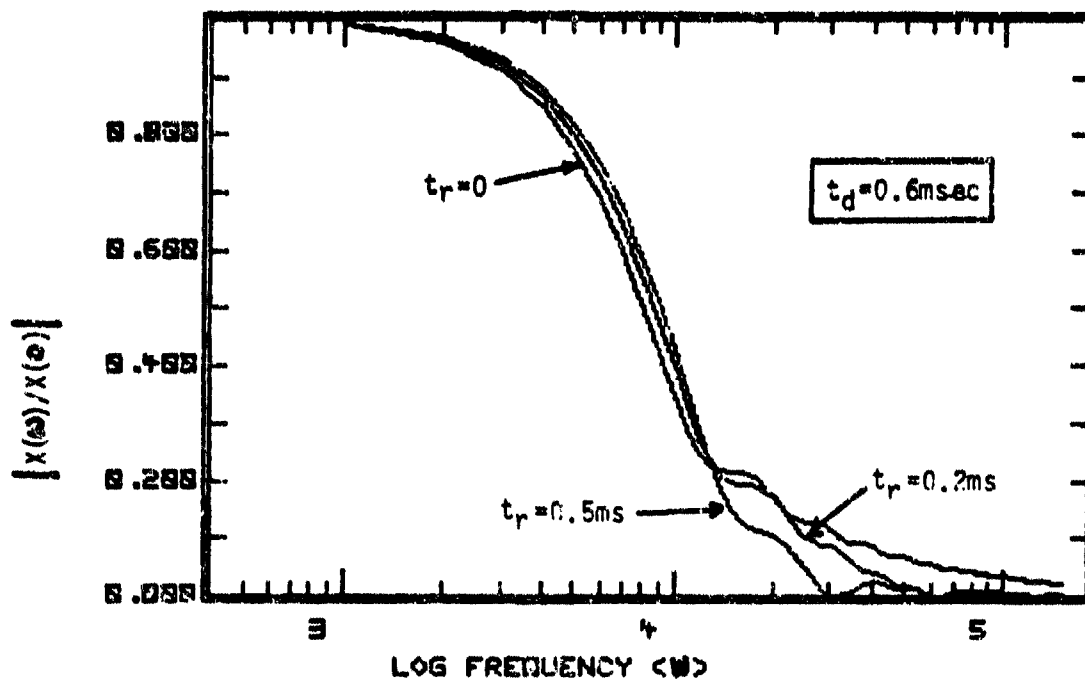


Figure 5.6 Fourier Amplitude Spectrum for Idealized Pressure Pulse 0.6 msec duration

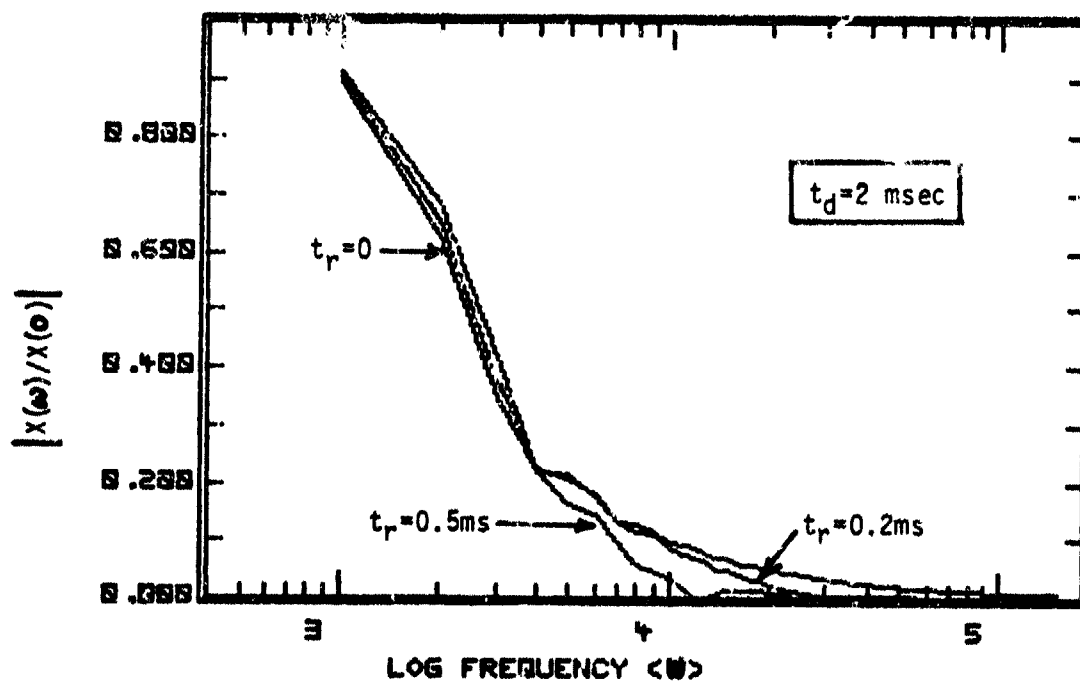


Figure 5.7 Fourier Amplitude Spectrum for Idealized Pressure Pulse 2 msec duration

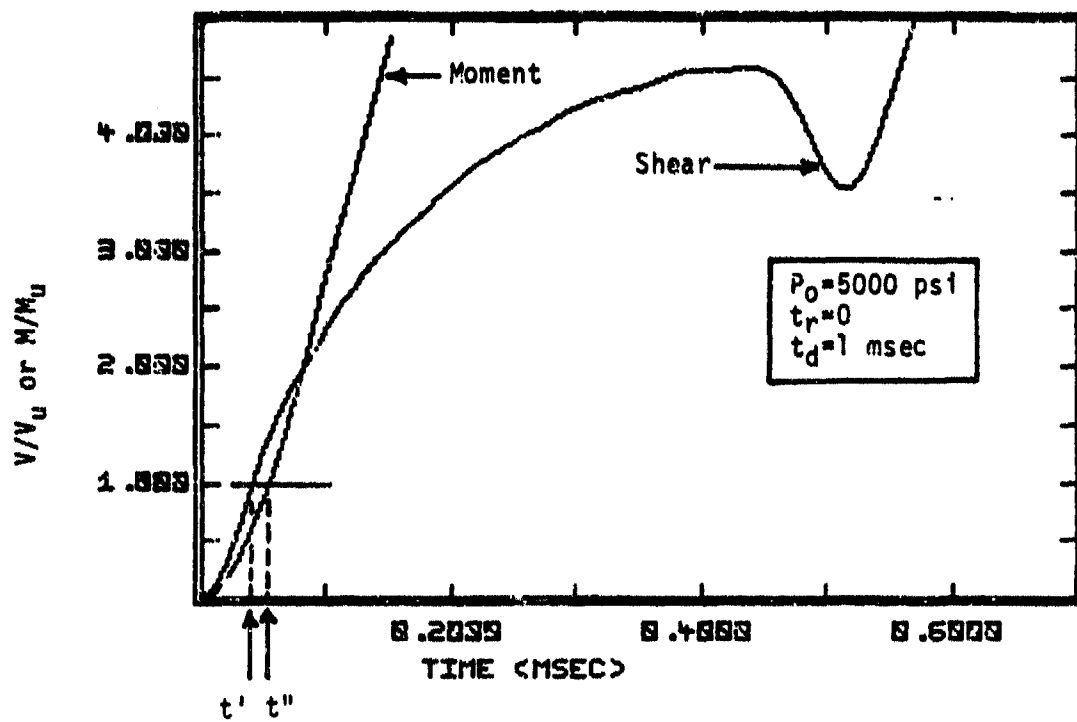


Figure 5.8 Normalized Support Shear and Moment vs. Time for Example Beam: Fixed-Ends, $P_0=5000$ psi

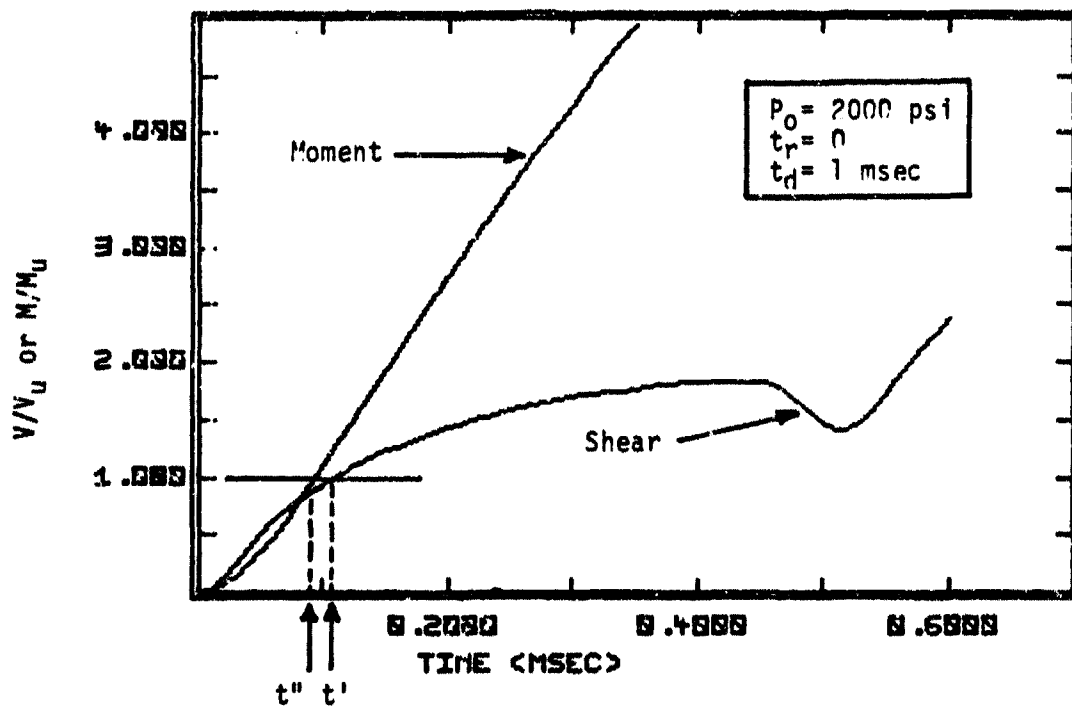


Figure 5.9 Normalized Support Shear and Moment vs. Time for Example Beam: Fixed-Ends, $P_0=2000$ psi

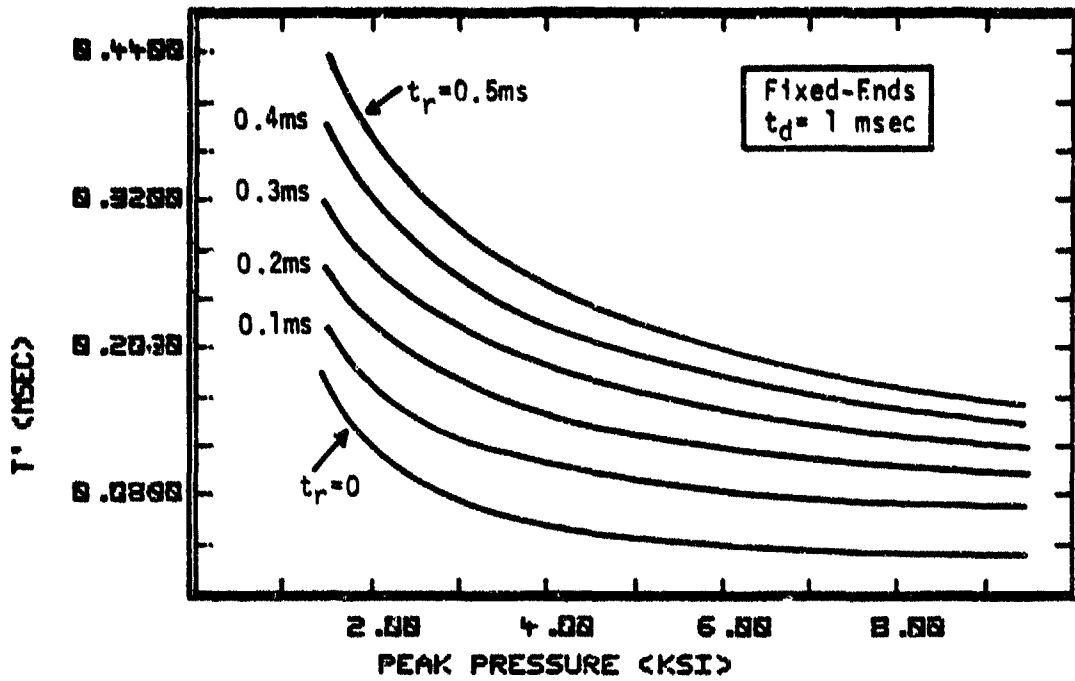


Figure 5.10 Direct Shear Failure Time, t' , vs. Peak Pressure for Example Beam

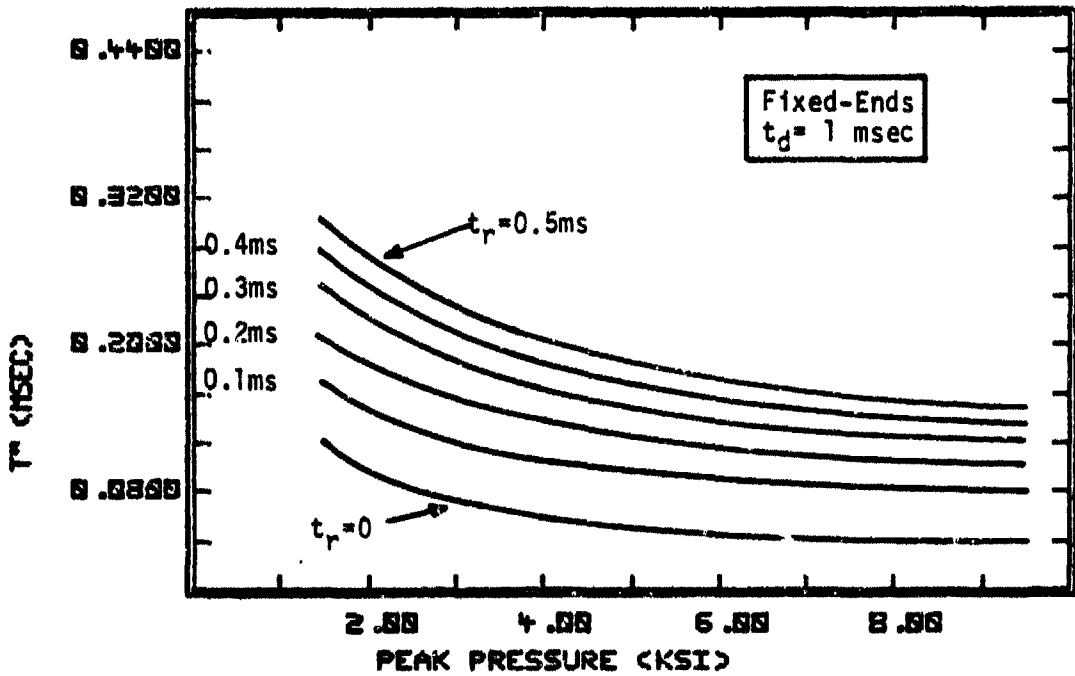


Figure 5.11 Flexure Failure Time, t'' , vs. Peak Pressure for Example Beam

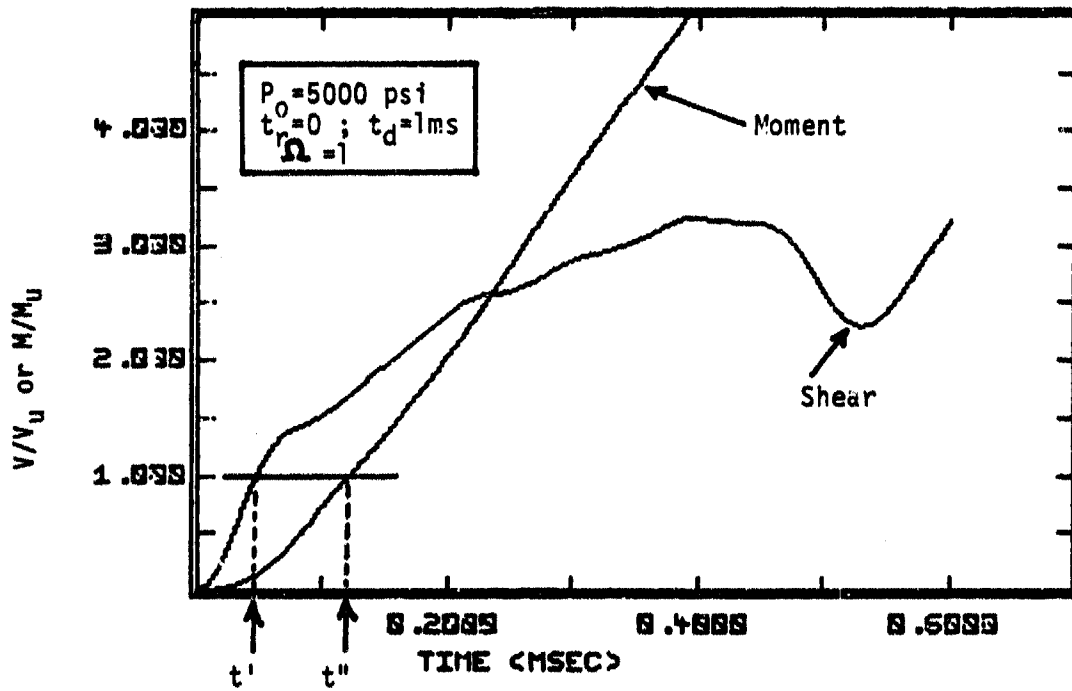
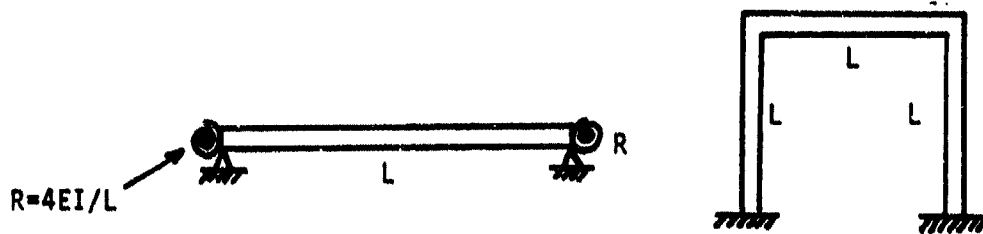
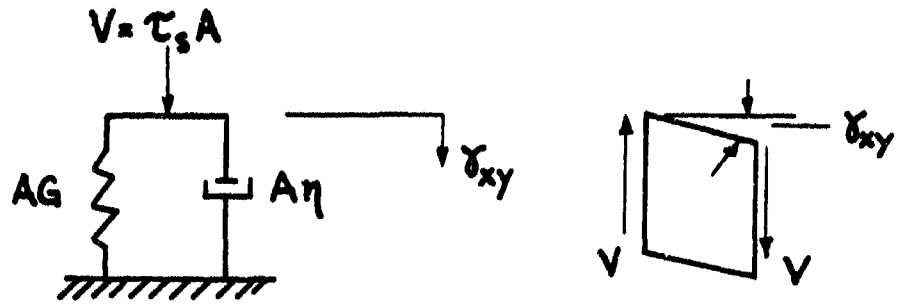
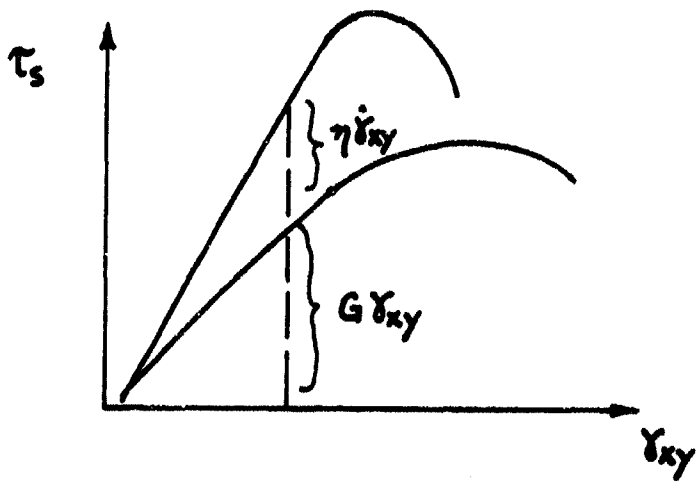


Figure 5.12 Normalized Support Shear and Moment vs. Time for Example Beam: $R=4EI/L$, $P_0=5000 \text{ psi}$



$$\tau_s = G \gamma_{xy} + \eta \dot{\gamma}_{xy}$$

a) Voigt Solid in Shear



b) Stress-Strain Relation in Shear

Figure 5.13 Linear Viscoelastic Model

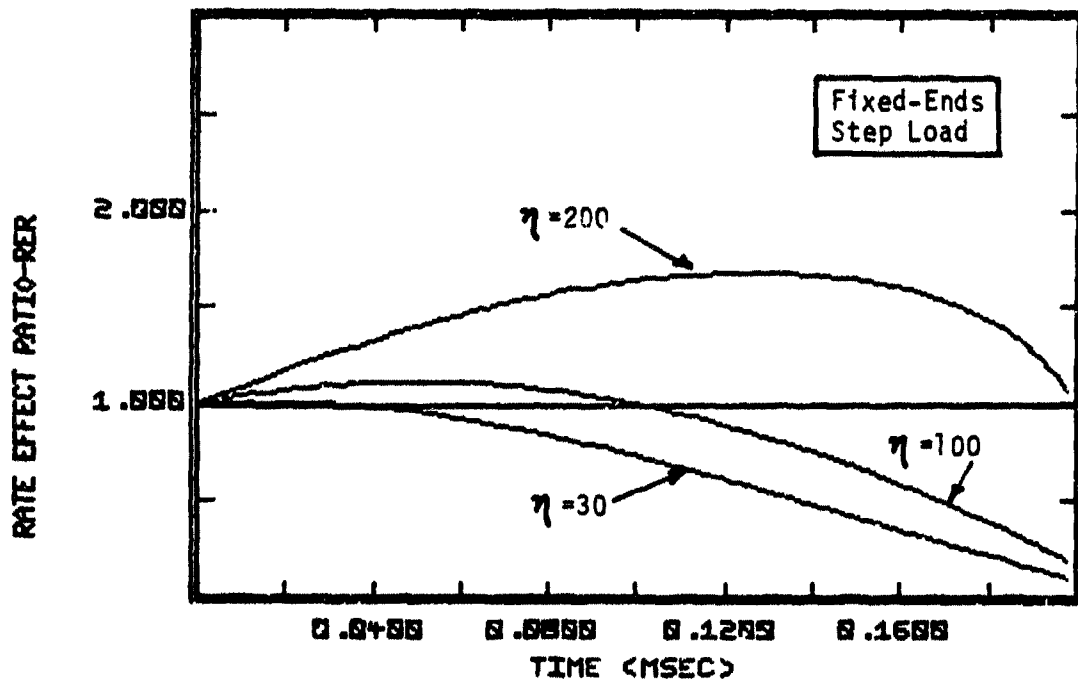
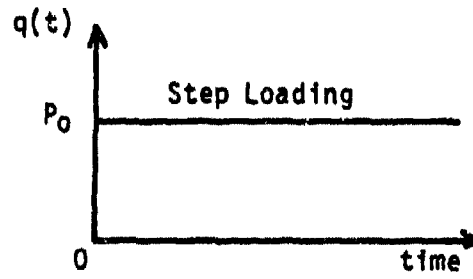


Figure 5.14 Rate Effect Ratio (RER) vs. Time for Example Beam

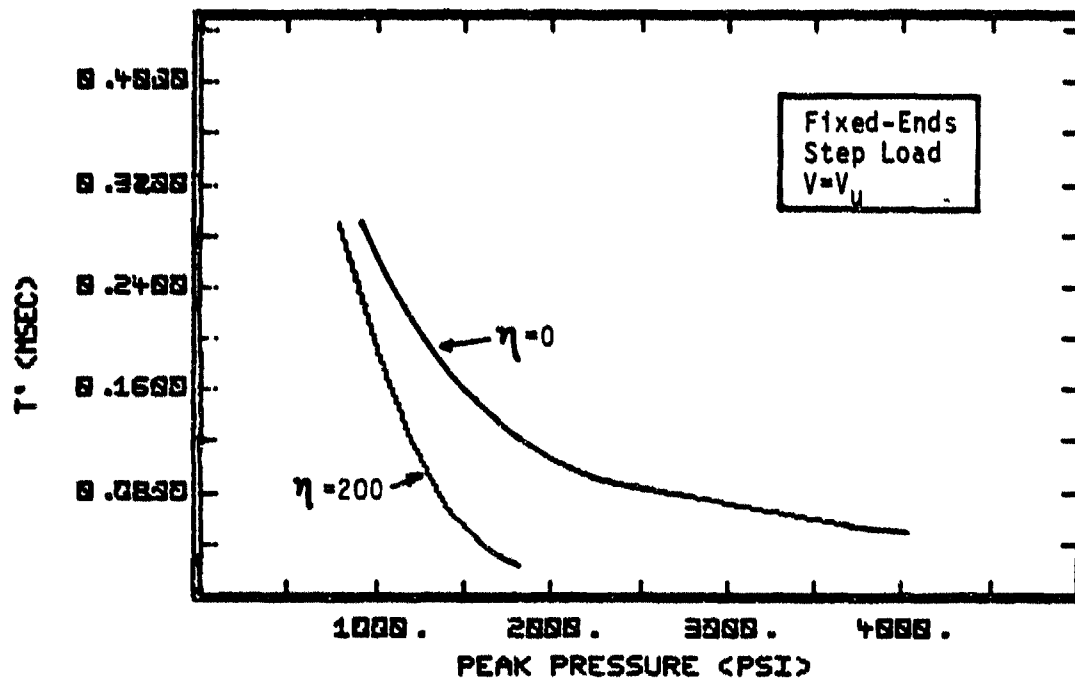


Figure 5.15 Strain Rate Effects on Shear Failure Time, t' , for Example Beam ($\Omega=1$)

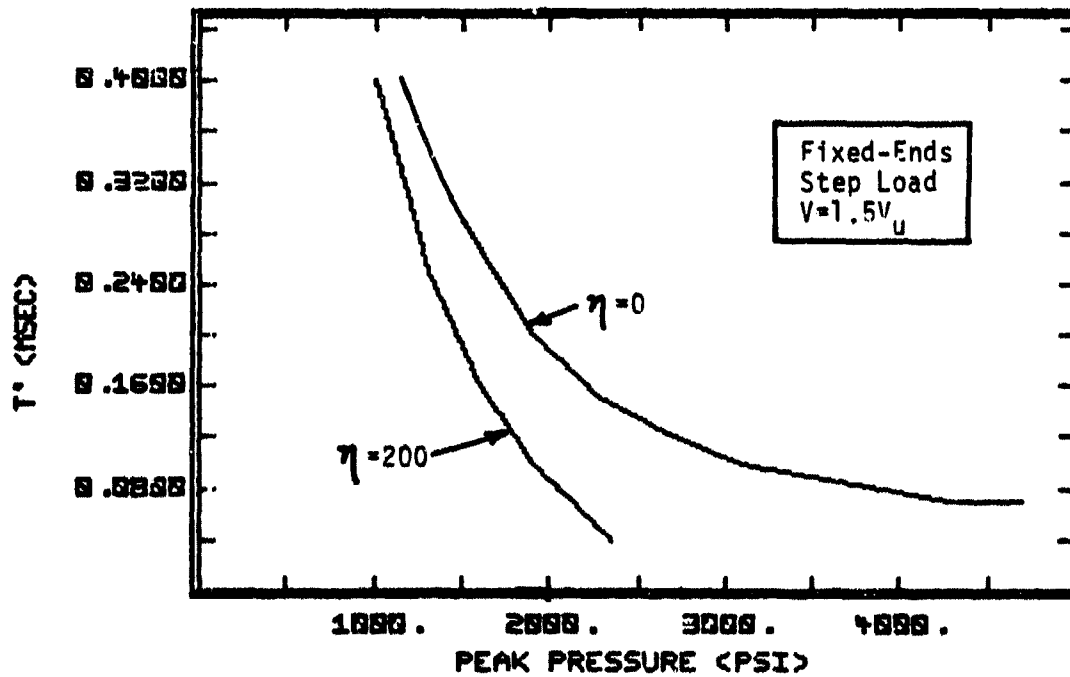


Figure 5.16 Strain Rate Effects on Shear Failure Time, t' , for Example Beam ($\Omega=1.5$)

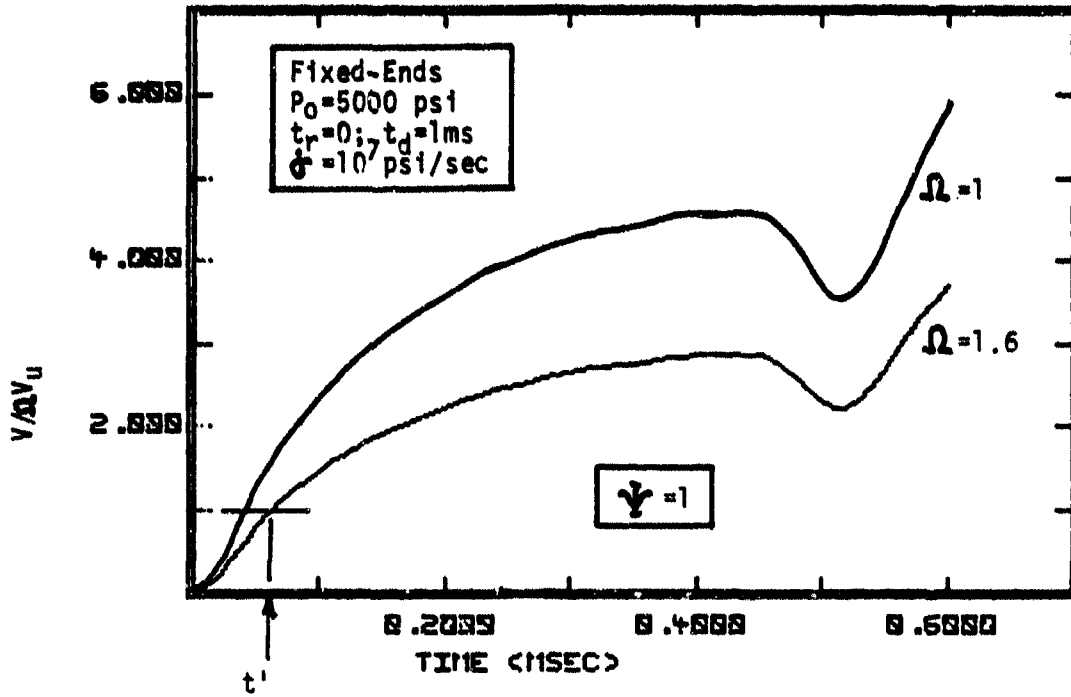


Figure 5.17 Strength Enhancement Effects on Normalized Support Shear of Example Beam

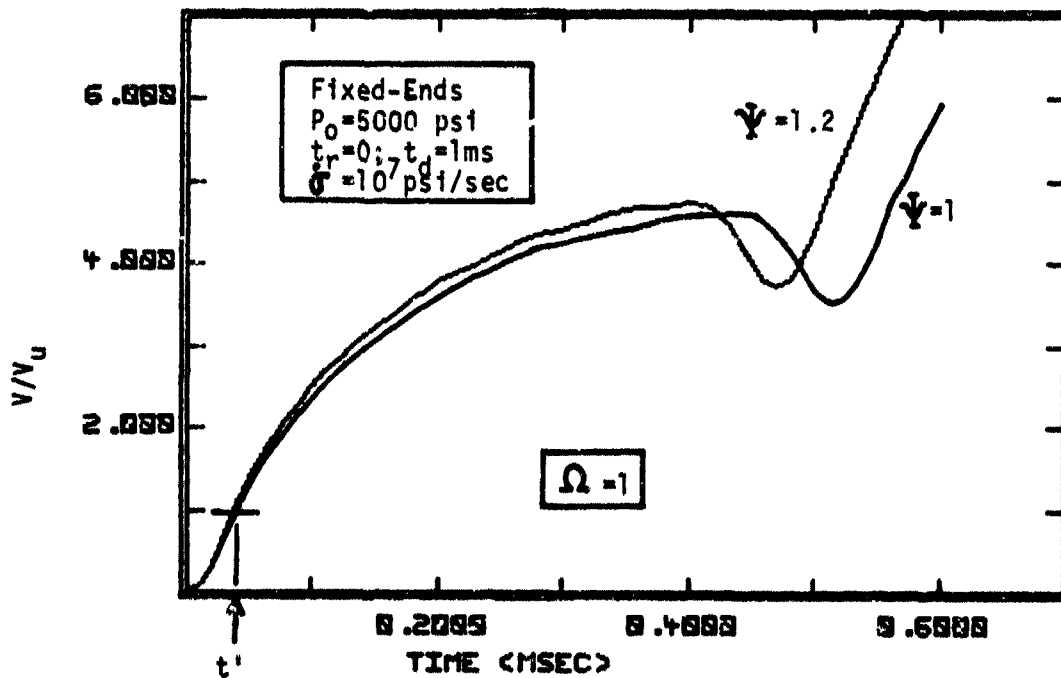
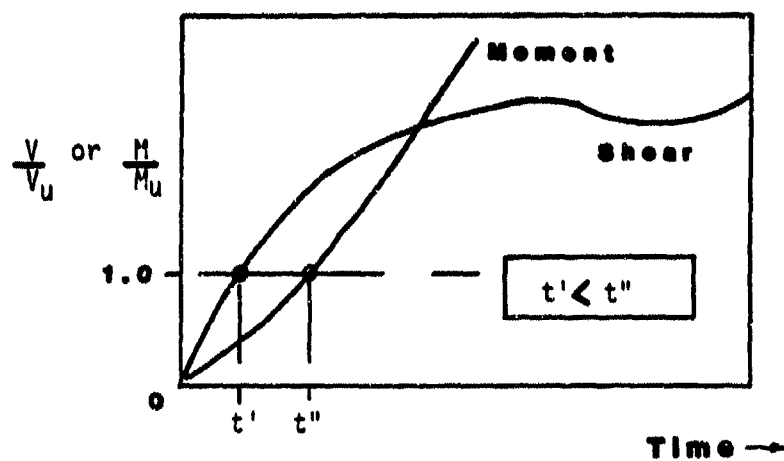
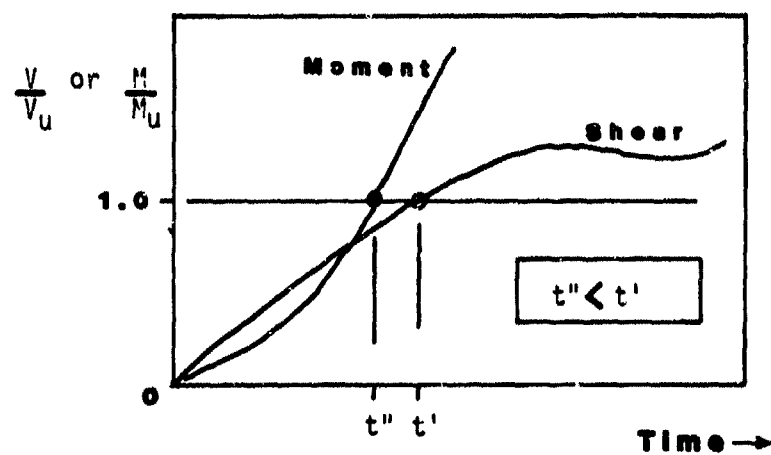


Figure 5.18 Modulus Enhancement Effects on Normalized Support Shear of Example Beam



a) Direct Shear Failure Predicted



b) Direct Shear Failure Not Predicted

Figure 5.19 Direct Shear Failure Time Parameters

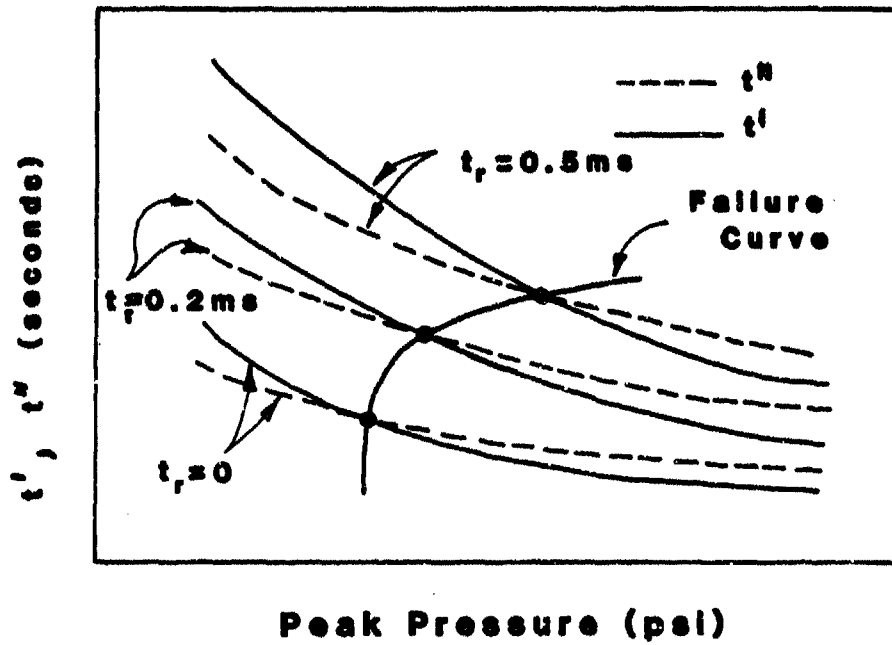


Figure 5.20 Construction of Failure Curves

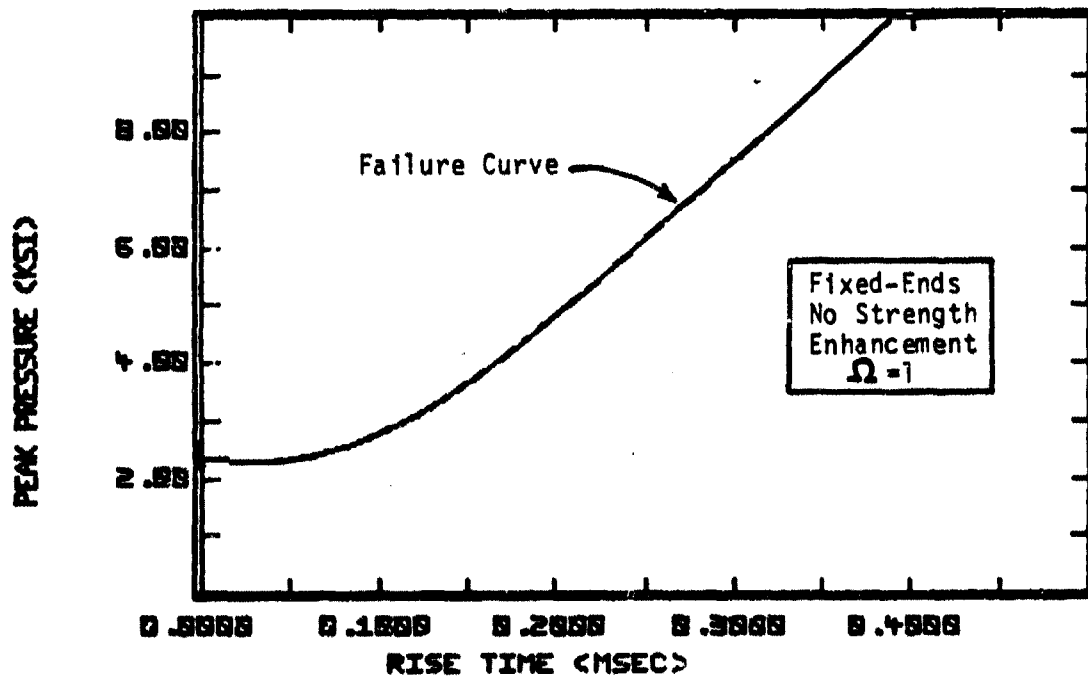


Figure 5.21 Failure Curve for Example Beam; Fixed-Ends, No Strength Enhancement

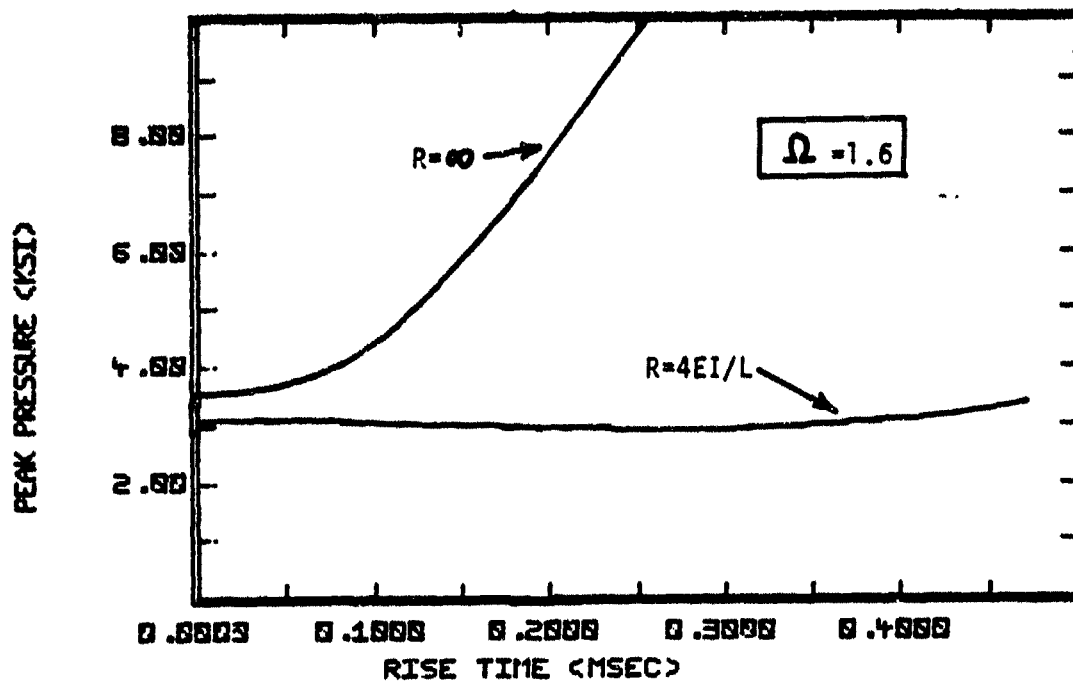


Figure 5.22 Influence of Beam-End Restraint on Failure Curve of Example Beam

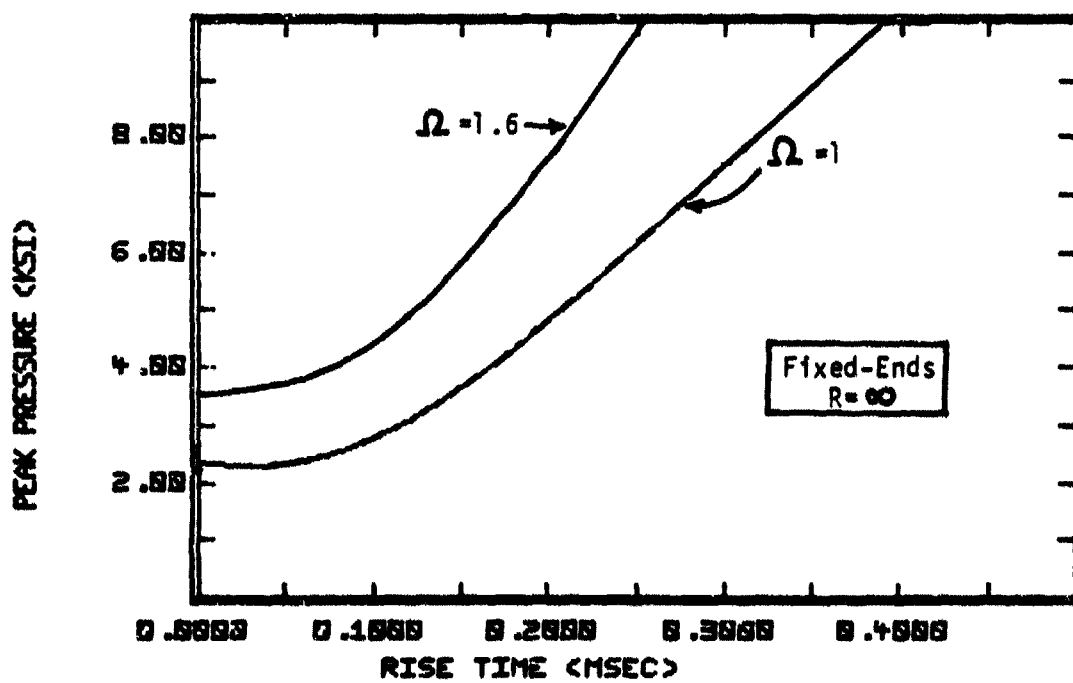


Figure 5.23 Influence of Strength Enhancement Factor on Failure Curve of Example Beam; Fixed-Ends

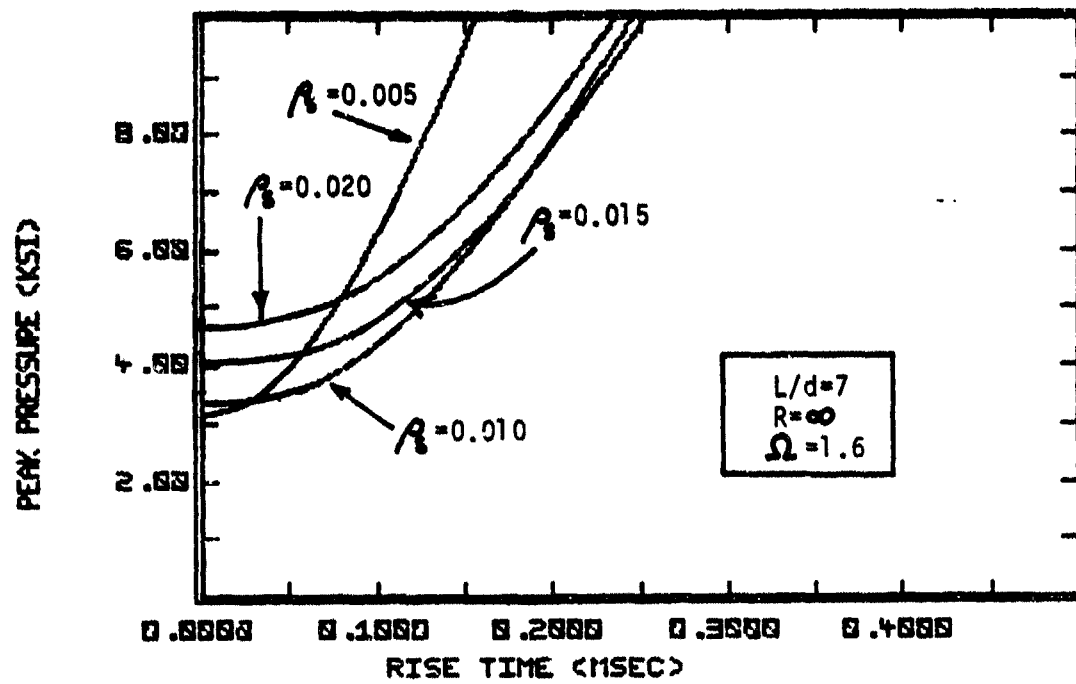


Figure 5.24 Influence of Reinforcement Ratio on Failure Curve of Example Beam; Fixed-Ends

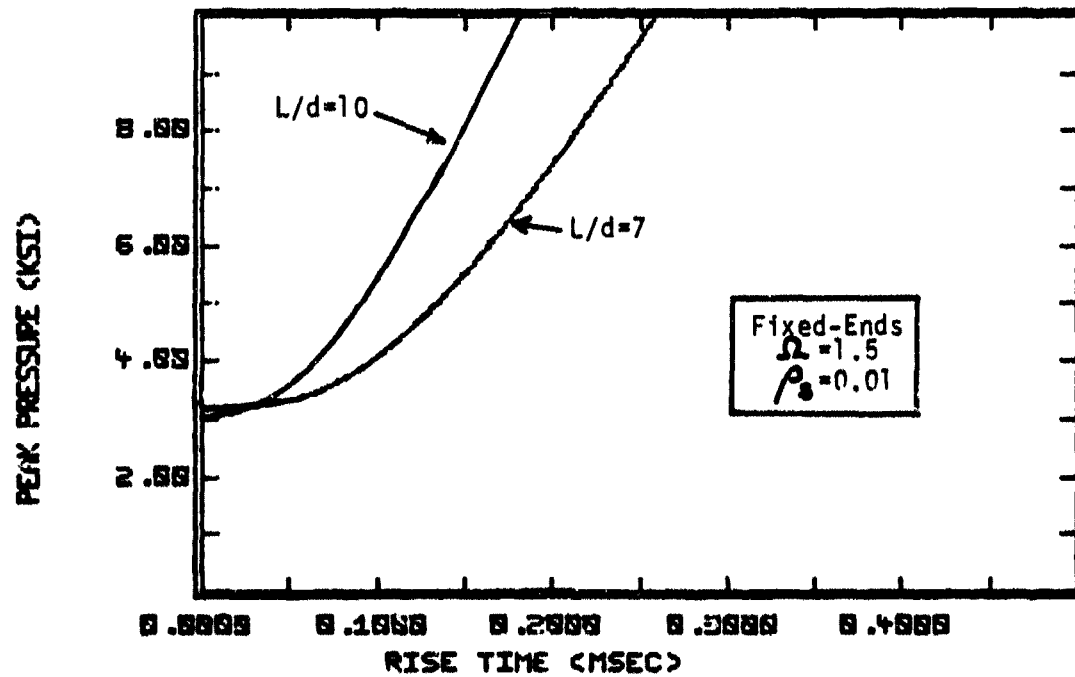


Figure 5.25 Influence of L/d Ratio on Failure Curve of Example Beam; Fixed-Ends

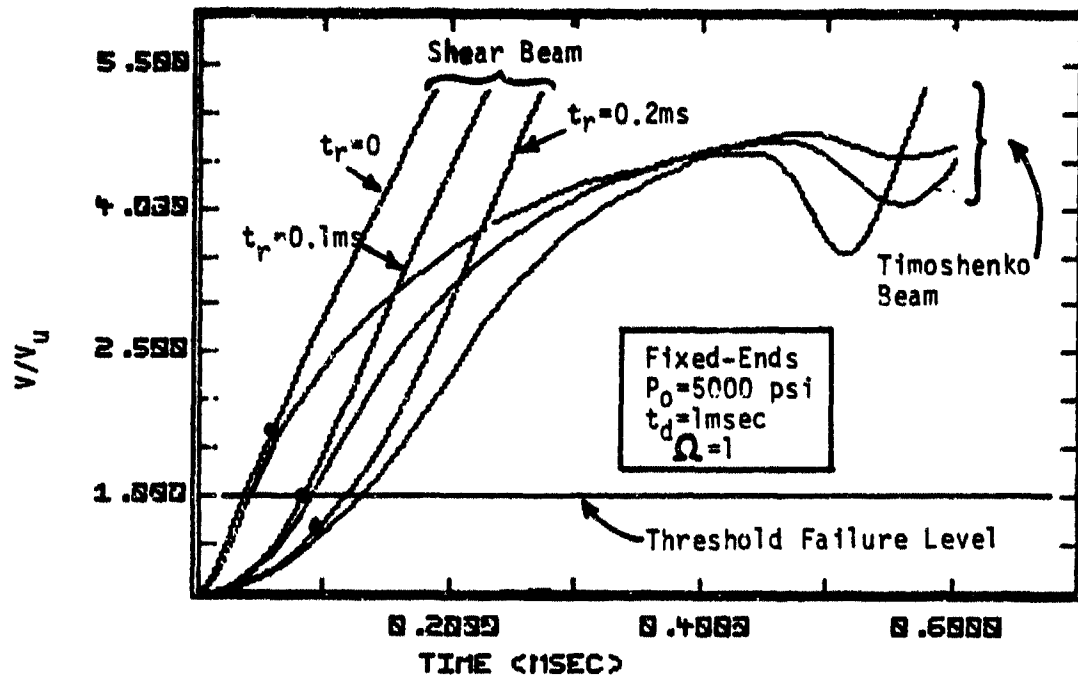


Figure 5.26 Comparison of Support Shear Forces for a Timoshenko Beam and a Shear Beam; Fixed-Ends

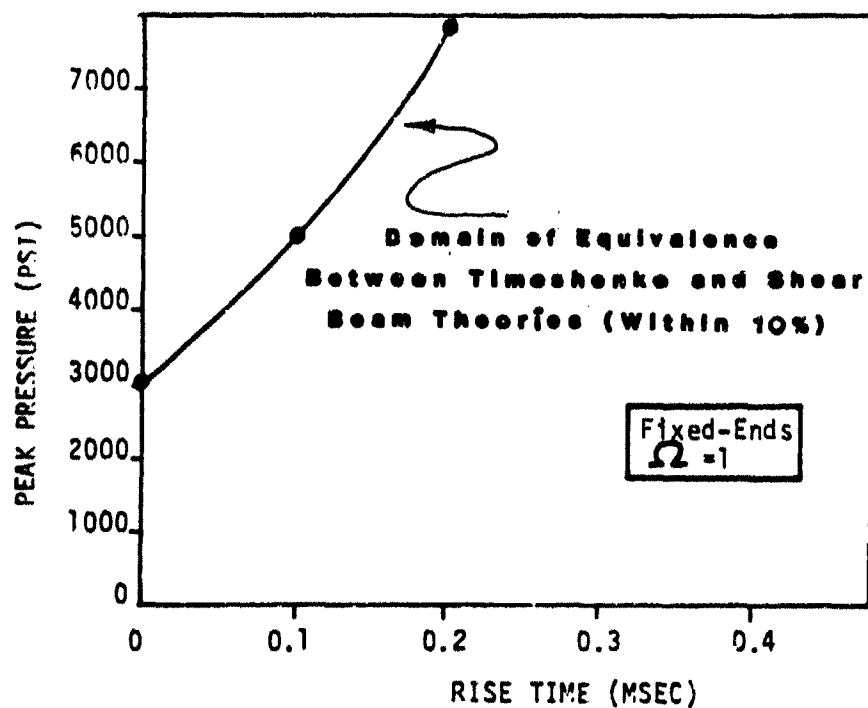


Figure 5.27 Domain of Equivalence for Support Shear Forces

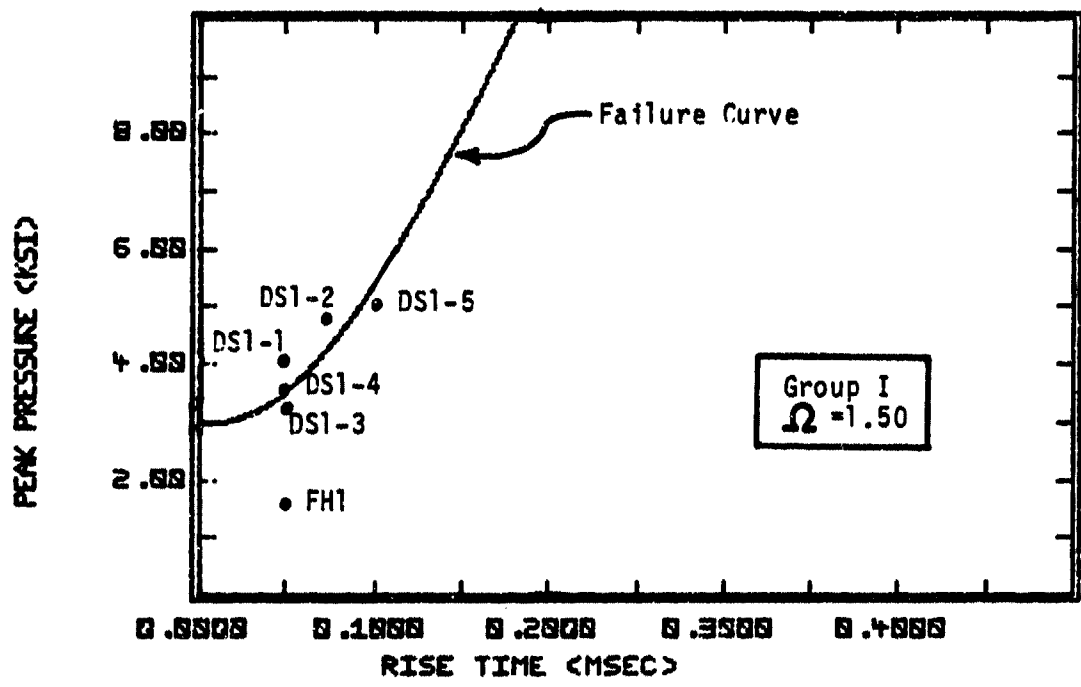


Figure 5.28 Comparison of Failure Curve and Test Data: Group I Beams

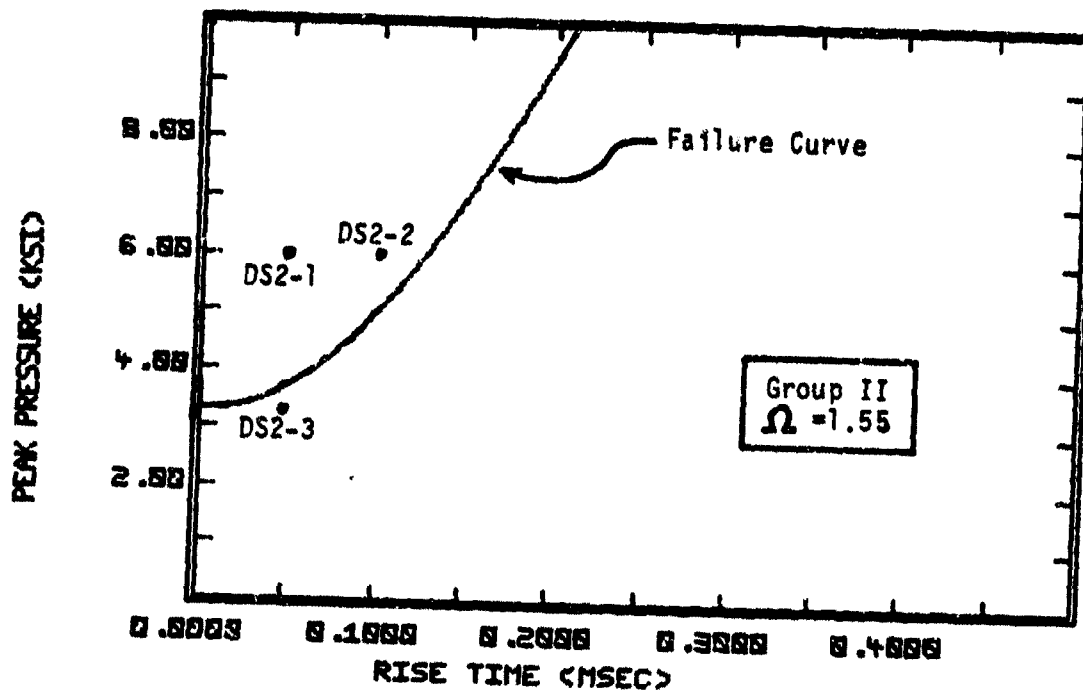


Figure 5.29 Comparison of Failure Curve and Test Data: Group II Beams

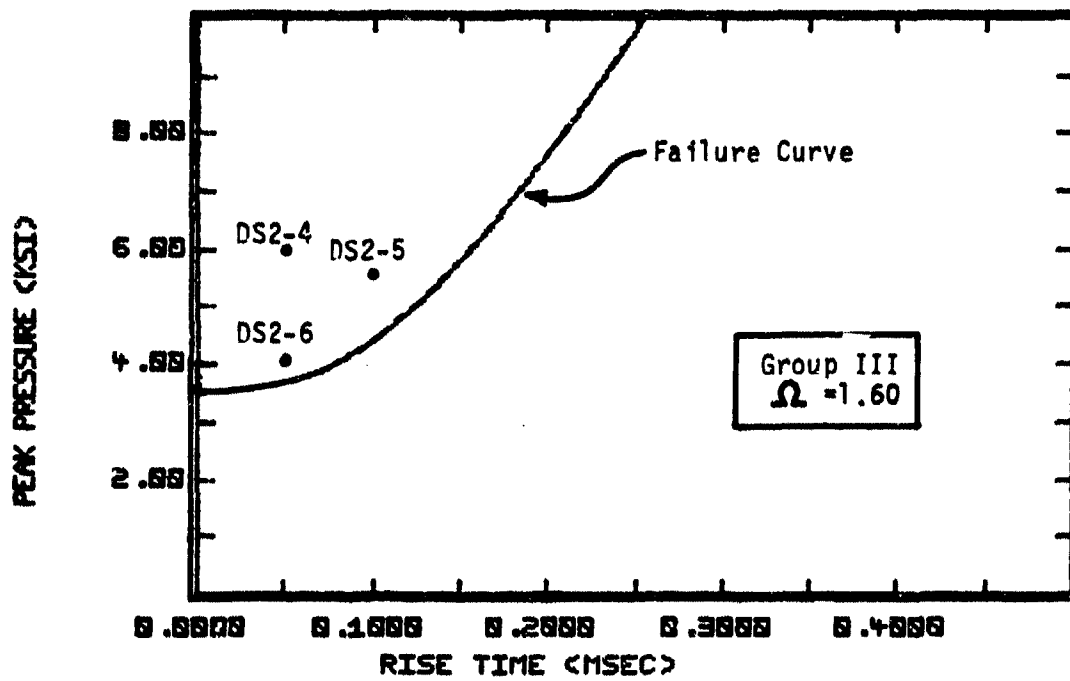


Figure 5.30 Comparison of Failure Curve and Test Data: Group III Beams

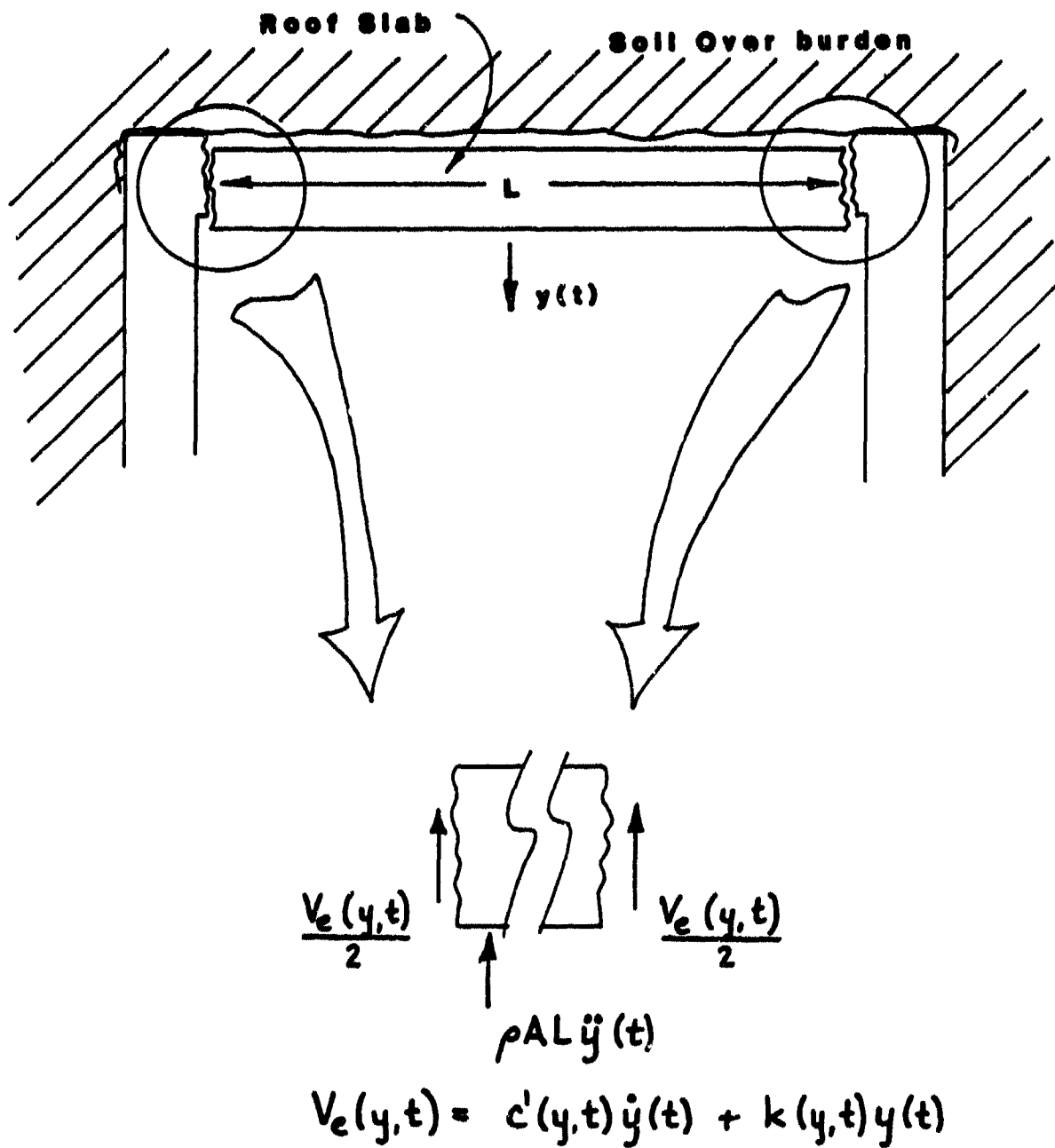
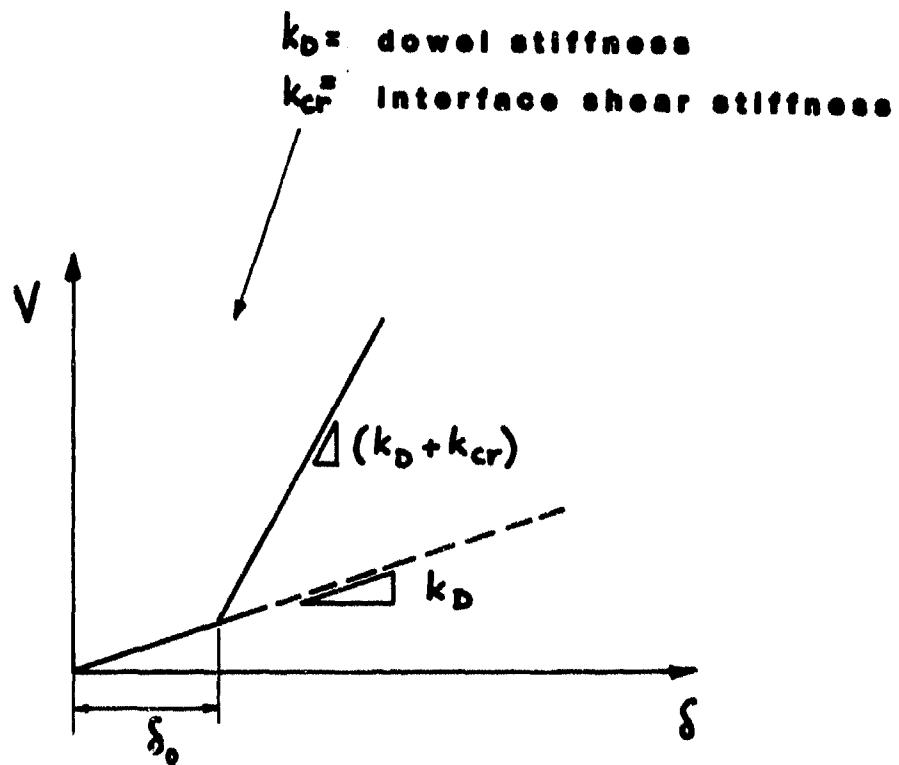
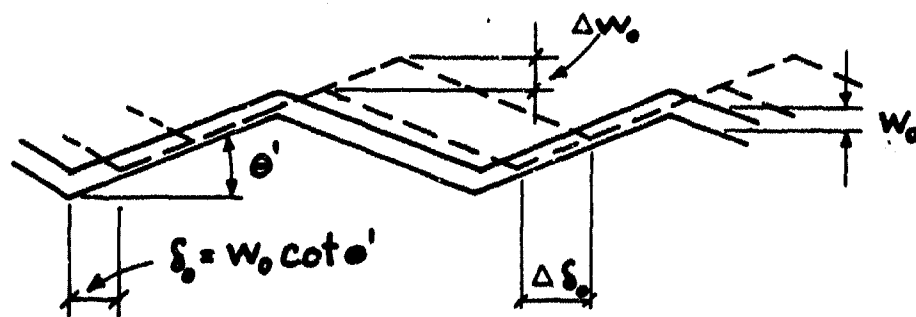


Figure 6.1 Post Failure Model: Rigid-Body Motion



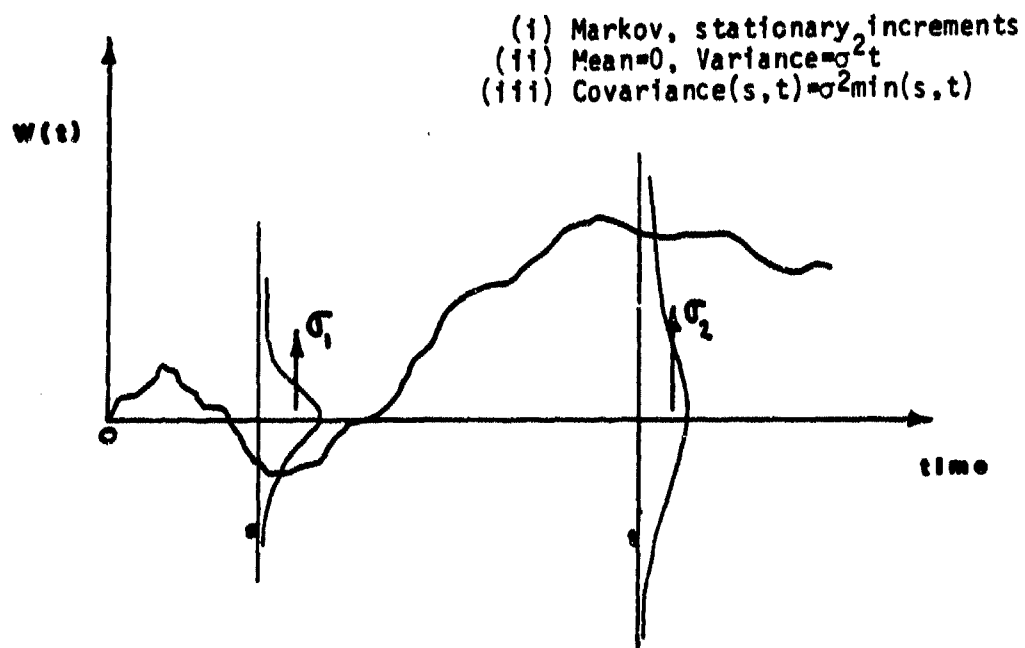
a) Crack Stiffness (Buyukozturk '79)



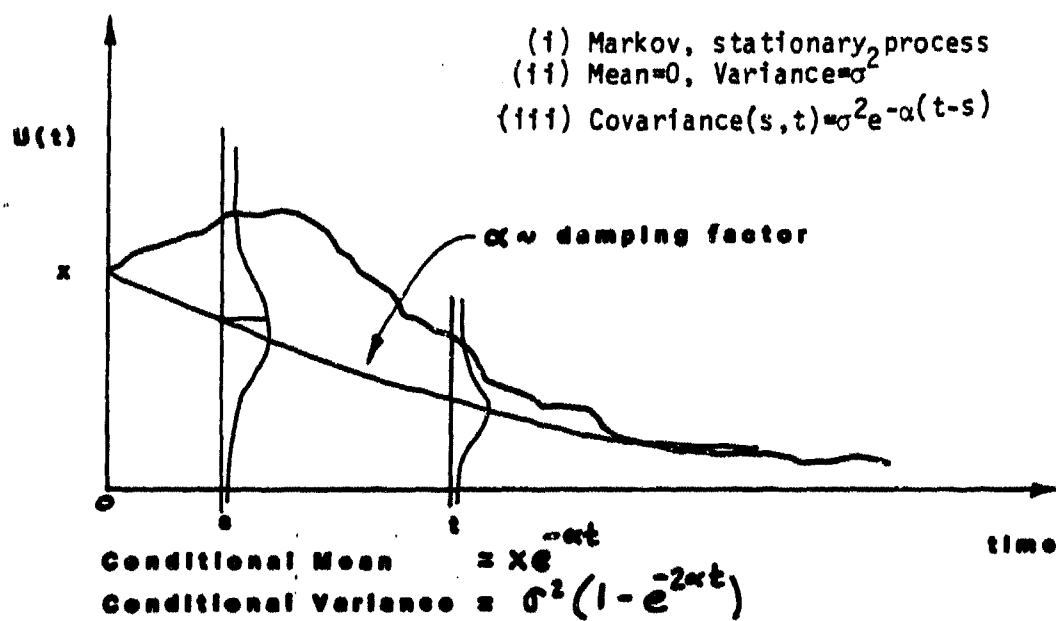
$w_0 =$ initial crack width

b) Crack Displacement

Figure 6.2 Shear Stiffness vs. Shear Displacement for a Precracked Shear Plane



Wiener Process, $W(t)$



Ornstein-Uhlenbeck Process, $U(t)$

Figure 6.3 Stochastic Processes: Wiener and Ornstein-Uhlenbeck

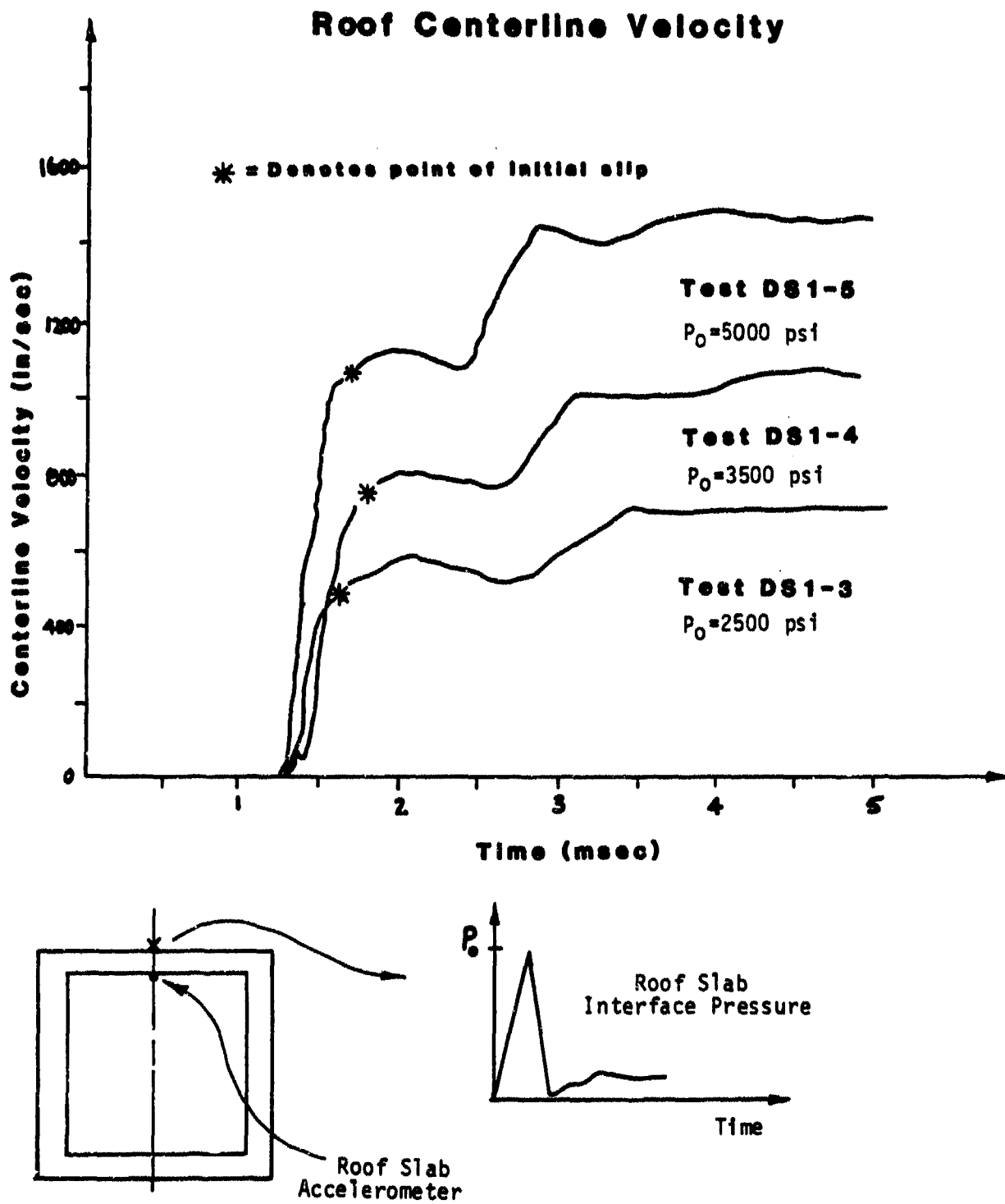


Figure 6.4 Test Roof Slab Velocity (Kiger'82)

APPENDIX A

Interface Pressure Loading

General

The interaction loading at a soil-structure interface can be illustrated by considering a disturbance in the medium (free-field velocity) which is propagated towards the structure, a portion of which is shown in Figure A.1. If the structure moves with the surrounding medium, i.e., if it acquires the same velocity as the free-field (at the location it occupies) would have, the structure experiences the same motion as the free-field and there is no interaction effect (Figure A.1a).

On the other extreme is the case when the structure remains stationary despite movement of the medium around it. At a rigid boundary an incident velocity pulse is reflected as a velocity pulse of equal magnitude propagating in the opposite direction (so that the resultant velocity at the rigid boundary is zero), and the stress at the interface is twice that of the incident wave. The amplification factor for interface pressure in this case is 2. Even for this extreme case, an amplification factor of 2 can be erroneous if applied over the complete duration of the free-field pulse. This is because there are several mechanisms by which the amplification due to reflected stresses can be relieved. As shown in Figure A.1b, relief may come from a free surface such as the ground surface (B) or an edge or corner of the structure (A) beyond which the free-field stress is not reflected.

The actual interaction process experienced by a structure is somewhere between the two extremes just described. The structure usually acquires some velocity of

its own which is different from the free-field velocity. Motion of the structure provides another mechanism to relieve the stress amplitude due to reflection of the initial compression wave off the free surface at the underside of the concrete slab (B) as in Figure A.1c. The extent of the relief depends on the motion of the structural component; at the side walls where motion is small there will be little relief, and at midspan of the slab the relief due to motion of the slab may be significant. Relief due to the free surface at the original ground surface (B) and due to the corner (A) usually are considered negligible.

Interface Stress

When a transient wave strikes an interface between two materials having different acoustic impedances (mass density times dilatational wave velocity), part of the energy of the incident wave will be reflected and part will be transmitted as seen in Figure A.2. When the direction of the wave is normal to the plane between the two materials, called normal incidence, the values of reflected stress, σ_r , and transmitted stress, σ_t , in terms of the incident stress, σ_i , are given by

$$\sigma_r = \left\{ \frac{\rho_2 c_2 - \rho_1 c_1}{\rho_2 c_2 + \rho_1 c_1} \right\} \sigma_i \quad (\text{A-1})$$

$$\sigma_t = \left\{ \frac{2\rho_2 c_2}{\rho_2 c_2 + \rho_1 c_1} \right\} \sigma_i \quad (\text{A-2})$$

where c_1 and ρ_1 are the dilatational wave velocity and mass density, respectively, of the medium in which the wave is originally traveling and c_2 and ρ_2 are the

corresponding parameters for the material on the other side of the interface. If the interface is unbonded, i.e., cannot carry a tensile force, compressive waves will be transmitted across the interface but tension waves will not. The arrival of a tension wave will, in the absence of another compressive wave of equal or larger magnitude propagating in the opposite direction, immediately part the unbonded interface preventing further interaction between the two materials.

The transmitted wave will always have the same sign as the incident wave. Also, the reflected wave will have the same sign as the incident wave if $\rho_2 c_2$ is greater than $\rho_1 c_1$ and will be of opposite sign if $\rho_2 c_2$ is less than $\rho_1 c_1$.

The two extreme cases mentioned earlier are of special interest as seen in Figure A.3. At a free edge $\rho_2 = 0$, the reflected wave will be equal in magnitude but opposite in sign to the incident wave (this arises because the stress on the surface has to vanish). At a rigid edge $\rho_2 c_2 = \text{infinite}$, the stress is doubled and the reflected wave has the same sign as the incident wave (this arises from the condition of zero velocity at a rigid interface boundary).

Interface Pressure Decay Characteristics

After an incoming wave experiences a reflection and transmission at an interface boundary between soil and concrete the pressure versus time character beyond the peak value becomes more complicated, involving pressure relief due to three different processes. The first process involves multiple wave reflections and transmissions at the soil-concrete interface and the concrete free edge. The second process involves interface pressure decay when the original incoming wave form also decays with time. And the third process involves pressure relief when

motion of the slab away from the soil reduces the interface pressure between the soil and concrete slab. This later process is often termed a soil-structure interaction.

The pressure decay process associated with wave reflections and transmissions can best be illustrated by using one-dimensional elastic wave theory and the aid of a characteristics diagram as developed by Wong '78 and shown in Figure A.4. The figure presents a plot of distance versus time for a two layer finite element model of soil and concrete. In this figure the lines with arrows show the direction of wave propagation and the velocity of propagation is determined by the slope of these lines — the steeper the slope the higher the velocity. The figure is for a step pulse (no decay with time) with a peak pressure of 1000 psi and it shows schematically the influence of several wave reflections and transmissions at the interface and free edge. For example, from point A to point C there are two round-trips of the wave through the concrete layer and the interface pressure at point C is determined simply by the algebraic sum of the magnitude of previous waves, i.e., $1000 + 800 - 300 - 250 = 1250$ psi. The time associated with this decay from 1800 psi to 1250 psi depends on the wave transit times and hence the thickness of the concrete slab. Therefore a quick decay is associated with a thin slab.

The decay characteristics associated with an initially decayed ground shock pressure pulse (incident wave) are shown schematically in Figure A.5. The curves in this figure are the results of a finite element study conducted by Wong '78, which have been rescaled to a time domain on the order of milliseconds. As can be

seen the interface pressure decays more rapidly as the duration of the original pulse decreases.

The interface pressure decay characteristics associated with slab motion are shown in Figure A.6. As shown the interface pressure is relieved much quicker under conditions where the two layers are allowed to separate. This occurs at an ideal free edge when the concrete slab moves away from the overlying soil until it actually separates and reduces the contact pressure to zero.

Slab Velocity

Associated with propagating stress waves is a particle velocity pulse given by the one-dimension relationship

$$\sigma = \rho c v \quad (A-3)$$

where σ is the stress, v the corresponding particle velocity, and ρc the acoustic impedance of the medium. The relationship holds for elastic materials. The interface stress (over some area) can be thought of as the action which causes the slab to move as a rigid body with velocity v .

Peak velocity of a slab is attained at the time the interface stress reduces to zero. For an interface which cannot sustain tension, such as exists between concrete and soil, the velocity will remain at its peak value and will not decay. Physically, this means that the slab temporarily moves away from the soil when it achieves a

higher velocity than the soil. At the extreme case of a rigid boundary, the concrete slab cannot move and there is no relief due to motion.

Possible Dynamic Failure Mechanism

Having discussed the issues of stress reflection and transmissions and the issue of particle velocity associated with one-dimensional wave propagation theory, it is feasible to envision the initial formation of a direct shear failure at a slab support due to the passage of a wave front through the thickness of the member. This heuristic discussion certainly does not completely describe the entire dynamic failure process but it does provide one reason why dynamic direct shear may be initiated in a different fashion than has been seen in slab response under static loads.

This possible scenario for dynamic failure in direct shear is characterized by the rapid propagation of a near-vertical crack through the depth of the roof member. This crack is produced by high shearing stresses near the roof supports. The occurrence of these high shear stresses at the roof support can be explained by simple one-dimensional elastic wave propagation theory. Stress concentrations develop when part of a shock wave front is reflected while another part of the same wave front is transmitted at the support for the buried reinforced-concrete box under the influence of a planar, vertically propagating, one-dimensional wave front. This phenomenon can be seen by referring to Figure A.7.

As shown in Figure A.7, area I is an open space having an impedance of near zero (for calculations it is identically zero) and area II has a higher impedance than area I. On reaching the plane defined by the line AD, that part of a compressional

wave front lying between points B and C will undergo total reflection. The rest of the front will continue downward unimpeded. As a consequence of the conservation of momentum across boundaries (a free surface is a boundary) the element BC begins to move with twice the velocity of the elements AB and CD. Here, BC is a reflecting surface and AB/CD are transmitting surfaces. The result of this differential motion is the buildup of intense stresses in the neighborhood of the points B and C. Consequently small fractures and small regions of crushed concrete are initiated at the corners in the wake of a shock wave. In a two-dimensional sense, shear waves and longitudinal waves will interact and produce a complex series of wave patterns near points B and C.

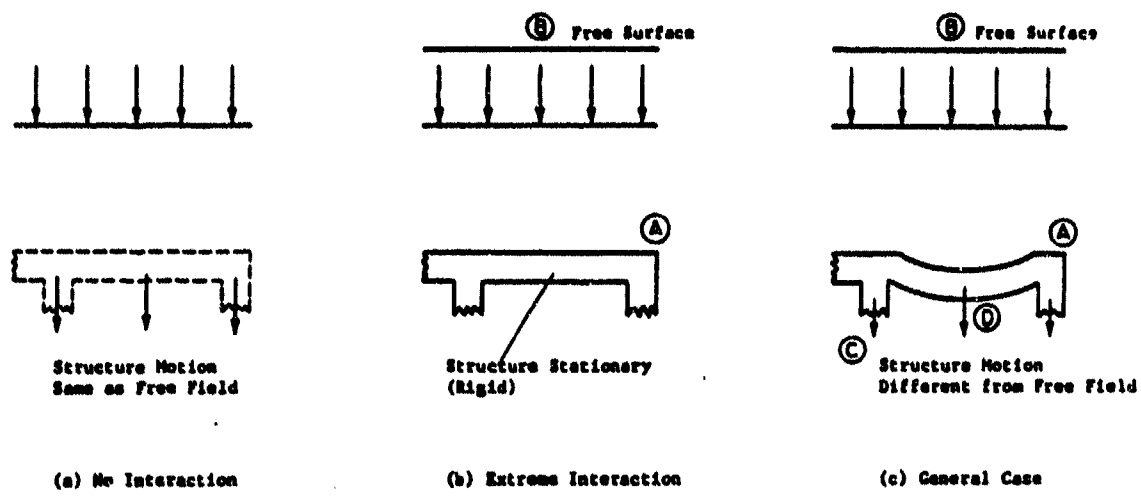


Figure A.1 Soil-Structure Interaction (Wong'78)

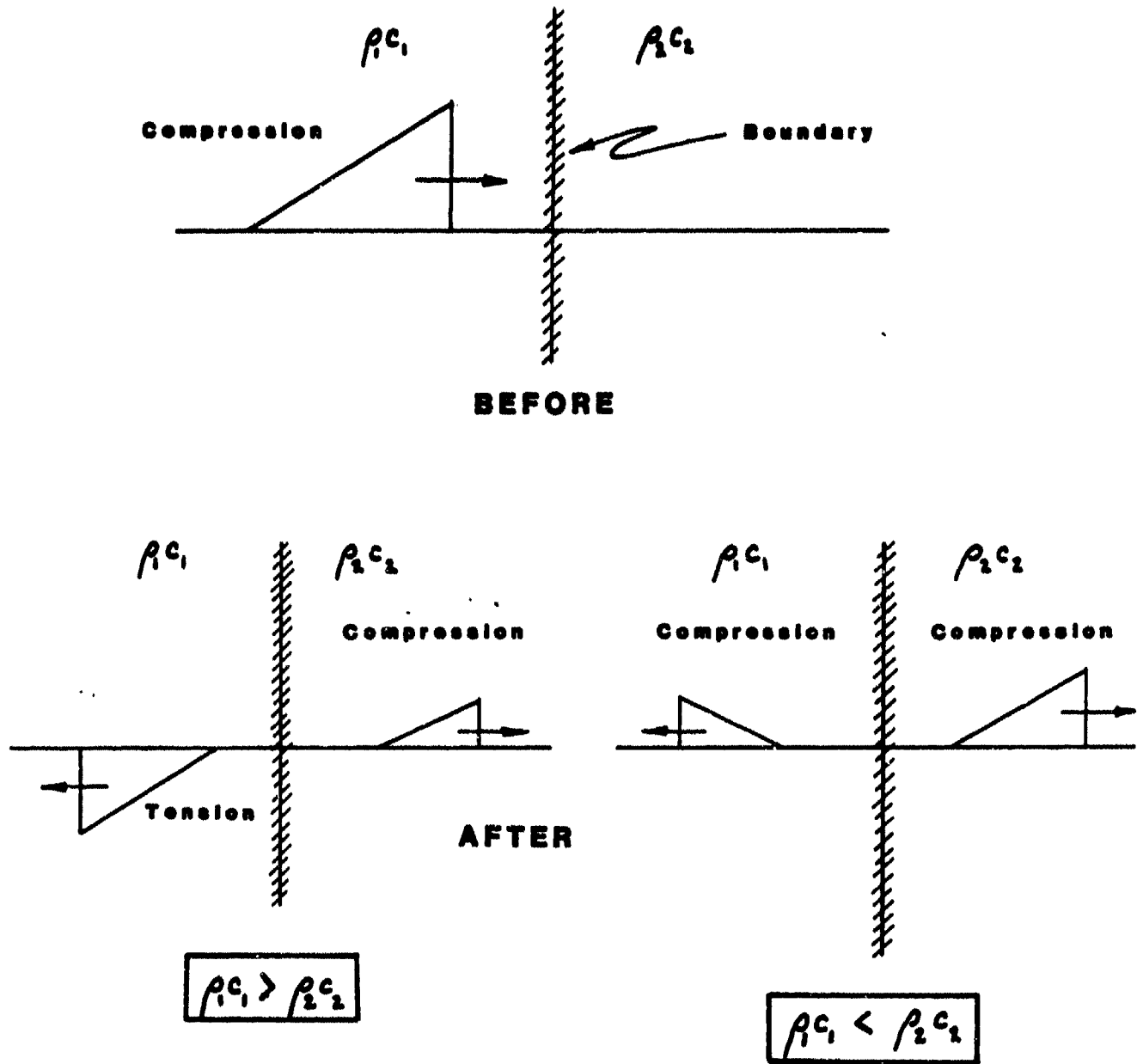


Figure A.2 Stress Wave Propagation at a Boundary Between Dissimilar Elastic Materials

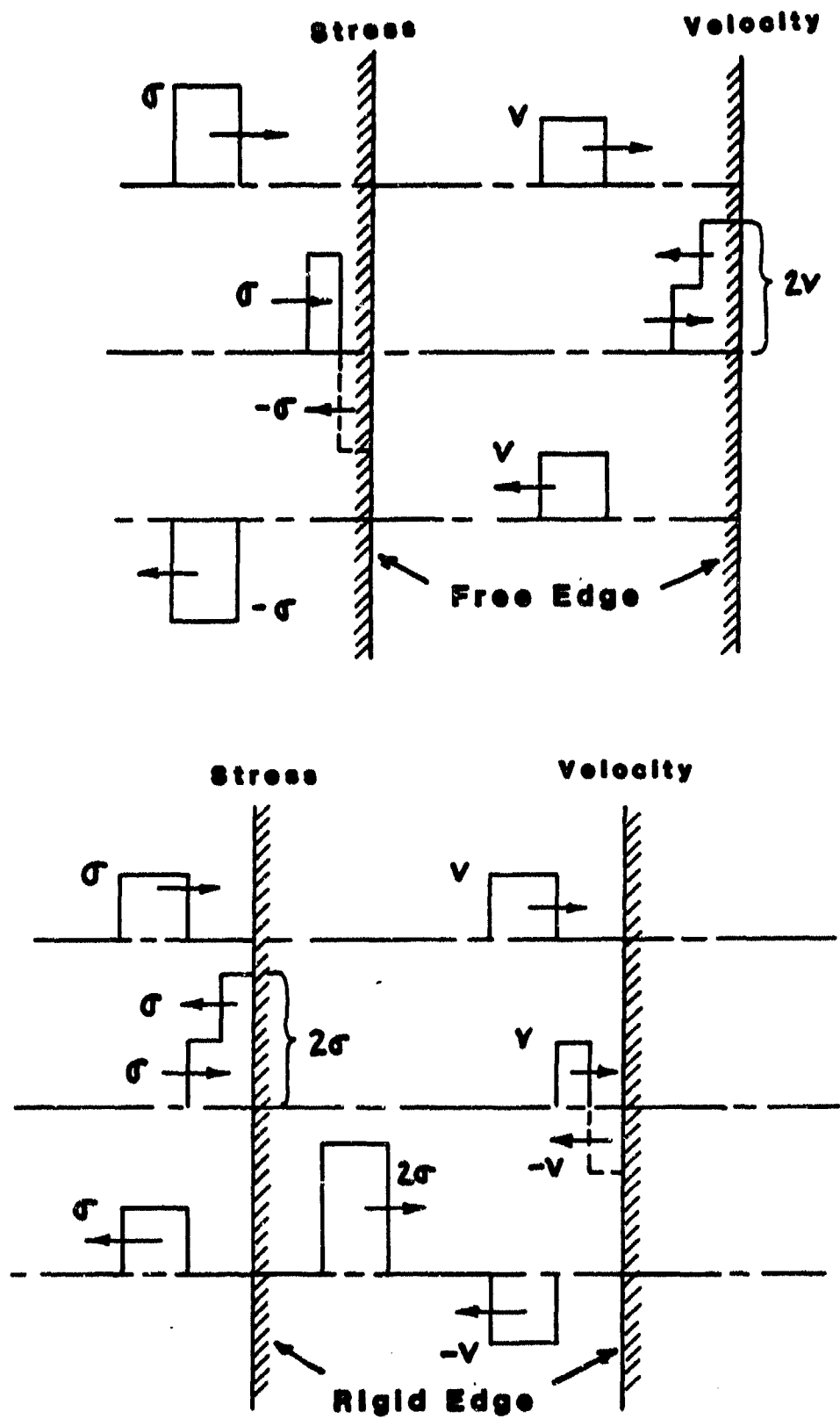


Figure A.3 Reflections and Transmissions at Free and Rigid Boundaries

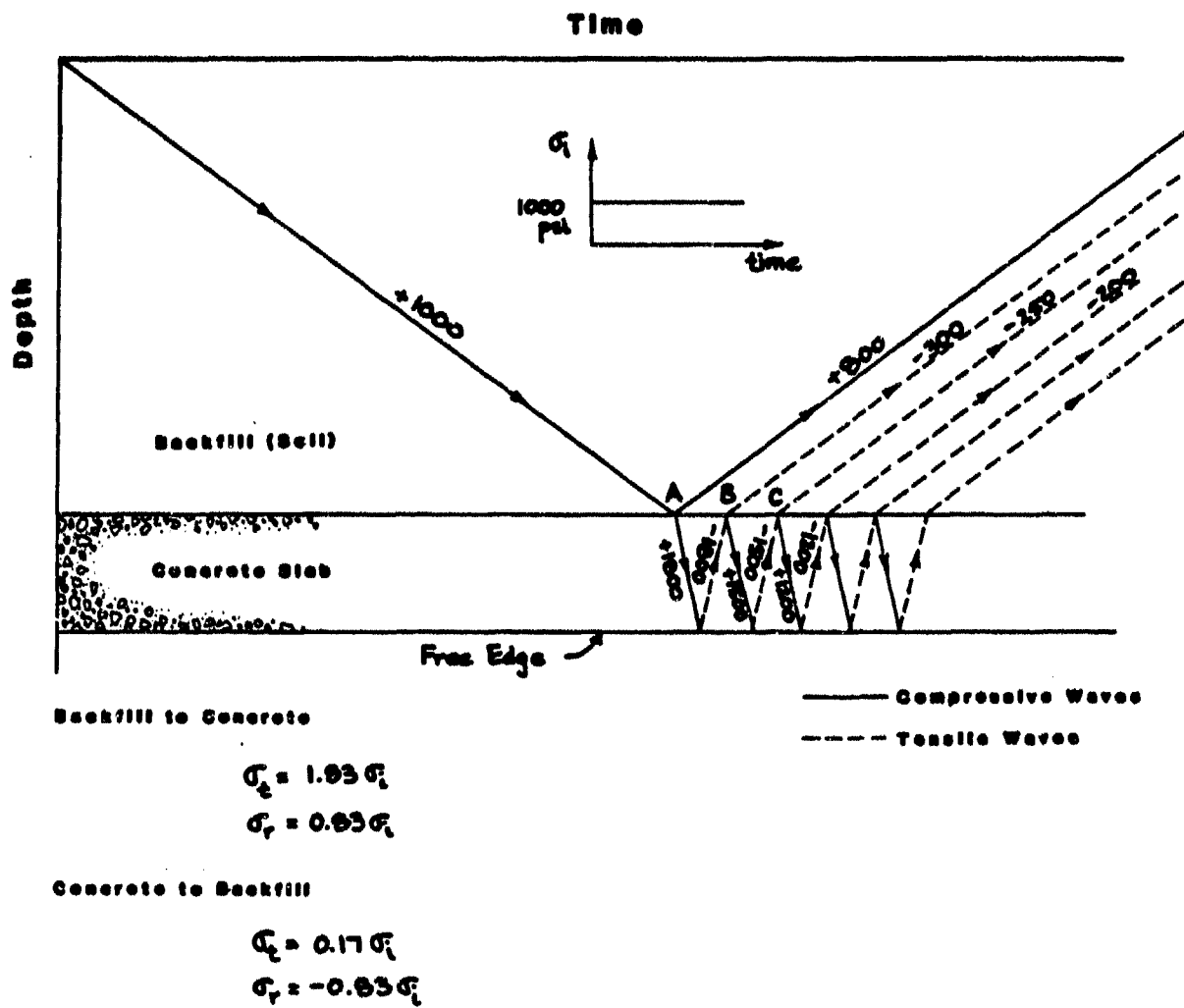


Figure A.4 Characteristic Diagram, One-Dimensional Elastic Wave Interaction (Wong'78)

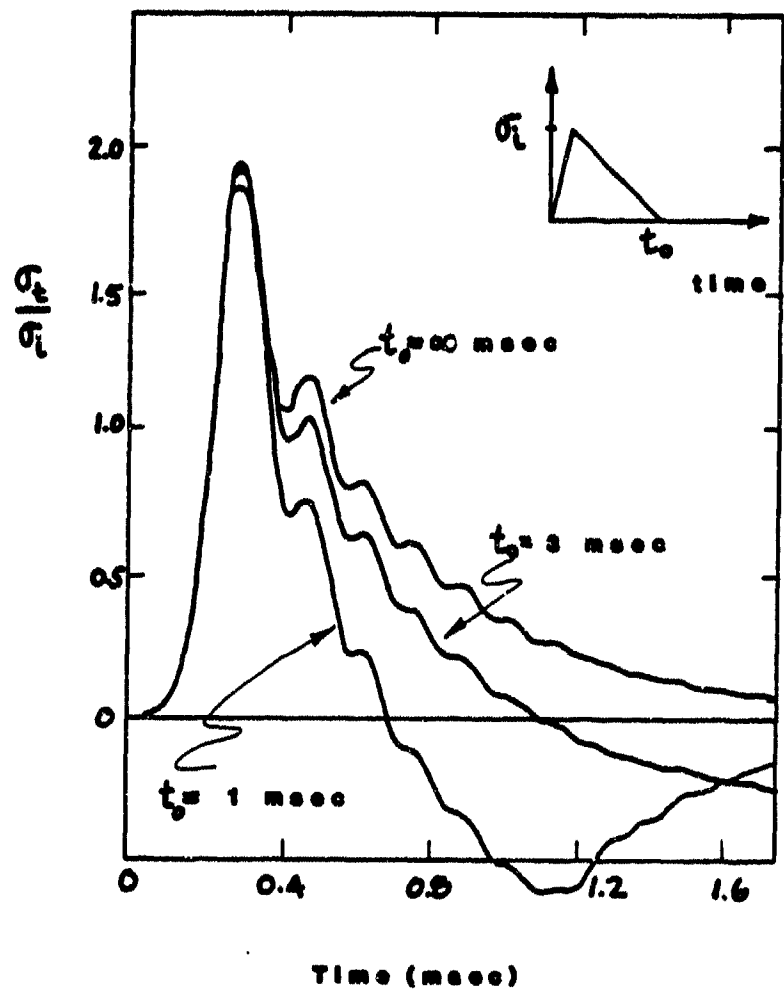


Figure A.5 Interface Pressure for Different Incident-Pulse Durations (Wong'79)

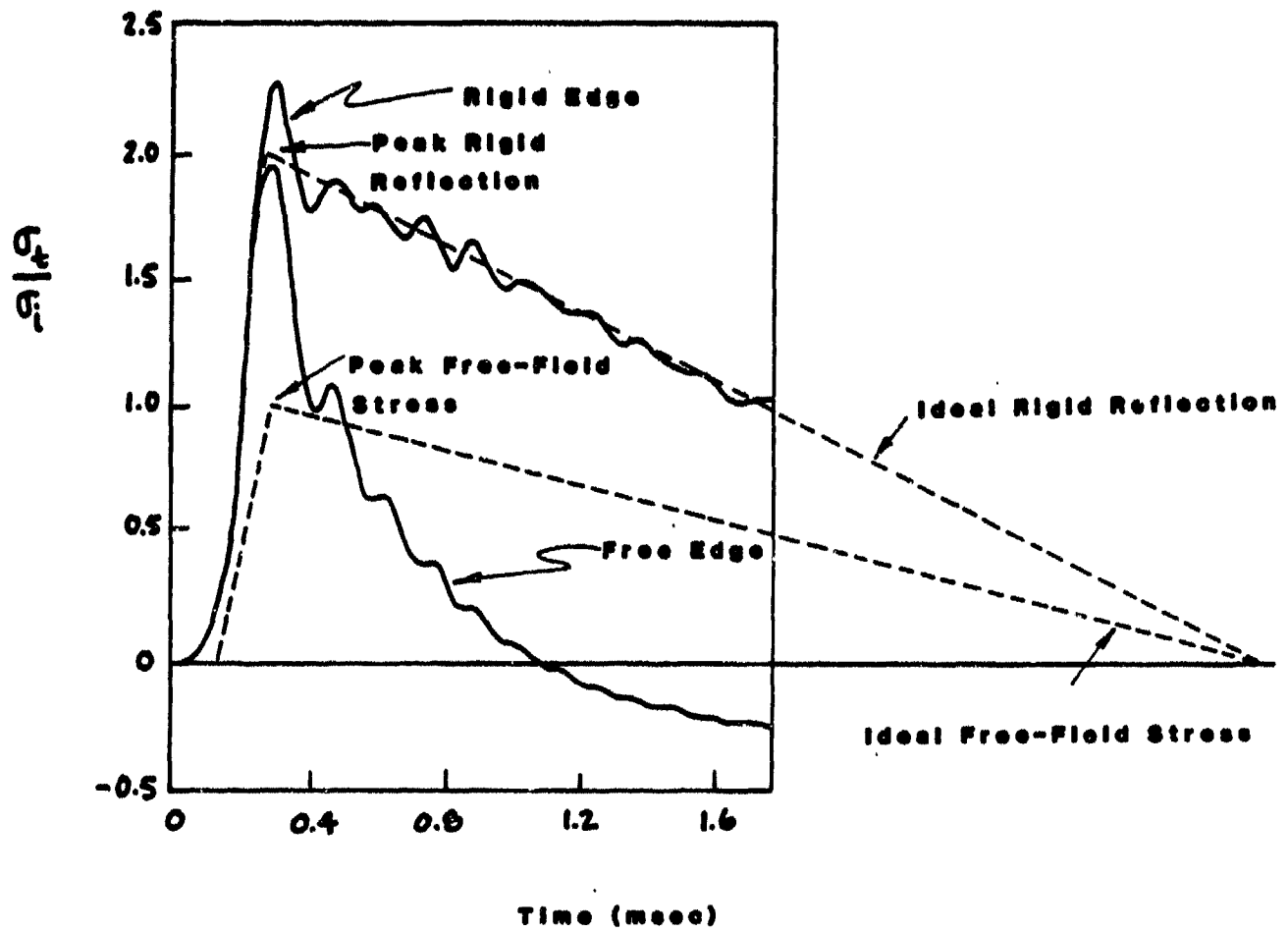


Figure A.6 Comparison of Interface Pressure Decay for Different Boundary Conditions (Wong'78)

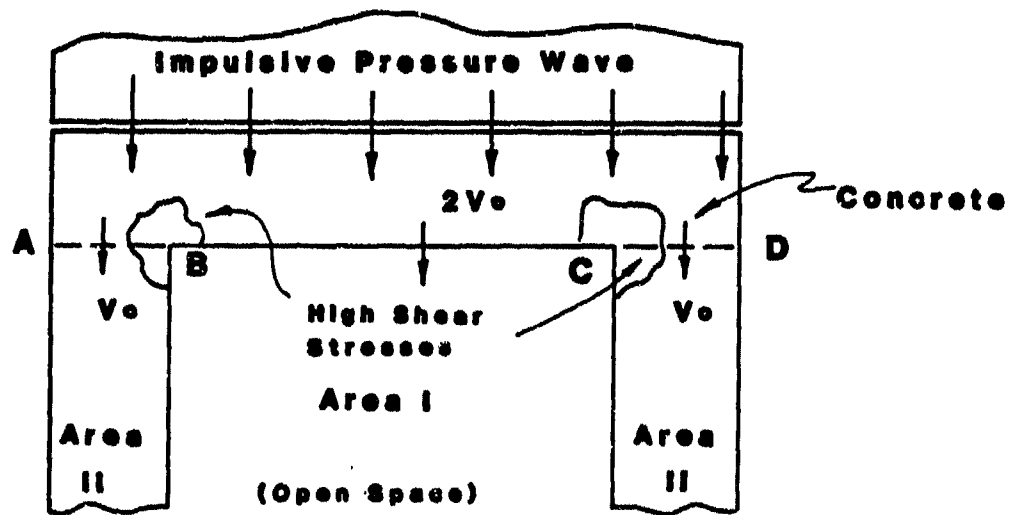


Figure A.7 Wave Propagation Through a Roof Slab

APPENDIX B

Concrete Fracturing

General

Concrete is a complex material. It is formed by a combination of components involving a mix of coarse aggregates, sand, unhydrated cement particles, cement gel, capillary pores, and entrapped air voids. Despite the large amount of results of experiments and investigations into the nature and character of concrete, there persists a tremendous divergence in reported mechanical properties (see Gerstle et al '80). The large variability in these mechanical properties depends on the uncertain nature of the concrete constituents, mixing, placement, compaction, and curing process. And perhaps no greater uncertainty exists than that which is associated with attempts to determine the conditions under which concrete will fail when subjected to high rates of loading. An understanding of the phenomenon of concrete fracture is helpful in reducing this uncertainty.

Static Fractures

Under static loads crack propagation can be detected by the reduction in slope of the uniaxial stress-strain curve, by an increase in the Poisson ratio, or by a reduction in the sonic velocity through a concrete specimen. In the static case, cracks typically develop normal to the plane of maximum tensile stress, as shown for the cases of uniaxial tension, uniaxial compression, and biaxial compression in Figure B.1.

As seen in Figure B.1 a columnar fracture pattern develops under uniaxial compression and a laminar fracture pattern develops under biaxial compression

(Nichols '76). It is relevant that in uniaxial compression cracking occurs in the direction of the applied stress because in all other directions there is no normal component of compressive stress. Cracking occurs at the aggregate-paste interface, in the cement paste, or in the aggregate particles depending on the relative stiffness and strength of the two materials.

Dynamic Fracture

Rinehart '79 gives an excellent discussion of the conditions leading to fracture. This discussion is summarized here for the purpose of highlighting differences between static and dynamic situations. There are distinct differences between fracture phenomena occurring under impulsive loads and those associated with static loads. Under static loads the stresses and the strains are distributed throughout the concrete element, permitting every particle to participate in the initial formation of fractures. Once a fracture has been formed, local stress concentrations control subsequent propagation of the fractures. Under impulsive loads highly localized areas of high stresses and strains may exist independently of stress-strain conditions in another region. This transient stress condition may change so rapidly that fractures that form may not have time to propagate before the stress situation changes.

The formation of fractures can occur under various transient situations such as:

- 1) stress inhomogeneities that result from the interference of waves, frequently caused by the generation of additional waves from reflections at free surfaces;
- 2) relative lateral motion, associated with cylindrical and spherical waves; and,
- 3) large volumetric expansion upon release of load following compression.

Aside from impulsively generated fractures, other dynamic fractures are similar to statically generated fractures. For example, fields of dynamic shear stress which develop progressively as an impulsive load moves throughout a material causes shear failures similar to those caused by static loading (Rinehart '79).

In dynamic fracturing that is associated with shearing stresses, the trajectory of the macrofracture may be oriented differently with respect to the shear stress field than the individual microfractures that compose the macrofracture. Thus a shear stress field may cause microfractures to form which cannot propagate but which can, through their confluence, develop into a macrofracture.

These macrofractures can form as the final stage of extensive slip in a shearing action, a process initiated by shearing stresses, or they can form by cleavage of the material under a tensile stress. Rinehart '79 states, "the individual microfractures will always bear a preferred orientation with respect to the stress field, the one most favorable to their formation. The relative orientations of the microfractures and the macrofractures differ depending upon the nature of the generating stresses. When the path of the macrofracture lies along a trajectory of maximum shear, the microfractures will be oriented parallel to it if they are shear generated and will be inclined obliquely if they are tensile generated. When the path of the macrofracture is perpendicular to a principal tensile stress and the microfractures are of the cleavage type (a common spalling situation) the macrofracture and the microfractures making it up are oriented parallel to one another."

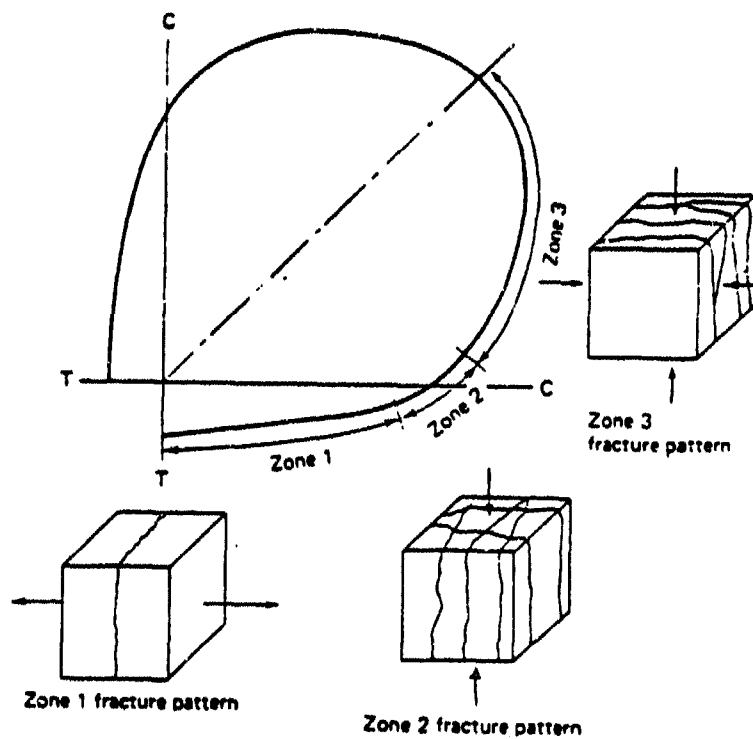


Figure B.1 Static Fracture Patterns in Concrete (Nichols '76)

APPENDIX C

Shear Transfer in Reinforced Concrete

General

Shearing forces in any reinforced concrete member including ordinary and deep beams, slabs, shear walls, and shear diaphragms can be carried by several force mechanisms. In addition to the direct transfer of shear force by uncracked concrete in the compression zone, contributions may include tensile force stirrups, dowel action in bars crossing shear cracks, friction and aggregate interlock of naturally rough surfaces appearing on the cracked surfaces, and the direct thrust between load points and reactions as permitted by internal force redistributions after shear cracking. The relative importance of these different mechanisms depends upon the geometry of the reinforced concrete member, the spatial distribution of loads and reactions, the magnitude and qualitative nature of the loads, the existence of concrete cracks, and other factors such as the arrangement and inclination of reinforcing steel. Many of the summaries and figures in the following sections are taken from a recent report prepared by the American Society of Civil Engineers (ASCE '1982).

Generic Behavior

The distribution of shear stress in concrete beams can be predicted by analysis by assuming the member to be homogeneous, isotropic, and elastic. Before cracking the reinforcement carries only low stress. Dowel effects are small. After cracking (see Figure C.1a) a significant redistribution of internal forces occurs. For static loads the total shear resistance in a typical region is comprised of the sum of the uncracked portion of the concrete section, the interface shear transfer

across the crack by aggregate interlock (friction), the dowel contribution of the longitudinal steel, and the force transferred by direct tension in the stirrups; identified for the case of inclined cracking, respectively, as V_{cz} , V_{ay} , V_d , and V_s . These resistive force components are shown in Figure C.1b.

Vertical equilibrium of the free body in Figure C.1b requires that the external shear force will be equal to the sum of all of these internal forces. In predicting strength in shear the stirrup force is usually taken equal to $V_s = A_v f_y$ where A_v is the total area of steel crossing the crack and f_y the yield strength of the steel. The contribution of the four components is shown qualitatively in Figure C.1c as a function of applied external shear V_{ext} . Components V_s , V_{ay} , and V_d have little or no influence until flexural cracking, after which dowel action and interface shear transfer contribute.

After inclined cracking, the part of the shear carried by the stirrups V_s , increases nearly linearly while the sum of the other three components stays nearly constant. When the stirrups yield their contribution stays constant; however, because of widening of the cracks and splitting in the concrete along the longitudinal steel, V_{ay} and V_d fall off rapidly. This overloads the remaining cracked concrete and very soon results in failure.

Dowel Action

Reinforcing bars across a crack which has been subjected to shearing displacements represent the shear force which may be transferred by dowel action. This mechanism is shown for a typical beam in Figure C.2. The shear force V_d applied to the main reinforcement tends to cause downward bending of the bar. This is

resisted by the concrete which provides an upward reaction force V_1 . If the concrete cover distance S_1 is large, such as for mass concrete, local crushing of the concrete may occur near the crack face. For beams in which S_1 is only a few inches, splitting of the concrete along the bar is probable due to the vertical tensile stress produced in the concrete at the plane of the reinforcement. This tendency to split along the bar is augmented by the wedging action by the bar deformations as the bar tends to slip longitudinally through the concrete from flexural loading of the member. Following splitting the effectiveness of dowel action is a function of the distance S_2 from the shear crack to the first stirrup supporting the dowel.

Experimental studies on dowel action have been conducted by Fenwick and Pauley '68, Dulacska '72, Pauley et al '74, Krefeld and Thurston '66, Taylor '74, Sharma '69, Houde and Mirza '74, and Kemp and Wilhelm '77. Many of these experiments were similar to the one performed by Dulacksa '72 and shown in Figure C.3. The effect of dowel action is isolated from interface shear transfer by means of eliminating the latter by smoothing and lubricating the contact faces of the shear plane.

The parameters of interest in the dowel studies on beams include the angle of inclination of the reinforcement, the dowel diameter, dowel strength, concrete tensile and compressive strengths, reinforcement percentage of shear plane area, beam net width, bottom concrete cover, bar spacing, and the presence of transverse stirrups. These dowel studies can be separated into two groups — one where small diameter bars with large concrete covers were investigated, and the other where large diameter bars with relatively small concrete covers were studied. Basic conclusions of these studies are summarized here.

For the group of tests with small bar diameters and large concrete cover it has been shown, generally, that failure of the specimen occurred due to either yielding of the reinforcement or concrete crushing beneath the bar. Fenwick and Paulay '68 concluded that dowel capacity was strongly influenced by the position of the bar in the specimen and by dowel embedment length and that under optimum conditions dowel action could resist 25-30% of the shear resisted by the interface shear transfer mechanism. Paulay et al. '74 found that the resistance provided by dowel action was proportional to the reinforcement area.

The tests on large diameter bars with small concrete cover revealed that failure was initiated by the formation of splitting cracks around the bar periphery and subsequent spalling of concrete cover. Krefeld and Thurston '66 and Taylor '74 found that dowel strength increased with concrete tensile strength, increased concrete cover, and increased beam net width. Sharma '69 concluded that dowel capacity increased when the bond quality between bars was improved and that stirrups increased dowel capacity only if they were close to a crack. Houde and Mirza '74 found that dowel capacity was enhanced by increased concrete strength and beam net width, but it wasn't influenced as much by bar size or embedment length. Kemp and Wilhelm '77, in a study of bond behavior, found that the presence of dowel forces and tensile forces in the concrete did not significantly affect the cracked pattern observed when only axial forces were applied. Finally, Taylor '74 found that the dowel stiffness was linear for very low loads and that after cracking the dowel load drops to half its ultimate value. This dowel load-displacement curve is shown in Figure C.4.

Interface Shear Transfer

Considering experimental investigations of interface shear transfer Fenwick & Paulay '68, Houde & Mirza '74, Paulay & Loeber '74 conducted direct shear tests to evaluate the effect of parameters such as initial crack width, aggregate size, and the restraining effect permitted by the longitudinal reinforcement crossing the crack.

Fenwick & Paulay '68 performed direct shear tests which permitted transfer of pure shear stresses across a precracked shear plane, while the crack width was held constant. The tests were designed to study the effect of initial crack width and concrete strength on the interface shear transfer mechanism. It was found that the shear stiffness increased with decreasing initial crack width and increasing concrete strength. Empirical equations for the interface shear stress transferred across a crack resulted from a regression analysis of the experimental data and it depended on initial crack width, concrete compressive strength, and the shear displacement.

Houde & Mirza '74 performed direct shear tests on precracked concrete block specimens. After the concrete blocks were cracked along the shear plane and the initial crack width was set to a predetermined value the specimens were sheared monotonically to failure. This test program evaluated the effect of the initial crack width, the concrete strength, and the aggregate size. Results indicated that the variation of shear stiffness of cracked concrete with concrete compressive strength was similar to that found by Fenwick & Paulay. In the range of maximum aggregate size tested (3/8 - 3/4 inches), the influence of the maximum aggregate size was found to be negligible compared to the effect of the crack width and concrete strength. Houde & Mirza developed a shear stress -- displacement

relationship expressing the shear stress in terms of initial crack width and shear displacement.

Paulay and Loeber '74 also studied interface shear transfer using the direct shear specimens shown in Figure C.5. The concrete specimens were highly reinforced with ties and flexural steel in order to avoid any premature flexural or diagonal cracks near the shear plane. The crack width was held constant while the specimen loaded monotonically to failure. Typical results are shown in Figure C.6. The shear stiffness of the specimen decreased with increasing crack width. Figure C.7 shows the mean shear stress -- shear displacement relationship with constant shear stress to crack width ratio. Results show that aggregate shape and size had very little influence on the shear displacement relationships.

Birkeland & Birkeland '66 have presented a shear-friction hypothesis to describe the maximum shear force that can be transferred across the crack. The model they used is similar to the one shown in Figure C.8. The shear load applied to the specimen produces tangential and normal displacements at the shear plane. Normal displacements will develop axial tensile stresses in the reinforcement crossing the crack which will induce vertical compressive stresses in the concrete. The resistance to sliding will then be provided by the frictional force generated by the vertical compressive stresses in the concrete. Shear-friction theory provides the lower bound to the experimental data available on push off type specimens. It must be noted that this procedure is valid only for conditions in which the failure is obtained by yielding of the reinforcement across the crack; this allows for the mobilization of shear friction. In the shear-friction theory dowel action is

neglected and the frictional resistance along the crack is presumed to account for the strength of the element.

Mast '68 also compared the shear friction theory to experimental results of composite beams. Similar to the results presented by Birkeland & Birkeland, the shear-friction equation with horizontal tension can be expressed in terms of the total cross sectional area of reinforcement, the yield strength of the reinforcing steel, and the tensile horizontal load at ultimate strength. Of course the shearing force can be equated to the normal force through the coefficient of friction between the two crack surfaces. In shear-friction this coefficient of friction is fictitiously high to compensate for the neglect of dowel action.

Combined Mechanisms

In all practical situations where shear forces have to be transferred across the crack, both the interface shear transfer and the dowel action mechanism should occur simultaneously. In the preceding sections the individual mechanisms were isolated to assess their most important parameters. In the following sections a summary of the existing literature on the combined action of static interface shear transfer and dowel action is presented.

Mattock '74, '76 conducted several investigations into the ultimate shear strength of initially cracked and uncracked concrete. All specimens were loaded by pure shear on a shear plane until failure occurred by yielding of the reinforcement. The investigation studied the effect on the ultimate shear strength of the different percentages and arrangements of reinforcement, concrete and reinforcement strength, presence of direct stresses acting parallel and transverse to the shear

plane, presence of moments and tensile forces normal to the shear plane, aggregate type, presence of construction joints on the shear plane, and the effect of cyclic shear stresses. Typical test results are shown in Figure C.9. The ultimate shear stress increases almost linearly with the index ρf_y from a finite value for ρf_y equal to zero to a limit dependent on the concrete strength for high ρf_y values. With a monolithic shear plane, strengths are consistently greater than the precracked shear plane. As shown in Figure C.9 for ρf_y lying between A or A' and B, failure is relatively gentle and is due to a breakdown of the concrete after the reinforcement crossing the shear plane yields. For ρf_y values lying between B and C failure occurred abruptly before the reinforcement yielded. In this region the failure loads are similar for uncracked and precracked specimens.

Reinhardt and Walraven '80 tested pushoff type specimens similar to those of Mattock. They found that with more reinforcement with smaller bar diameters the stiffness of the embedded steel was found to increase due to increased steel area in bond. Concrete strength and roughness of the crack plane affect interlock resistance and crack opening during sliding. The angle of bar inclination was found to be partly a stiffness and partly a geometry effect.

For specimens in which the applied shear force was transferred by combined action of the interface shear transfer and dowel action Jimenez et al '79 observed that the shear slips were small. This implies a higher shear stiffness compared to dowel action or interface shear action acting alone. This is due to the role that the reinforcing bars play in restraining the crack width, resulting in a higher contribution of the interface shear transfer. It was also observed that reinforcement size was an important parameter in the shear transfer mechanism.

· Large dowel bars attract higher dowel forces causing splitting of concrete along the bar and hence collapse of the shear transfer mechanism.

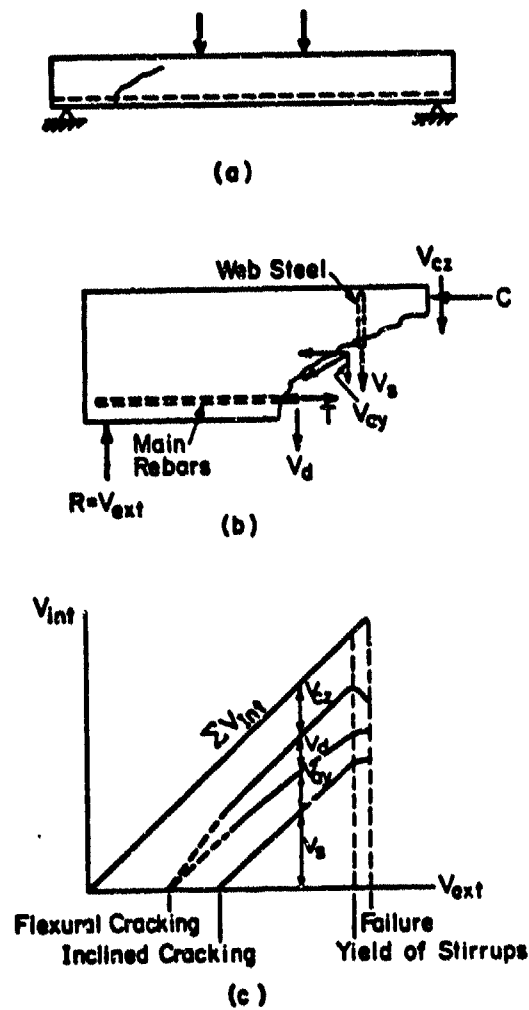


Figure C.1

Shear Transfer in Diagonally Cracked Beam: a) Cracked Beam, b) Free-body Diagram Along the Crack, c) Distribution of Internal Shear Forces (ASCE '82)

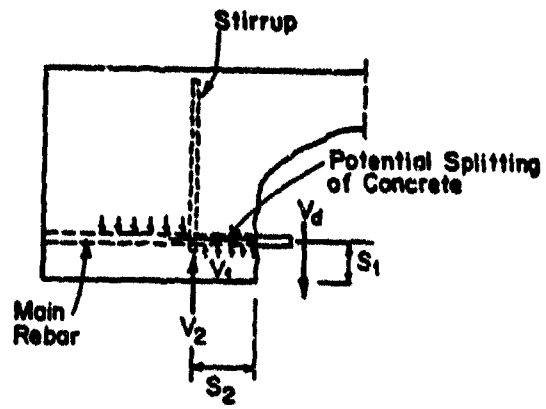


Figure C.2 Dowel Action of Main Reinforcement (ASCE'82)

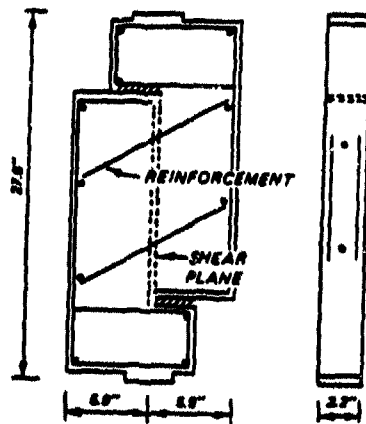


Figure C.3 Dulac's Test Specimen (ASCE'82)

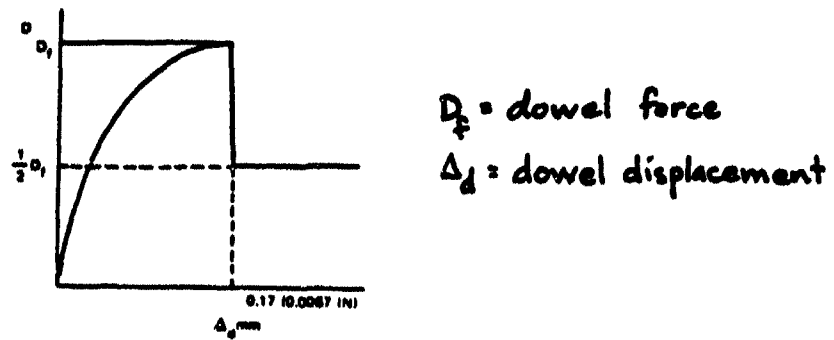


Figure C.4 Dowel Load-Displacement Curve from Taylor (ASCE '82)

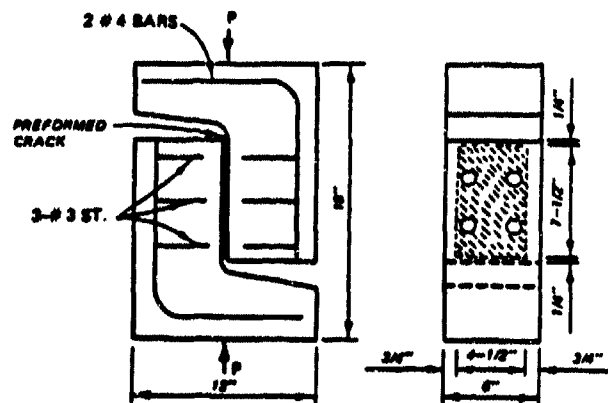


Figure C.5 Specimen Used in Paulay and Loeber's Investigation (ASCE '82)

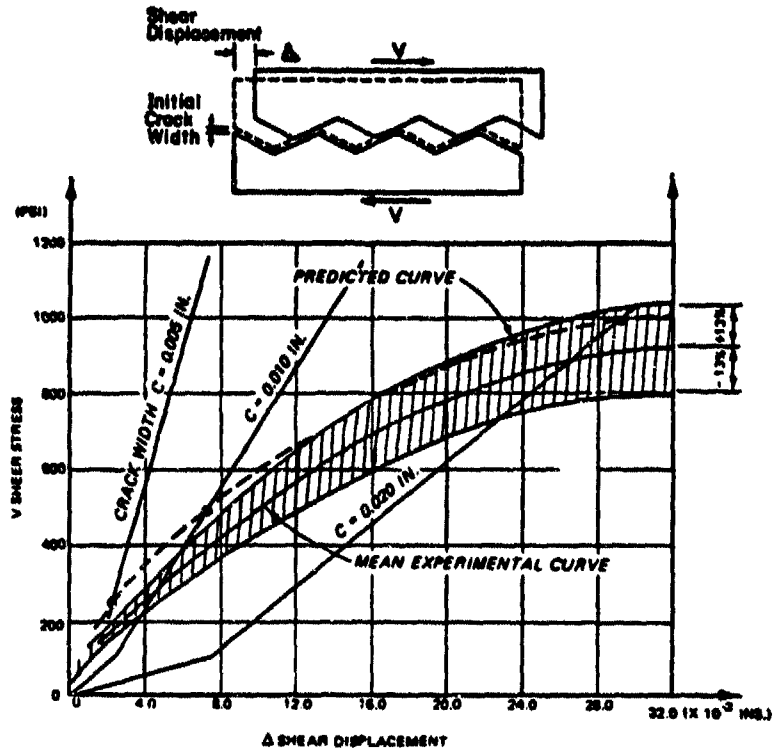


Figure C.6 Regression Analysis with Constant Shear Stress to Crack Width Ratio (ASCE'82)

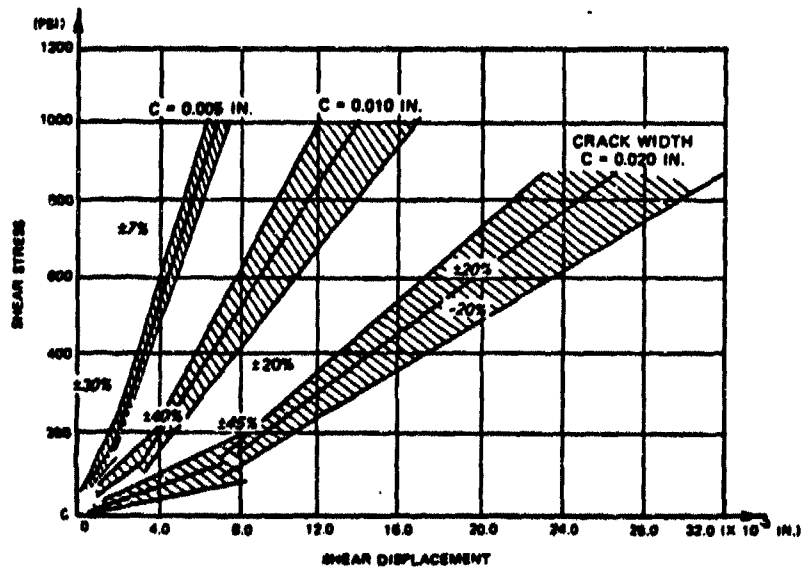
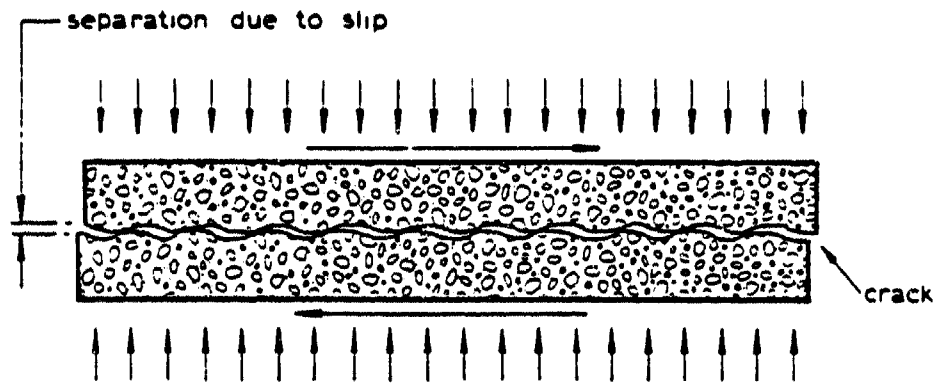
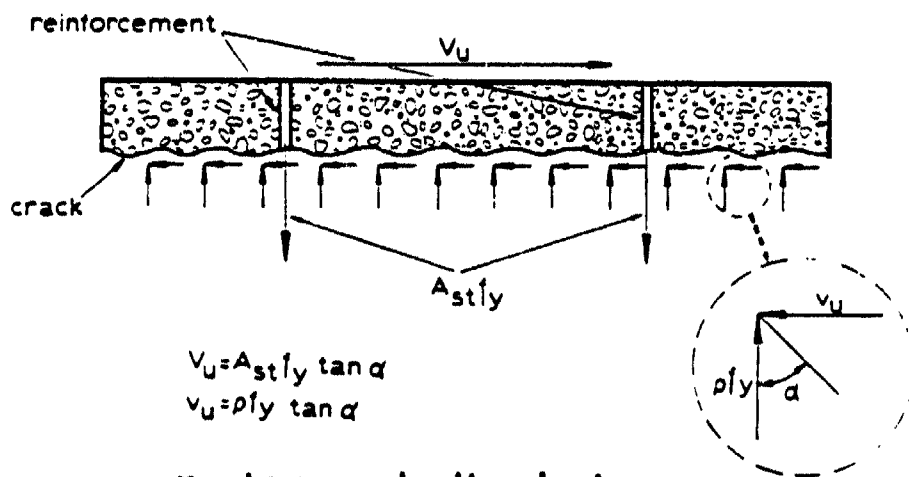


Figure C.7 Mean Shear Stress-Shear Displacement Relations for Constant Crack Width Tests (ASCE'82)



(a) Stresses on a crack



$$V_u = A_s f_y \tan \alpha$$

$$v_u = p f_y \tan \alpha$$

(b) Equilibrium at ultimate load

Figure C.8 Shear Friction Analogy (Somerville '74)

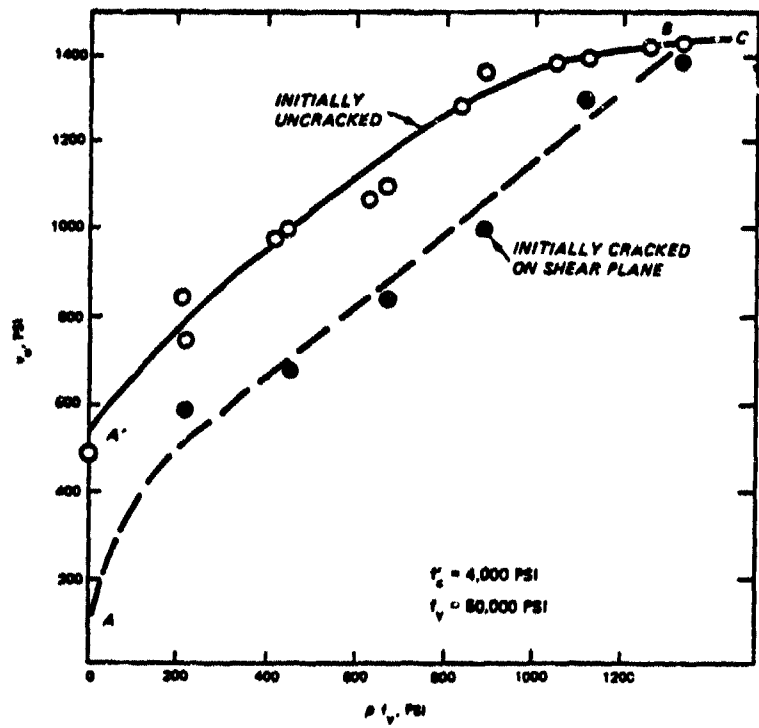


Figure C.9 Variation of Shear Strength with Reinforcement Parameter ρf_y (ASCE '82)